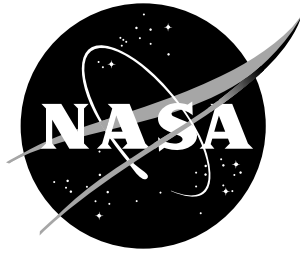


NASA Technical Memorandum 113137



Near Field Pressure Fluctuations in the Exit Plane of a Choked Axisymmetric Nozzle

Michael K. Ponton, John M. Seiner, and Martha C. Brown

November 1997

The NASA STI Program Office ... in Profile

Since its founding, NASA has been dedicated to the advancement of aeronautics and space science. The NASA Scientific and Technical Information (STI) Program Office plays a key part in helping NASA maintain this important role.

The NASA STI Program Office is operated by Langley Research Center, the lead center for NASA's scientific and technical information. The NASA STI Program Office provides access to the NASA STI Database, the largest collection of aeronautical and space science STI in the world. The Program Office is also NASA's institutional mechanism for disseminating the results of its research and development activities. These results are published by NASA in the NASA STI Report Series, which includes the following report types:

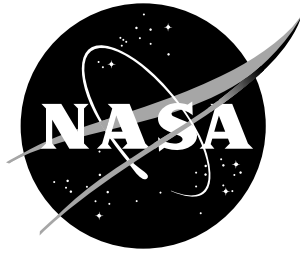
- TECHNICAL PUBLICATION. Reports of completed research or a major significant phase of research that present the results of NASA programs and include extensive data or theoretical analysis. Includes compilations of significant scientific and technical data and information deemed to be of continuing reference value. NASA counter-part of peer reviewed formal professional papers, but having less stringent limitations on manuscript length and extent of graphic presentations.
- TECHNICAL MEMORANDUM. Scientific and technical findings that are preliminary or of specialized interest, e.g., quick release reports, working papers, and bibliographies that contain minimal annotation. Does not contain extensive analysis.
- CONTRACTOR REPORT. Scientific and technical findings by NASA-sponsored contractors and grantees.
- CONFERENCE PUBLICATION. Collected papers from scientific and technical conferences, symposia, seminars, or other meetings sponsored or co-sponsored by NASA.
- SPECIAL PUBLICATION. Scientific, technical, or historical information from NASA programs, projects, and missions, often concerned with subjects having substantial public interest.
- TECHNICAL TRANSLATION. English-language translations of foreign scientific and technical material pertinent to NASA's mission.

Specialized services that help round out the STI Program Office's diverse offerings include creating custom thesauri, building customized databases, organizing and publishing research results ... even providing videos.

For more information about the NASA STI Program Office, you can:

- Access the NASA STI Program Home Page at <http://www.sti.nasa.gov/STI-homepage.html>
- E-mail your question via the Internet to help@sti.nasa.gov
- Fax your question to the NASA Access Help Desk at (301) 621-0134
- Phone the NASA Access Help Desk at (301) 621-0390
- Write to:
NASA Access Help Desk
NASA Center for AeroSpace Information
800 Elkridge Landing Road
Linthicum Heights, MD 21090-2934

NASA Technical Memorandum 113137



Near Field Pressure Fluctuations in the Exit Plane of a Choked Axisymmetric Nozzle

*Michael K. Ponton, John M. Seiner, and Martha C. Brown
Langley Research Center, Hampton, Virginia*

National Aeronautics and
Space Administration

Langley Research Center
Hampton, Virginia 23681-2199

November 1997

Available from the following:

NASA Center for AeroSpace Information (CASI)
800 Elkridge Landing Road
Linthicum Heights, MD 21090-2934
(301) 621-0390

National Technical Information Service (NTIS)
5285 Port Royal Road
Springfield, VA 22161-2171
(703) 487-4650

Summary

Near field pressure data are presented for an unheated jet issuing from an underexpanded sonic nozzle for two exit lip thicknesses of 0.200 and 0.625 nozzle diameters. Because both the amplitude and the frequency of the screech mechanism have been shown to be sensitive to the initial nozzle exit geometry, the data presented are at nozzle operating conditions where screech is dominant in the acoustic emission. Fluctuating measurements were obtained on the nozzle exit surface as well as in the acoustic near field. These measurements can be used to better characterize the initial acoustic shear layer excitation due to the natural screech feedback process. Such a characterization would be useful in the development of active control methodologies, incorporated in the nozzle exit plane, that can reduce the presence of screech.

Introduction

The acoustic emission from supersonic shock-containing jets may be dominated by an intense tonal component referred to as screech. Such a domination is dependent on the thermodynamic operating conditions of the nozzle and the angle of measurement. The seminal work of Powell [1] described screech as being associated with a feedback process as follows: (a) an embryonic disturbance is shed in the initial shear layer region of the jet; (b) the disturbance is amplified as it convects downstream; (c) the amplified disturbance interacts with the shock cell system causing plume oscillation; (d) the oscillation produces sound; and (e) the sound propagates upstream toward the nozzle exit and excites the initial shear layer thus closing the feedback loop.

Experimental work [2, 3] suggest that free shear flows contain organized wavelike structures in addition to the random turbulent fluctuations. Because the spatial magnitude of these structures are of orders near that of the mean flow, they are referred to as large-scale structures and also as

instability waves due to their local wavelike characteristics [4]. Tam, Seiner and Yu [5] introduced the use of linear spatial stability theory to describe the relationship between screech and the large scale turbulent structure of the jet.

Seiner [6] indicates that the frequency of the most highly amplified instability wave is the same as that measured for screech. Thus, a better understanding of the screech mechanism can be derived from Schlieren investigations of the large scale structures [7, 8, 9, 10] as well as with acoustic measurements [9, 11, 12, 13, 14, 15]. The screech mechanism has been extensively studied for a variety of nozzle geometries that include rectangular [8, 16, 17, 18, 19, 20, 21, 22, 23, 24, 25, 15], asymmetric [26, 20], multiple jet [27, 28, 29, 30], and axisymmetric [1, 7, 31, 32, 33, 14].

Numerous investigations continue to exist to reduce the presence of screech. These studies are not purely academic: full scale studies [34] have shown significant acoustic energy associated with this noise mechanism causing, in some cases, sonic fatigue of airborne structures [35]. To facilitate their study of broadband shock associated noise, Harper-Bourne and Fisher [36] introduced tabs into the initial shear layer region of the jet to reduce the screech “tones.” They also performed investigations into the effects on the screech amplitude of an acoustic reflector placed in the nozzle exit plane. Denham [37] demonstrates reductions in the screech amplitude using acoustic excitation and Norum [38] shows that screech can be modified by incorporating slots in choked tube jets. More recently, Huang et al. [39] are using electrostatic microactuators to control screech.

The purpose of this report is to provide data which can be used to better understand the initial acoustic shear layer excitation due to the screech feedback process. With this understanding, future investigators will be in a better position to modify the screech cycle via modifications to the initial nozzle conditions.

Symbols

D	inside diameter of the nozzle exit
M_j	fully expanded Mach number based on nozzle pressure ratio
R	distance from the sensor to the nozzle centerline
SPL	sound pressure level, dB, in a 25 Hz band (re 20 μ Pa)
λ_s	acoustic wavelength of screech

Experimental Details

The experiment was conducted in the Anechoic Noise Facility (ANF) [40] at the NASA Langley Research Center. The interior dimensions of the ANF are 27.5 ft by 27 ft by 24 ft high within the acoustic wedge tips. The anechoic treatment minimally absorbs 99% of the incident sound for frequencies in excess of 100 Hz. The ANF is capable of supplying dry unheated air for continuous operation and the electronically controlled valves maintain the nozzle pressure ratio to within 0.3% of the desired set point. All pressure transducers used by the flow control system received daily calibration.

The nozzle assembly consisted of a contoured transition section connecting a 7.875 inch inside diameter supply air pipe to a 1.500 inch inside diameter pipe which then led to the nozzle. The 1.500 inch straight section was 26.000 inches in length with an outside diameter of 2.250 inches. The length of this assembly allowed minimal interference of flanges with the natural jet entrainment. The nozzle was convergent and conical (5° convergence angle) with an exhaust diameter of 1.000 inches. High precision collars were fabricated which, when placed over the nozzle exit, would increase the nozzle exit lip

thickness to 0.200 and 0.625 inches as indicated in Figure 1 (shaded regions). Note that great care was taken to minimize exterior nozzle assembly protrusions.

The near field acoustic spectra were obtained by a single 1/4 inch microphone and surface-mounted transducers on the nozzle exit lip. The microphone was located in the nozzle exit plane and positioned 2 inches from the centerline. Because the directivity of screech is at shallow angles to the jet axis, the near field microphone is located in a position at which the measurement of screech should easily be obtained for all nozzle pressure ratios investigated. The included angle between the microphone and nozzle axes was approximately 6° . The diameter of the surface-mounted pressure transducers were 0.095 inches and their positions are indicated in Figure 2.

The length of the nozzle assembly created a total pressure loss through the system. Thus, before the experiment was conducted the total pressure exiting the nozzle was measured and a relationship found between the actual total pressure and the pressure measured in the stagnation chamber leading to the nozzle assembly. The fully expanded Mach number, M_j , was based on the true nozzle pressure ratio (actual total pressure divided by the ambient pressure) by using their isentropic relationship.

Acoustic Results

Narrowband spectra were gathered for each sensor utilizing a Fast Fourier Transform analyzer set to a filter bandwidth of 25 Hz and a maximum frequency of 20 kHz. For the 0.625 inch lip thickness, 44 M_j values ranging from 1.04 to 1.90 were tested. Thirty one M_j values ranging from 1.04 to 1.64 were investigated for the 0.200 inch lip thickness (screech does not dominate acoustic spectra at high Mach numbers for thinner lip configurations). The data are presented by the desired fully expanded Mach number. Figures 3 through 46 are for the 0.625 inch lip and figures 47 through 77 are for the

0.200 inch lip thickness. Each figure contains all sensor spectra acquired and indicated using the respective R/D position.

Presented in figures 78 through 82 are the normalized acoustic wavelength and the corresponding sound pressure levels for some of the dominant screech components. The wavelength was computed using the ambient speed of sound. The data are for fundamental frequencies and not harmonics. Figures 78 through 80 are for the 0.625 inch lip and figures 81 and 82 are for the 0.200 inch lip thickness.

Concluding Remarks

Near field pressure data acquired at the NASA Langley Research Center are presented for a convergent conical nozzle operating underexpanded. Two exit lip thicknesses of 0.200 and 0.625 nozzle diameters were tested. The fully expanded Mach number range tested for each lip thickness was limited to the operating conditions that screech is the dominant noise source mechanism. Narrowband spectra are given for a single near field microphone located in the nozzle exit plane as well as fluctuating pressure measurements acquired on the nozzle exit. These measurements may prove useful in understanding the initial acoustic jet excitation due to the screech mechanism. Such information would be valuable in the development of active screech control methodologies.

References

1. Powell, A.: On the Mechanism of Choked Jet Noise. *Proceedings of the Physical Society*, vol. 66, pt. 12, 1953, pp. 1039-1056.
2. Brown, G. L.; and Roshko, A.: Density Effects and Large Structure in Turbulent Mixing Layers. *Journal of Fluid Mechanics*, vol. 23, pt. 4, 1974, pp. 775-816.
3. Cohen, J.; and Wygnanski, I.: The Evolution of Instabilities in the Axisymmetric Jet. *Journal of Fluid Mechanics*, vol. 176, 1987, pp. 191-219.
4. Tam, C. K. W.; and Morris, P. J.: The Radiation of Sound by the Instability Waves of a Compressible Plane Turbulent Shear Layer. *Journal of Fluid Mechanics*, vol. 98, 1980, pp. 349-381.
5. Tam, C. K. W.; Seiner, J. M.; and Yu, J. C.: Proposed Relationship Between Broadband Shock Associated Noise and Screech Tones. *Journal of Sound and Vibration*, vol. 110, 1986, pp. 309-321.
6. Seiner, J. M.: Advances in High Speed Jet Aeroacoustics. AIAA-84-2275, 1984.
7. Davies, M. G.; and Oldfield, D. E. S.: Tones From a Choked Axisymmetric Jet. *Acoustica*, vol. 12, no. 4, 1962, pp. 257-277.
8. Poldervaart, L. J.; Vink, A. T.; and Wijands, A. P. J.: The Photographic Evidence of the Feedback Loop of a Two-Dimensional Screeching Supersonic Jet of Air. *The 6th International Congress on Acoustics*, F-3-9, 1968, pp. 101-104.
9. Westley, R.; and Woolley, J. H.: The Near Field Sound Pressures of a Choked Jet During a Screech Cycle. *AGARD Conference Proceedings*, no. 42, 1969, pp. 23-1 to 23-13.
10. Matsuda, T.; Umeda, Y.; Ishii, R.; and Yasuda, A.: Numerical and Experimental Studies on Choked Underexpanded Jets. AIAA-87-1378, 1987.
11. Westley, R.; and Woolley, J. H.: The Near Field Sound Pressures of a Choked Jet When Oscillating in the Spinning Mode. AIAA-75-479, 1975.
12. Seiner, J. M.; Manning, J. C.; and Ponton, M. K.: The Preferred Spatial Mode of Instability for a Mach 2 Jet. AIAA-86-1942.
13. Ponton, M. K.: An Acoustic Study of the Preferred Instability Modes for Supersonic Jets. M.S. Thesis, The George Washington University, 1991.
14. Ponton, M. K.; and Seiner, J. M.: The Effects of Nozzle Exit Lip Thickness on Plume

- Resonance. *Journal of Sound and Vibration*, vol. 154, no. 3, 1992, pp. 531-549.
15. Walker, S. H.: Experiments Characterizing Nonlinear Shear Layer Dynamics in a Supersonic Rectangular Jet Undergoing Screech. Ph.D. Dissertation, University of Notre Dame, 1997.
 16. Powell, A.: On the Noise Emanating From a Two-Dimensional Jet Above the Critical Pressure. *The Aeronautical Quarterly IV*, 1953, pp. 103-122.
 17. Krothapalli, A.; Baganoff, D.; and Hsia, Y.: On the Mechanism of Screech Tone Generation in Underexpanded Rectangular Jets. AIAA-83-0727, 1983.
 18. Seiner, J. M.; Ponton, M. K.; and Manning, J. C.: Acoustic Properties Associated with Rectangular Geometry Supersonic Nozzles. AIAA-86-1867, 1986.
 19. Ponton, M. K.; Manning, J. C.; and Seiner, J. M.: Far-Field Acoustics of Supersonic Rectangular Nozzles with Various Throat Aspect Ratios. NASA TM-89002, 1986.
 20. Tam, C. K. W.: The Shock-Cell Structures and Screech Tone Frequencies of Rectangular and Non-Axisymmetric Supersonic Jets. *Journal of Sound and Vibration*, vol. 121, no. 1, 1988, pp. 135-147.
 21. Gutmark, E.; Schadow, K. C.; and Bicker, C. J.: On the Near Acoustic Field and Shock Structure of Rectangular Supersonic Jets. AIAA-89-1053, 1989.
 22. Rice, E. J.; and Taghavi, R.: Screech Noise Source Structure of a Supersonic Rectangular Jet. NASA TM-105384, 1992.
 23. Raman, G.; and Rice, E. J.: Instability Modes Excited by Natural Screech Tones in a Supersonic Rectangular Jet. NASA TM-106409, 1993.
 24. Raman, G.: Screech Tones From Rectangular Jets With Spanwise Oblique Shock-Cell Structures. NASA CR-198417, 1996.
 25. Kaji, S.; and Nishijima, N.: Pressure Field Around a Rectangular Supersonic Jet in Screech. *AIAA Journal*, vol. 34, no. 10, 1996, pp. 1990-1996.
 26. Wlezien, R. W.; and Kibens, V.: The Influence of Nozzle Asymmetry on Supersonic Jets. AIAA-86-0277, 1986.
 27. Seiner, J. M.; Manning, J. C.; and Ponton, M. K.: Model and Full Scale Study of Twin Supersonic Plume Resonance. AIAA-87-0244, 1987.
 28. Wlezien, R. W.: Nozzle Geometry Effects on Supersonic Jet Interaction. AIAA-87-2694, 1987.
 29. Seiner, J. M.; Manning, J. C.; and Ponton, M. K.: Dynamic Pressure Loads Associated with Twin Supersonic Plume Resonance. *AIAA Journal*, vol. 26, no. 8, 1988, pp. 954-960.
 30. Taghavi, R.; and Raman, G.: Enhanced Mixing of Multiple Supersonic Rectangular Jets by Synchronized Screech. AIAA-94-2325, 1994.
 31. Seiner, J. M.; and Norum, T. D.: Experiments of Shock Associated Noise on Supersonic Jets. AIAA-79-1526, 1979.
 32. Norum, T. D.; and Seiner, J. M.: Measurements of Mean Static Pressure and Far-Field Acoustics of Shock-Containing Supersonic Jets. NASA TM-84521, 1982.
 33. Yu, J. C.; and Seiner, J. M.: Nearfield Observations of Tones Generated from Supersonic Jet Flows. AIAA-83-0706, 1983.
 34. Seiner, J. M.; Manning, J. C.; and Ponton, M. K.: Model and Full Scale Study of Twin Supersonic Plume Resonance. AIAA-87-0244, 1987.
 35. Hay, J. A.; and Rose, E. G.: In-Flight Shock Cell Noise. *Journal of Sound and Vibration*, vol. 11, no. 4, 1970, pp. 411-420.
 36. Harper-Bourne, M.; and Fisher, M. J.: The Noise From Shock Waves in Supersonic Jets. *AGARD Conference Proceedings No. 131 on Noise Mechanisms*, AGARD-CP-131, 1973, pp. 11-1 to 11-13.
 37. Denham, Jr., J. W.: Investigation of Screech Tone Elimination in an Underexpanded Supersonic Jet. AIAA-83-0646, 1983.

38. Norum, T. D.: Screech Suppression in Supersonic Jets. *AIAA Journal*, vol. 21, no. 2, 1983, pp. 235-240.
39. Huang, C.; Papp, J.; Najafi, K.; and Nagib, H. M.: A Microactuator System for the Study and Control of Screech in High Speed Jets. *IEEE MEMS-96 Workshop*, 1995.
40. Hubbard, H. H.; and Manning, J. C.: Aeroacoustic Research Facilities at NASA Langley Research Center--Description and Operational Characteristics. NASA TM-84585, 1983.

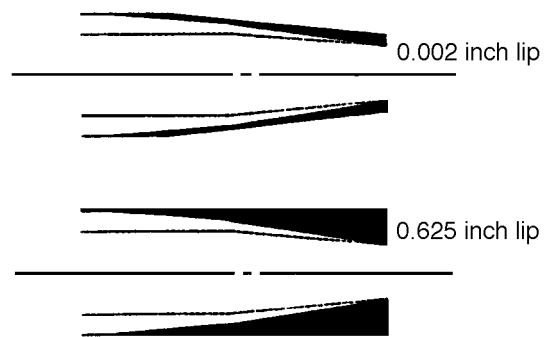


Figure 1. Position of collars (shaded regions) on the nozzle exterior

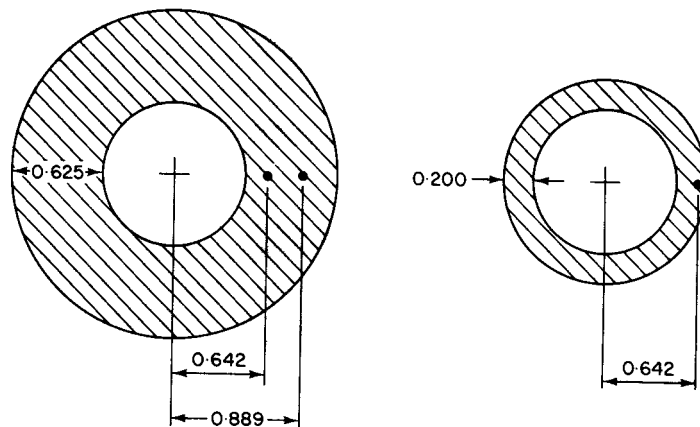
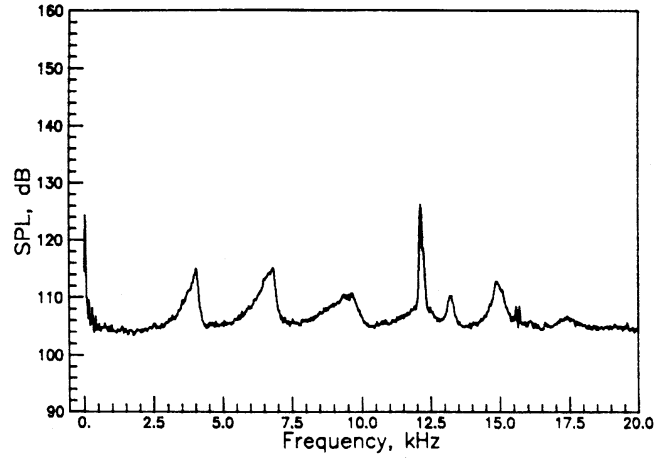
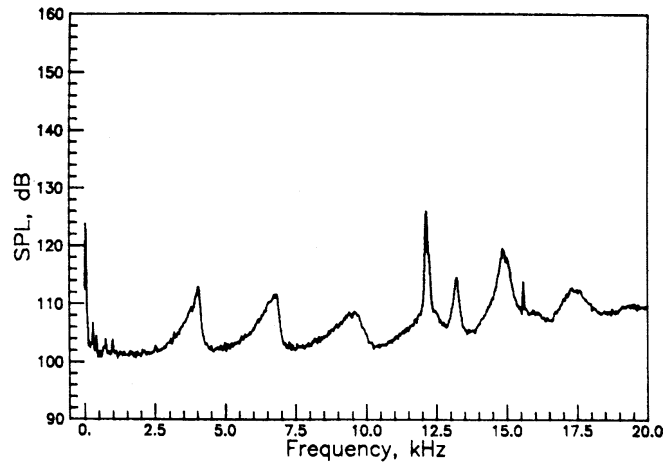


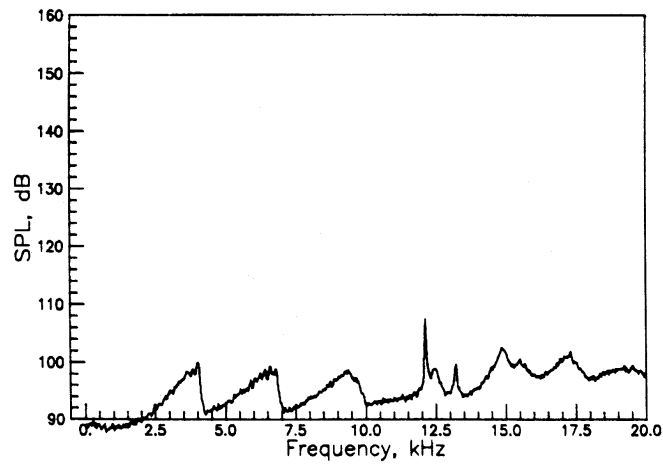
Figure 2. Location of surface-mounted transducers on the nozzle exit lip (dimensions in inches).



(a) $R/D=0.642$

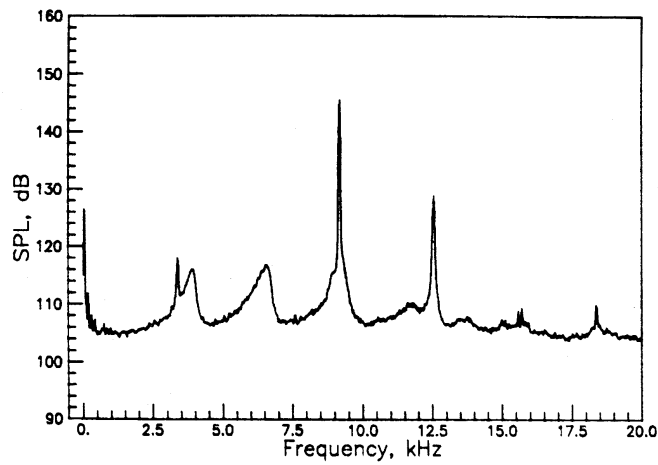


(b) $R/D=0.889$

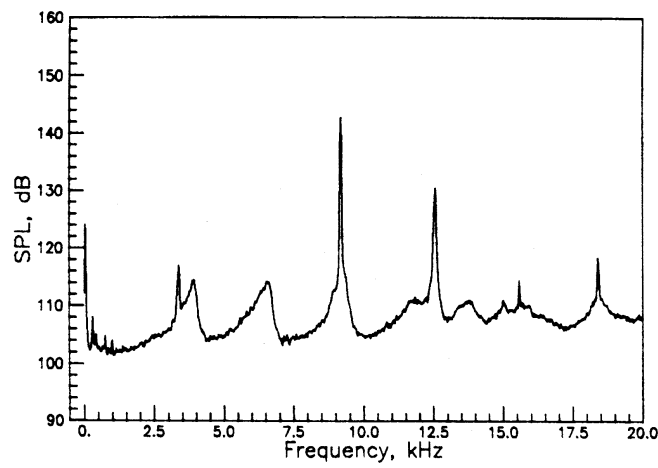


(c) $R/D=2.000$

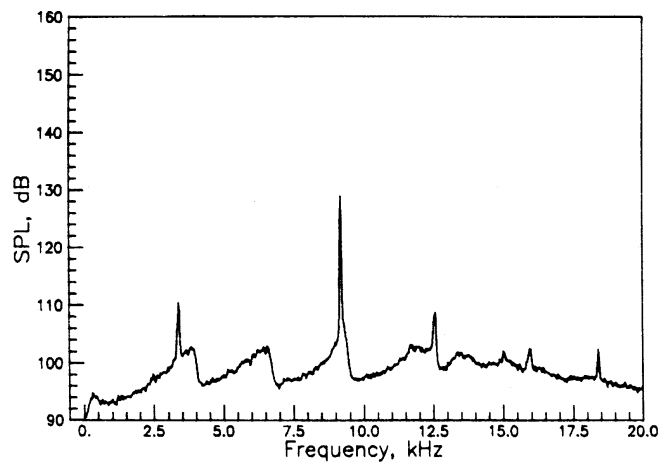
Figure 3. Narrowband spectra for the 0.625 inch lip thickness nozzle at $M_j=1.04$.



(a) $R/D=0.642$

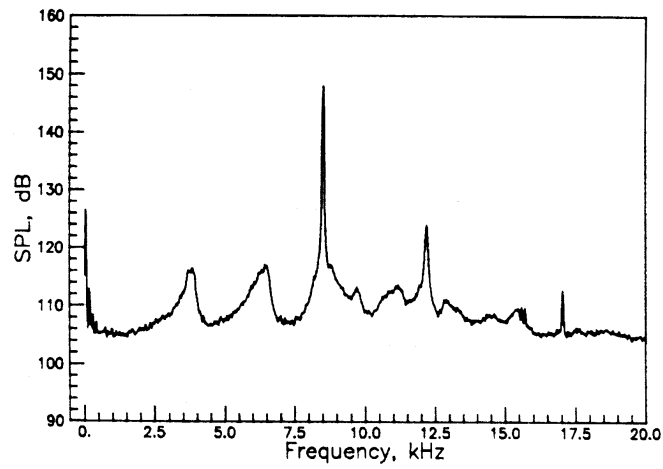


(b) $R/D=0.889$

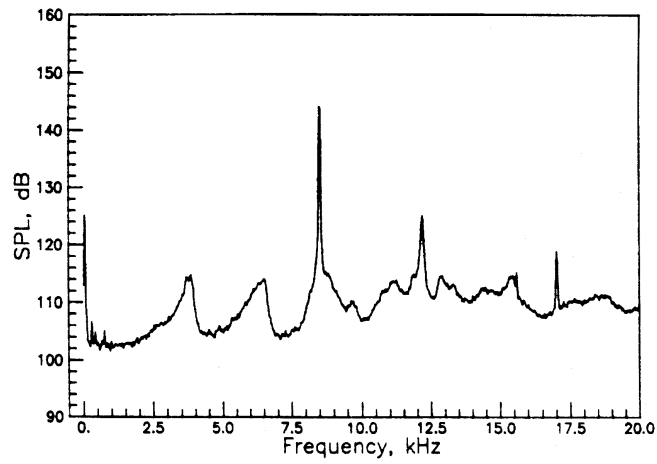


(c) $R/D=2.000$

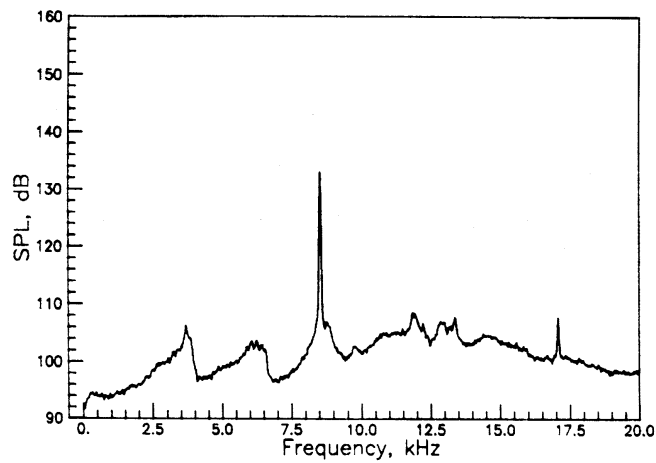
Figure 4. Narrowband spectra for the 0.625 inch lip thickness nozzle at $M_j=1.07$.



(a) $R/D=0.642$

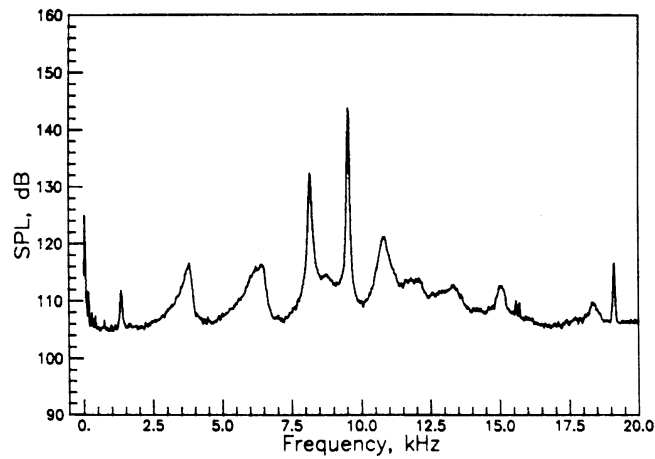


(b) $R/D=0.889$

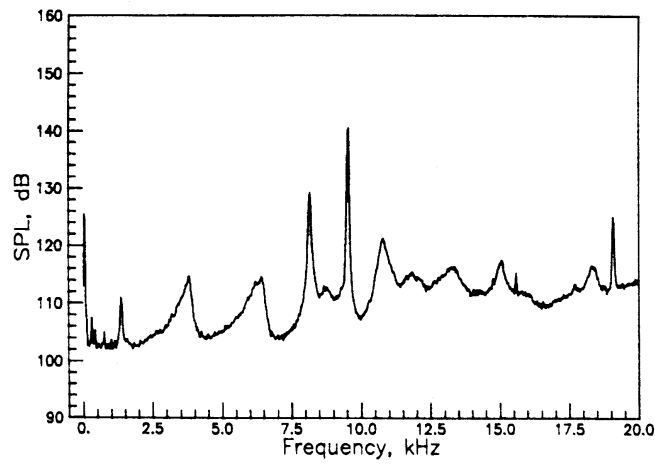


(c) $R/D=2.000$

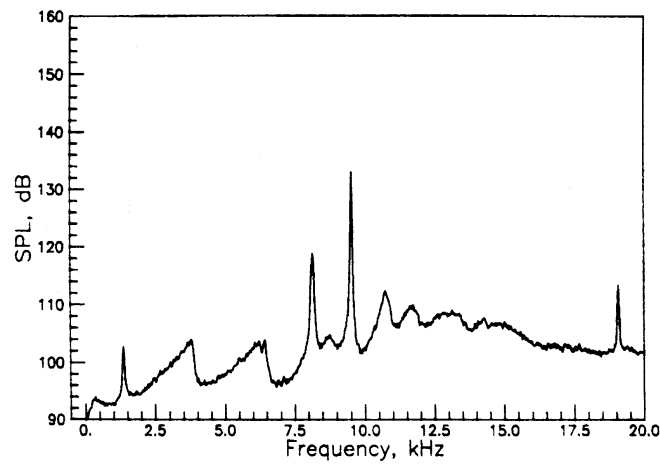
Figure 5. Narrowband spectra for the 0.625 inch lip thickness nozzle at $M_j=1.09$.



(a) $R/D=0.642$

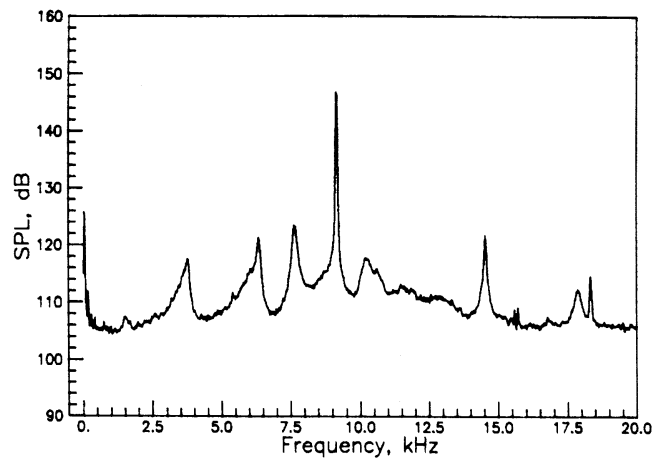


(b) $R/D=0.889$

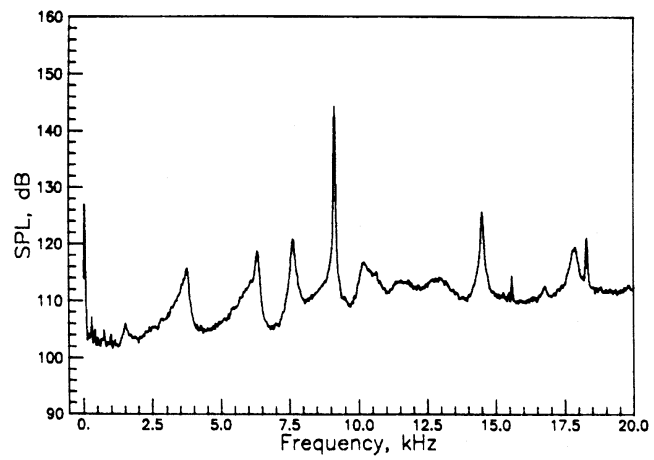


(c) $R/D=2.000$

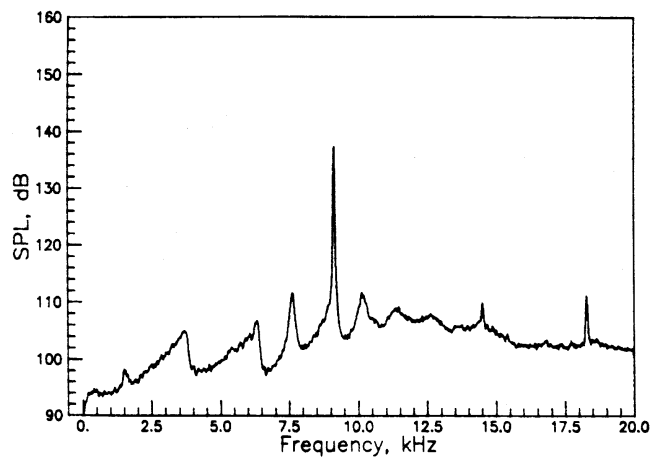
Figure 6. Narrowband spectra for the 0.625 inch lip thickness nozzle at $M_j=1.11$.



(a) $R/D=0.642$

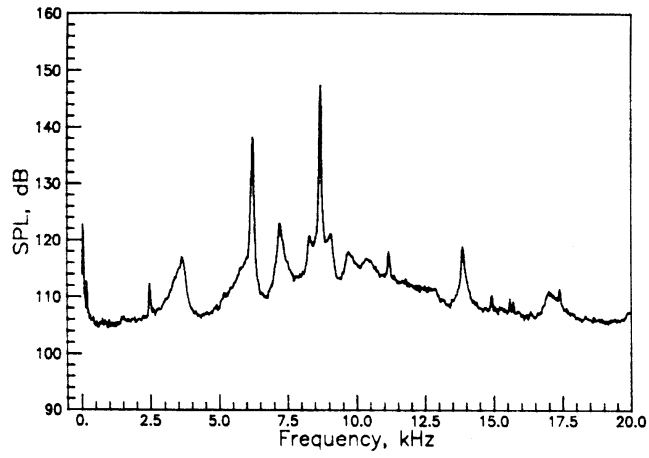


(b) $R/D=0.889$

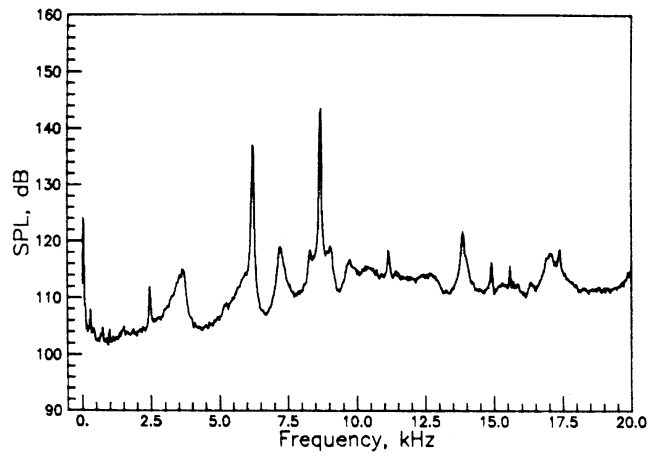


(c) $R/D=2.000$

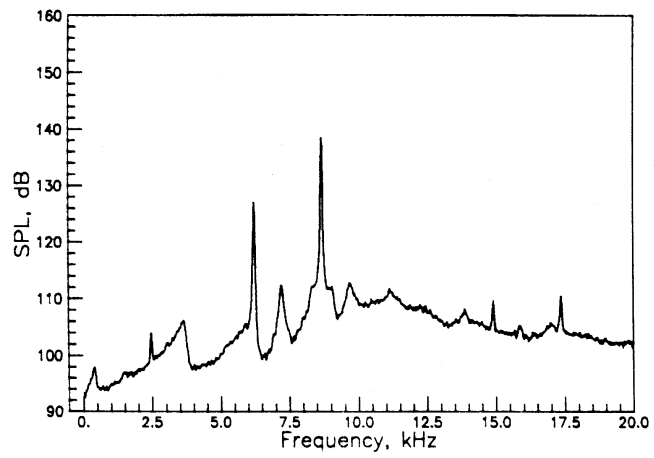
Figure 7. Narrowband spectra for the 0.625 inch lip thickness nozzle at $M_j=1.13$.



(a) $R/D=0.642$

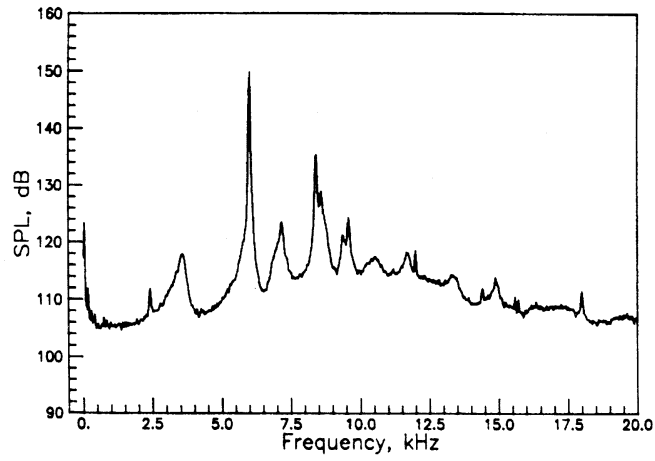


(b) $R/D=0.889$

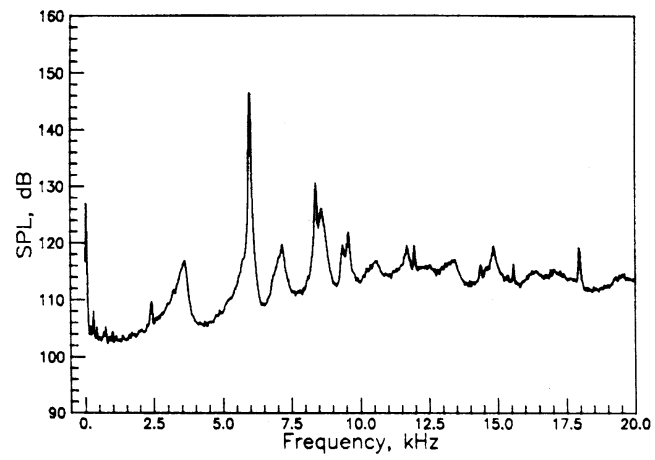


(c) $R/D=2.000$

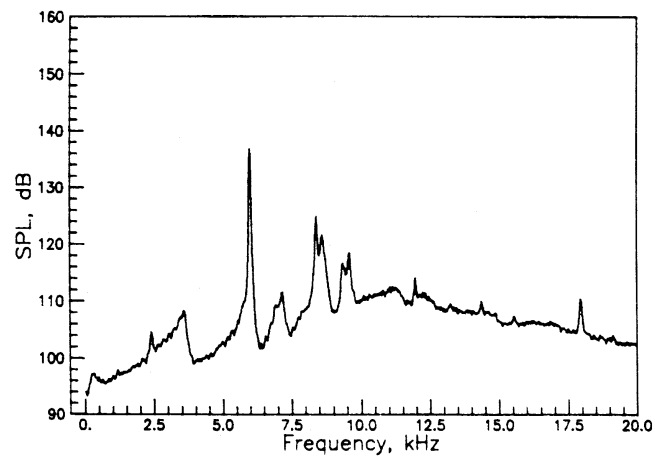
Figure 8. Narrowband spectra for the 0.625 inch lip thickness nozzle at $M_j=1.15$.



(a) $R/D=0.642$

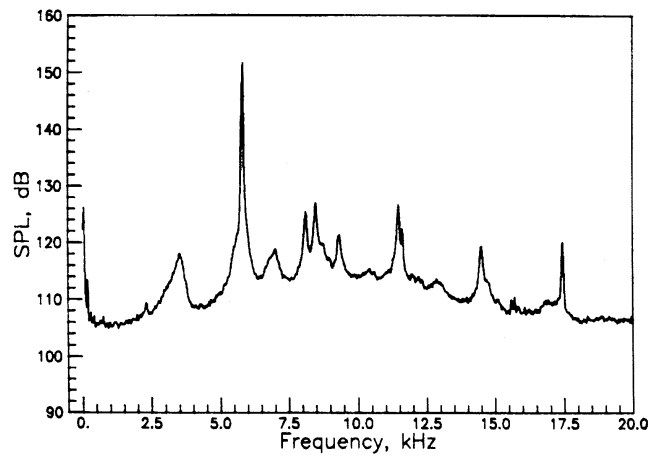


(b) $R/D=0.889$

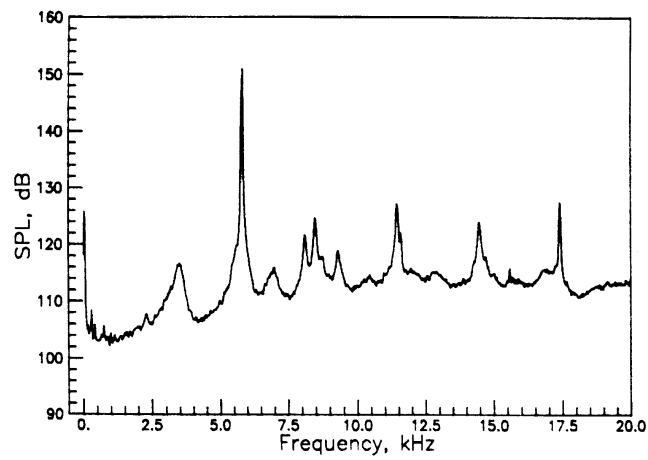


(c) $R/D=2.000$

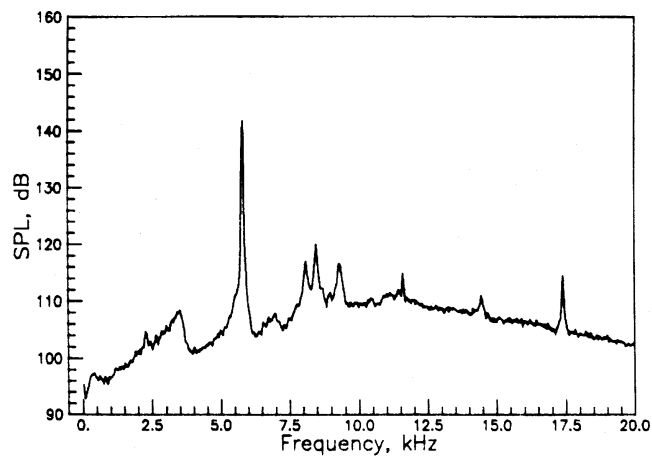
Figure 9. Narrowband spectra for the 0.625 inch lip thickness nozzle at $M_j=1.17$.



(a) $R/D=0.642$

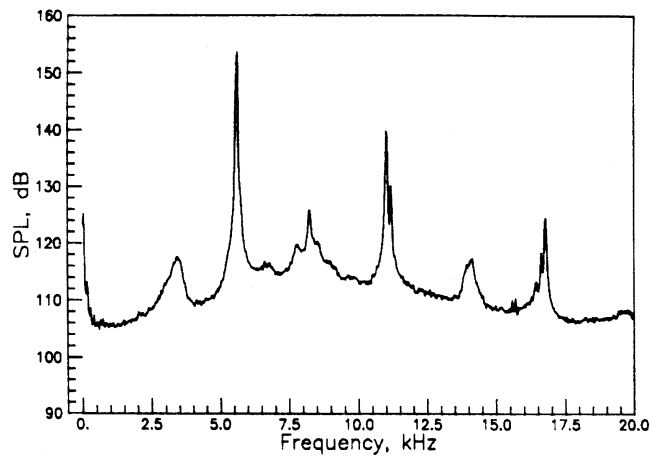


(b) $R/D=0.889$

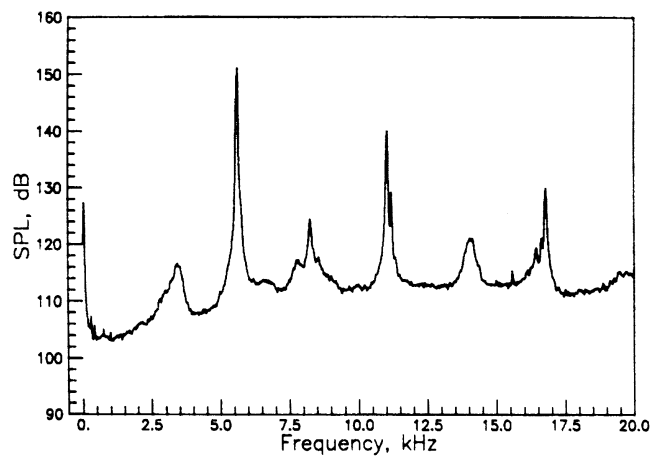


(c) $R/D=2.000$

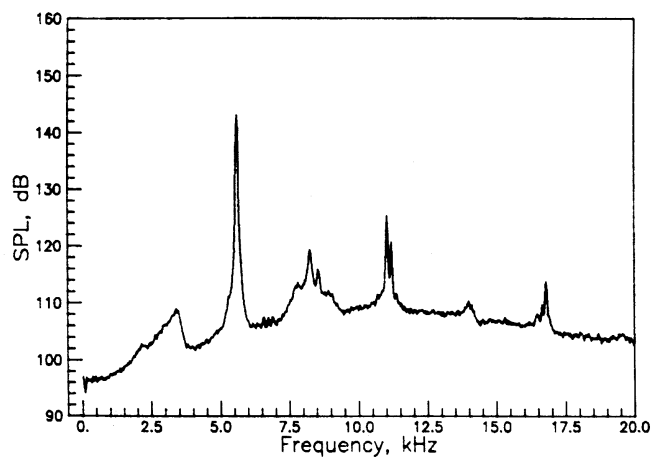
Figure 10. Narrowband spectra for the 0.625 inch lip thickness nozzle at $M_j=1.19$.



(a) $R/D=0.642$

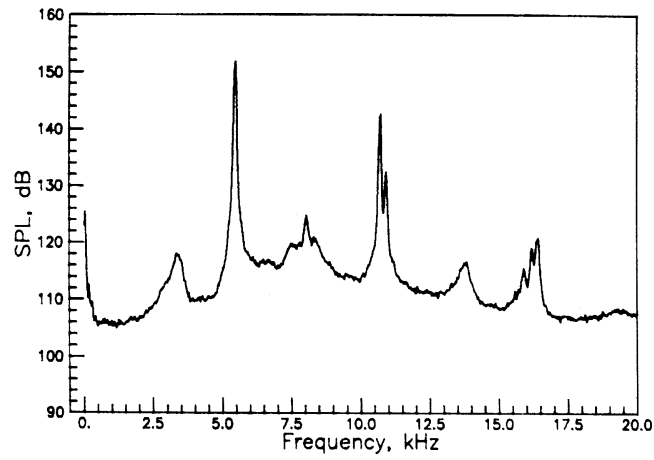


(b) $R/D=0.889$

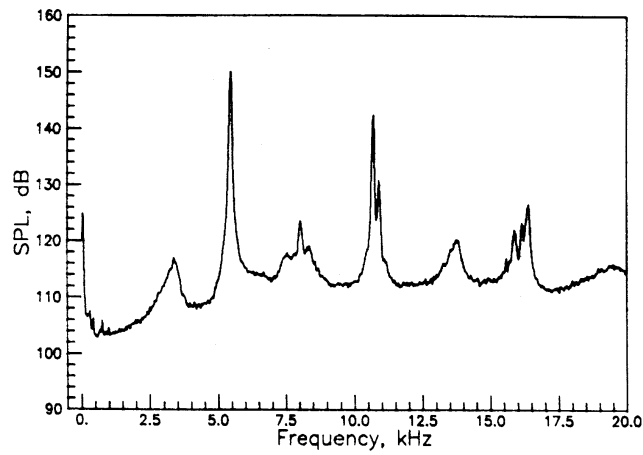


(c) $R/D=2.000$

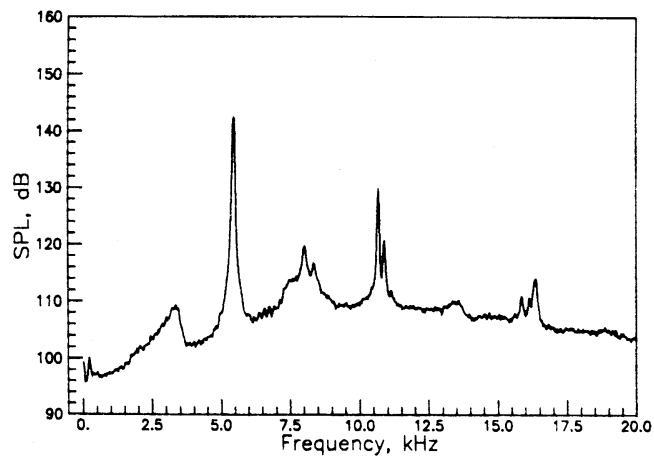
Figure 11. Narrowband spectra for the 0.625 inch lip thickness nozzle at $M_j=1.21$.



(a) $R/D=0.642$

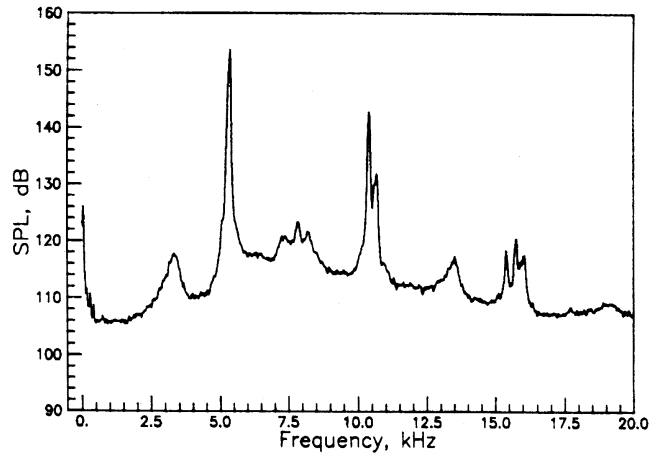


(b) $R/D=0.889$

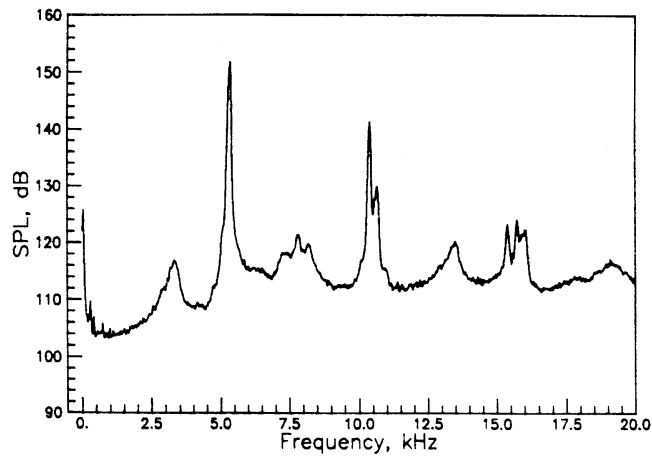


(c) $R/D=2.000$

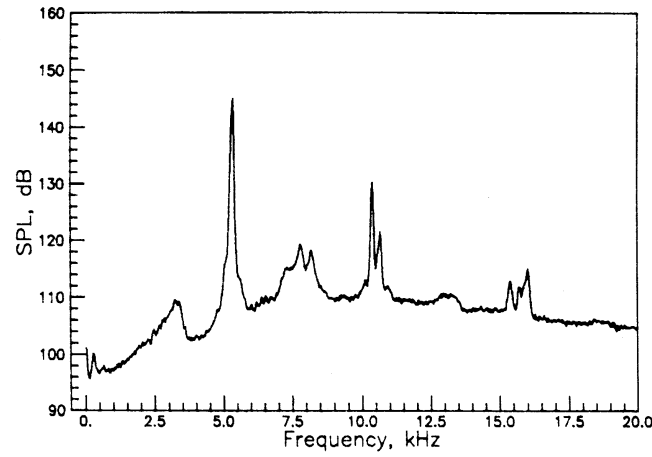
Figure 12. Narrowband spectra for the 0.625 inch lip thickness nozzle at $M_j=1.23$.



(a) $R/D=0.642$

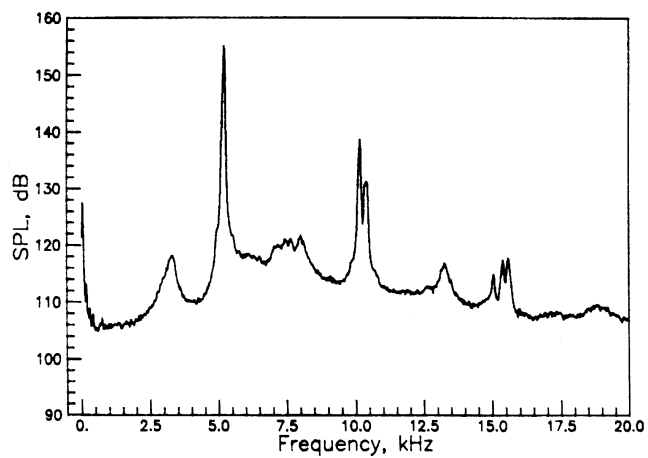


(b) $R/D=0.889$

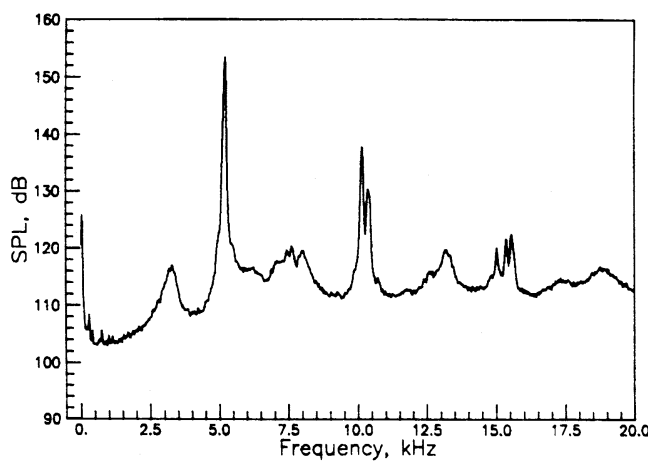


(c) $R/D=2.000$

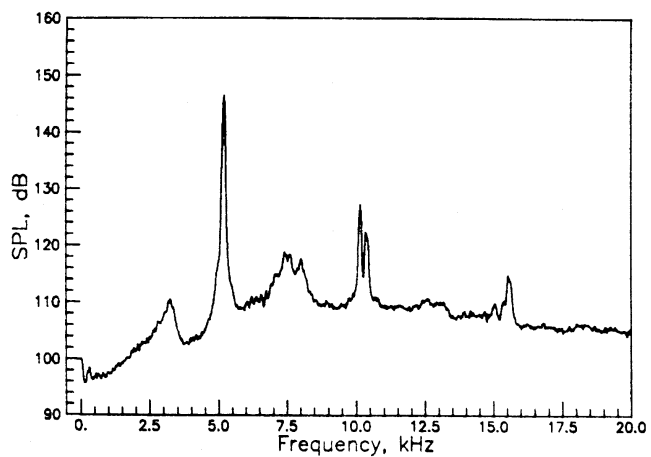
Figure 13. Narrowband spectra for the 0.625 inch lip thickness nozzle at $M_j=1.25$.



(a) $R/D=0.642$

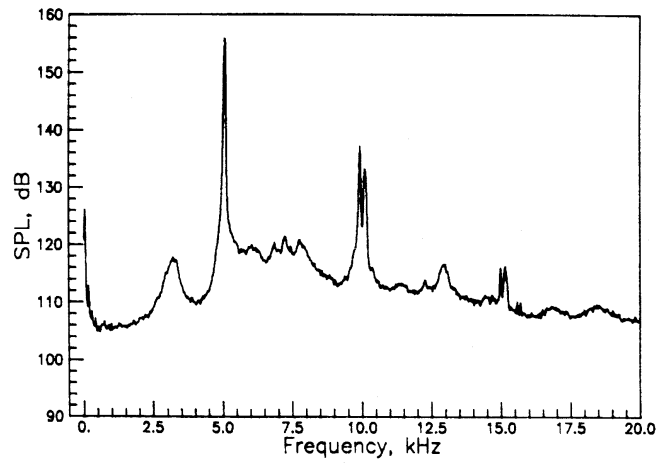


(b) $R/D=0.889$

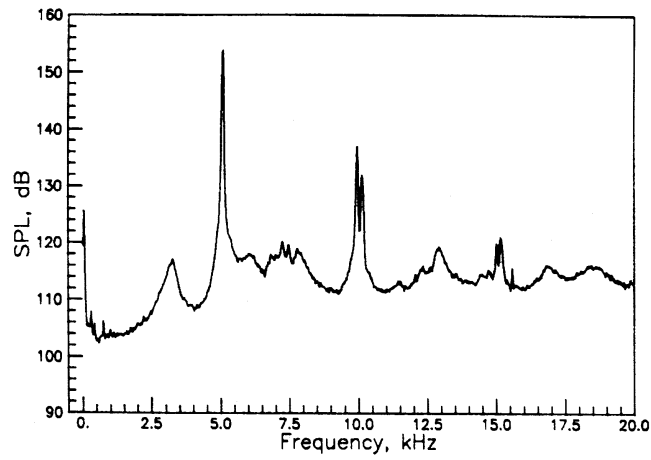


(c) $R/D=2.000$

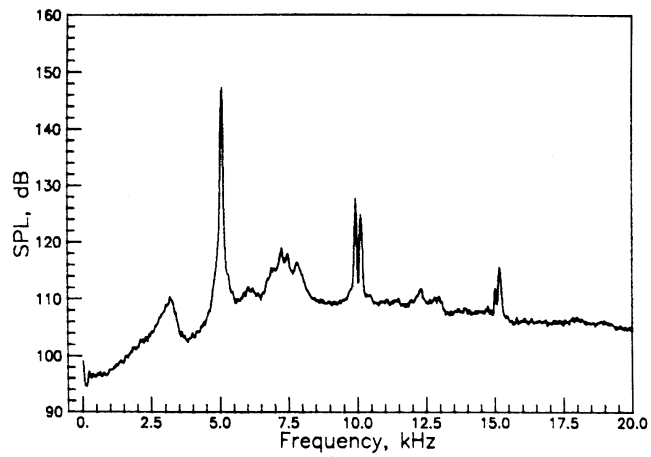
Figure 14. Narrowband spectra for the 0.625 inch lip thickness nozzle at $M_j=1.27$.



(a) $R/D=0.642$

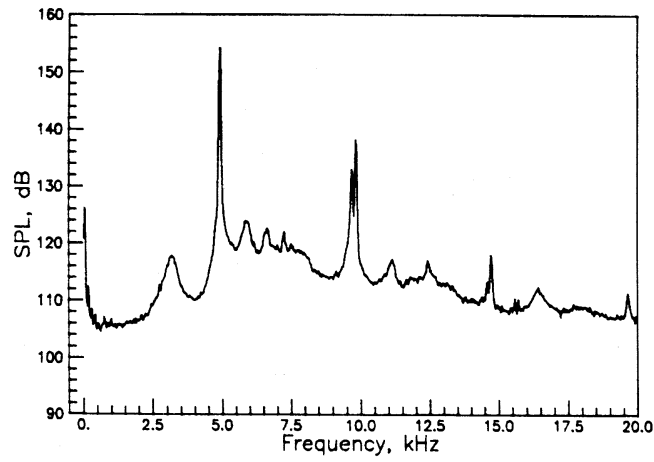


(b) $R/D=0.889$

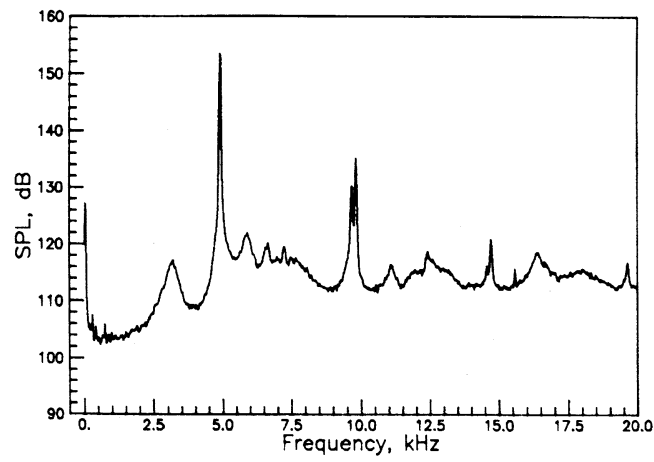


(c) $R/D=2.000$

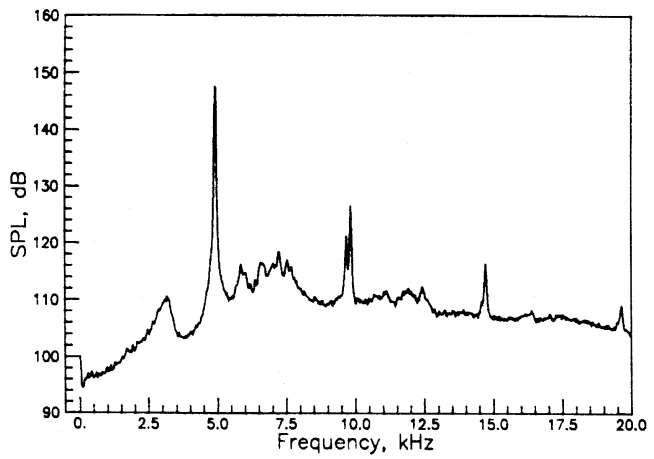
Figure 15. Narrowband spectra for the 0.625 inch lip thickness nozzle at $M_j=1.29$.



(a) $R/D=0.642$

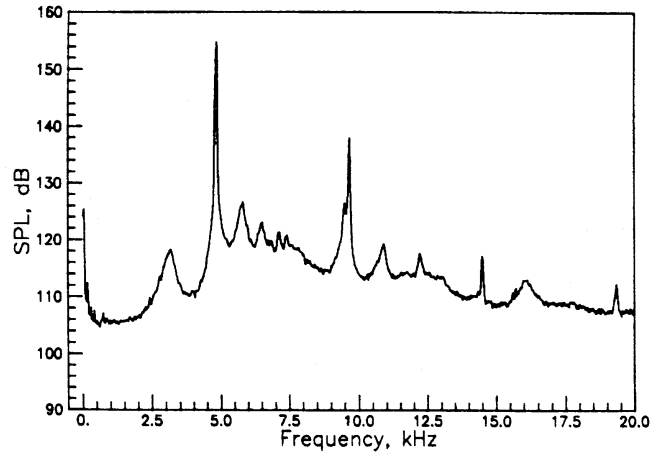


(b) $R/D=0.889$

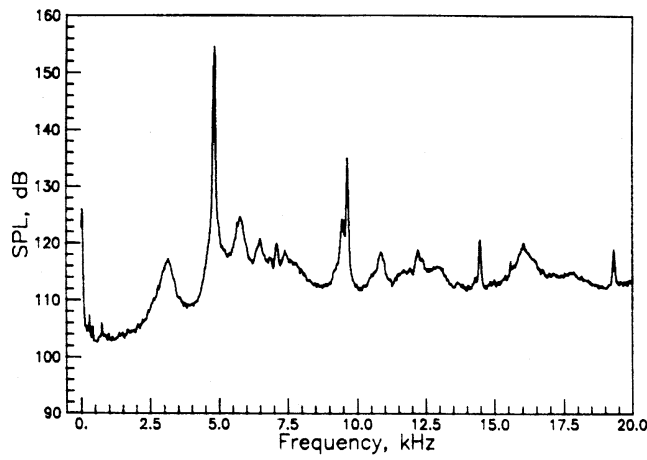


(c) $R/D=2.000$

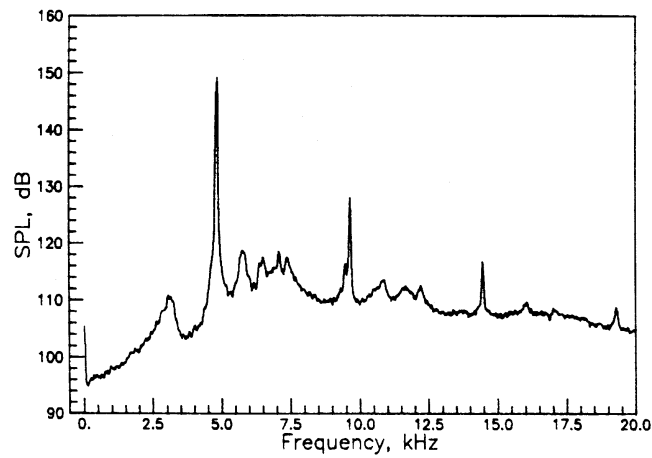
Figure 16. Narrowband spectra for the 0.625 inch lip thickness nozzle at $M_j=1.31$.



(a) $R/D=0.642$

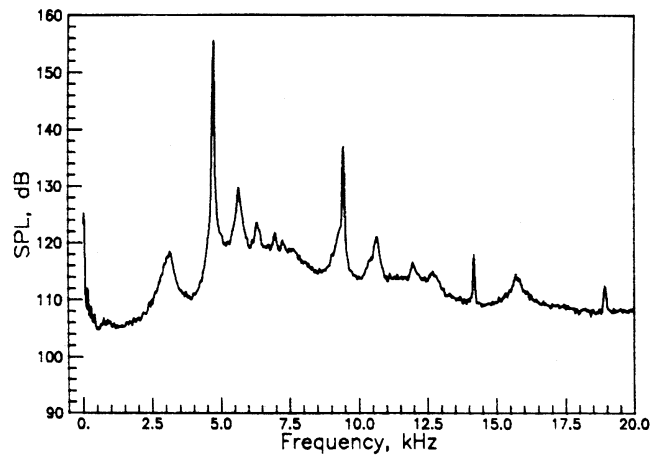


(b) $R/D=0.889$

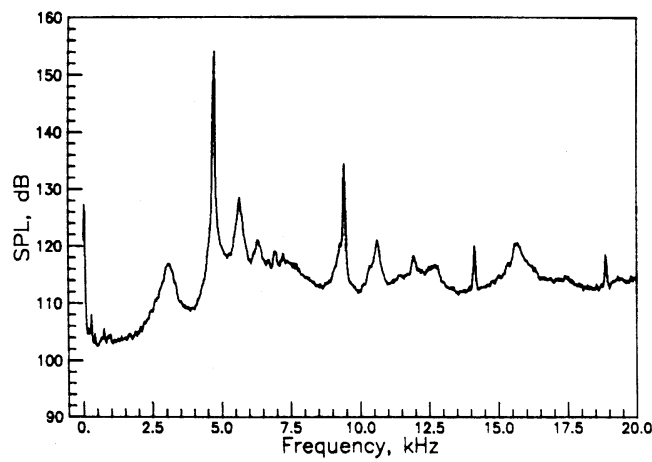


(c) $R/D=2.000$

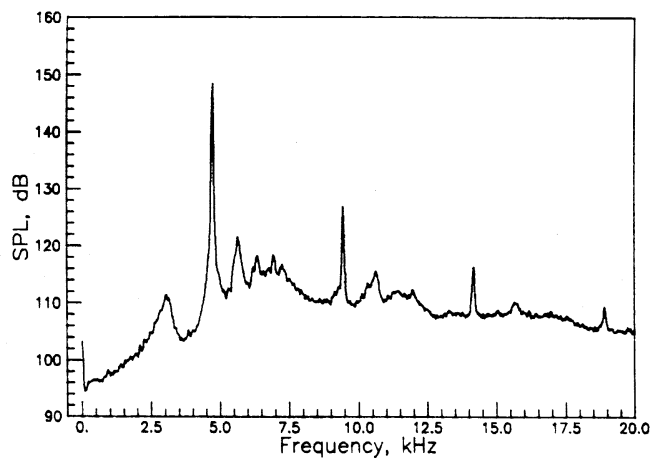
Figure 17. Narrowband spectra for the 0.625 inch lip thickness nozzle at $M_j=1.33$.



(a) $R/D=0.642$

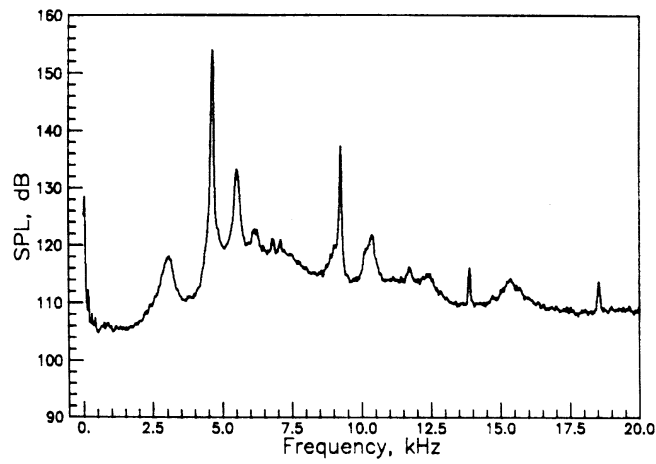


(b) $R/D=0.889$

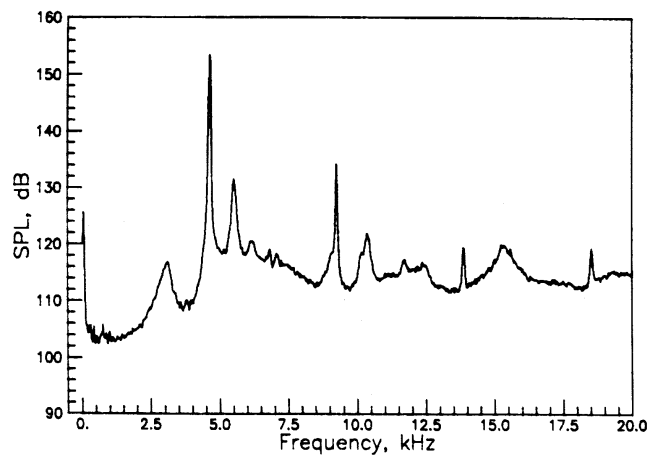


(c) $R/D=2.000$

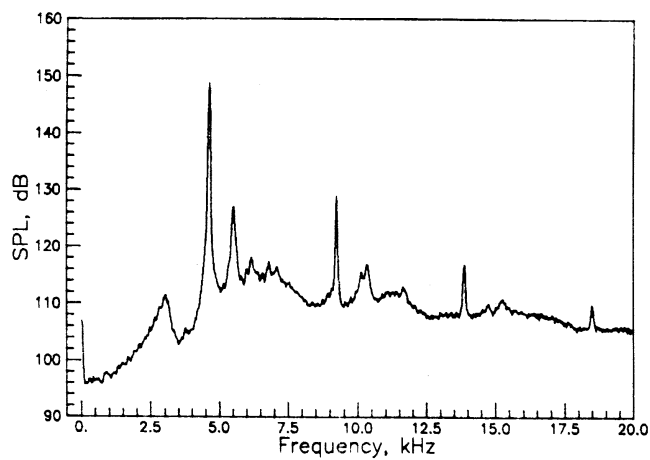
Figure 18. Narrowband spectra for the 0.625 inch lip thickness nozzle at $M_j=1.35$.



(a) $R/D=0.642$

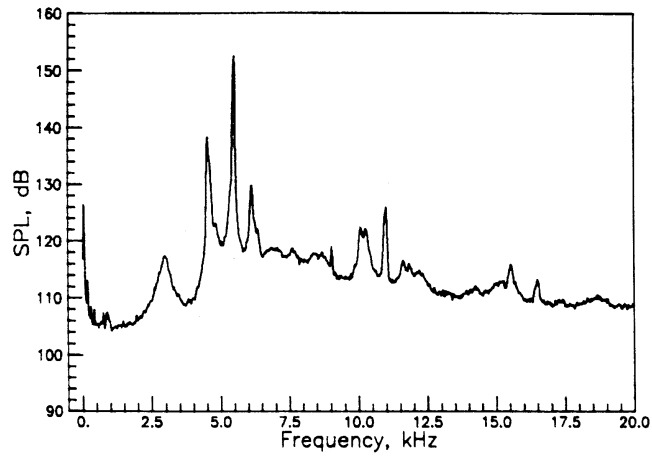


(b) $R/D=0.889$

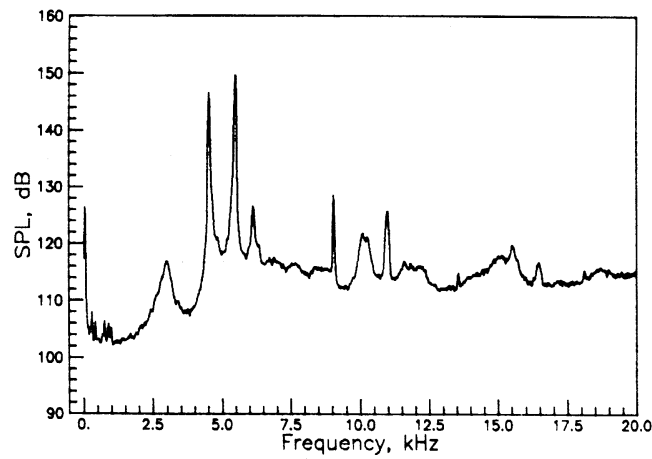


(c) $R/D=2.000$

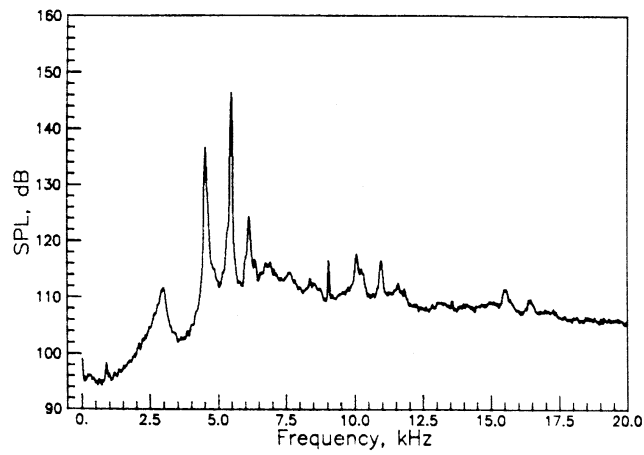
Figure 19. Narrowband spectra for the 0.625 inch lip thickness nozzle at $M_j=1.37$.



(a) $R/D=0.642$

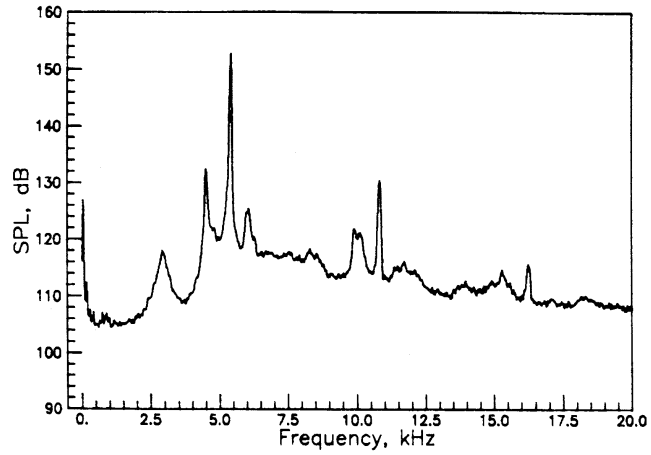


(b) $R/D=0.889$

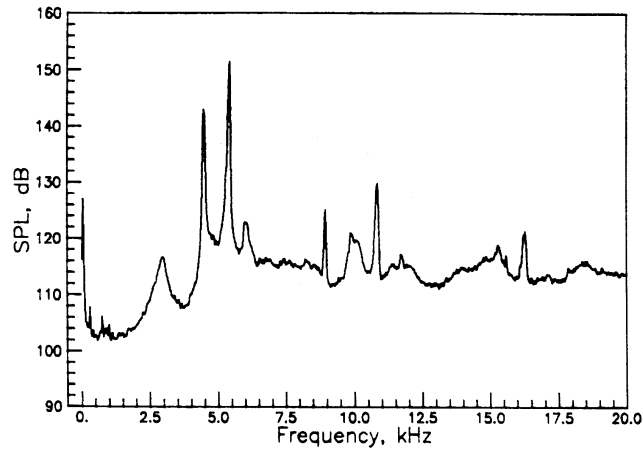


(c) $R/D=2.000$

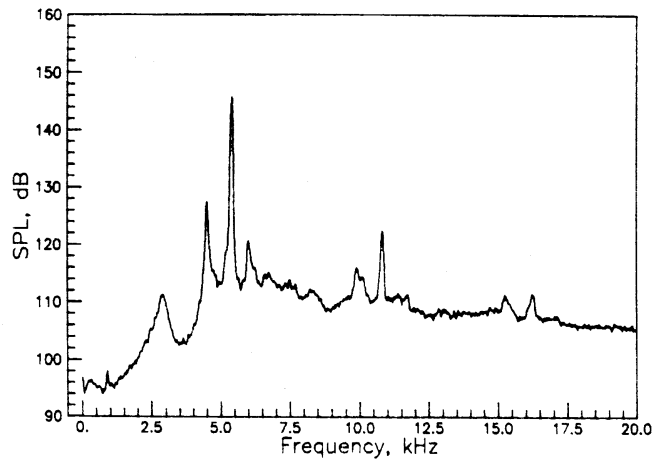
Figure 20. Narrowband spectra for the 0.625 inch lip thickness nozzle at $M_j=1.39$.



(a) $R/D=0.642$

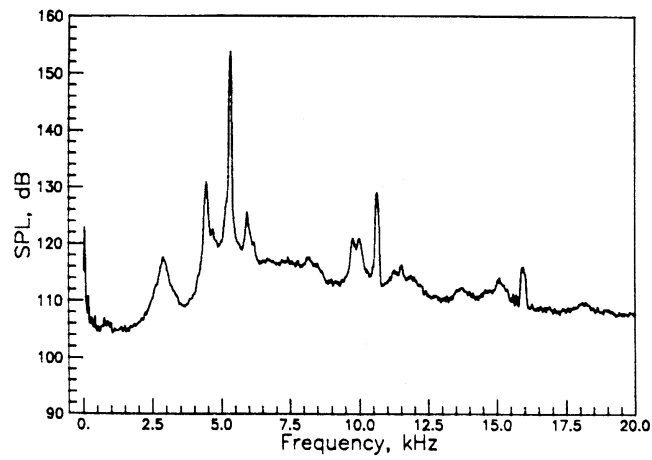


(b) $R/D=0.889$

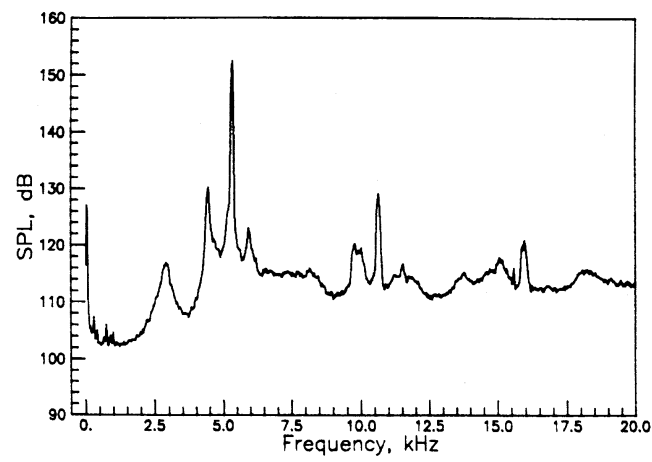


(c) $R/D=2.000$

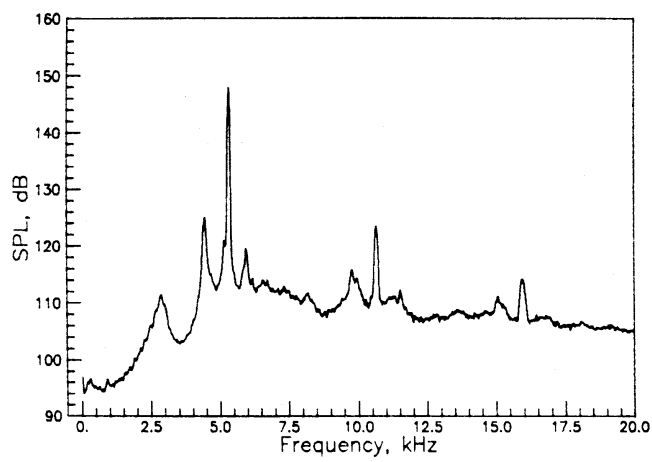
Figure 21. Narrowband spectra for the 0.625 inch lip thickness nozzle at $M_j=1.41$.



(a) $R/D=0.642$

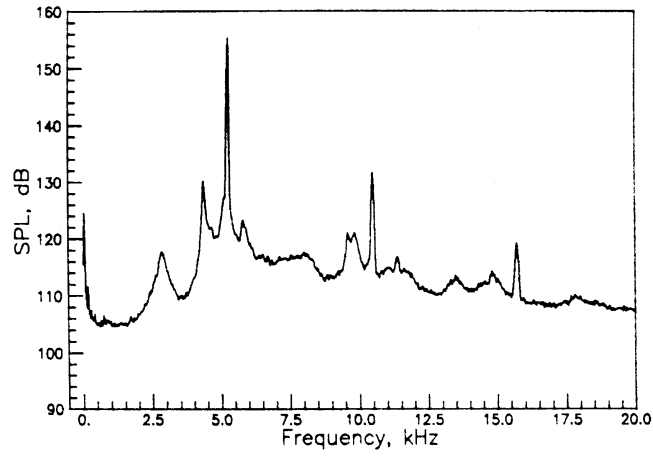


(b) $R/D=0.889$

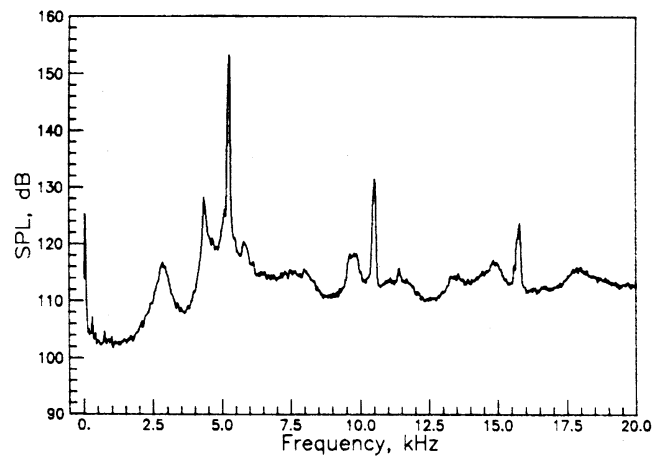


(c) $R/D=2.000$

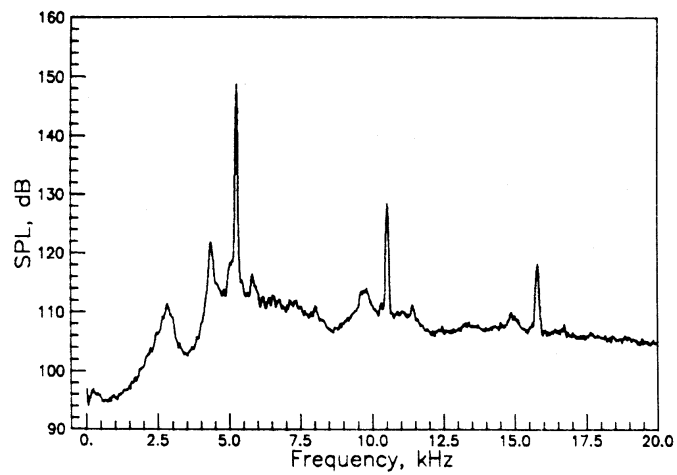
Figure 22. Narrowband spectra for the 0.625 inch lip thickness nozzle at $M_j=1.42$.



(a) $R/D=0.642$

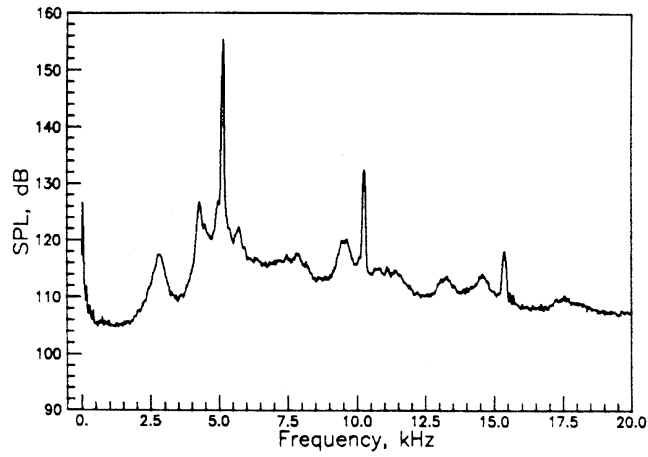


(b) $R/D=0.889$

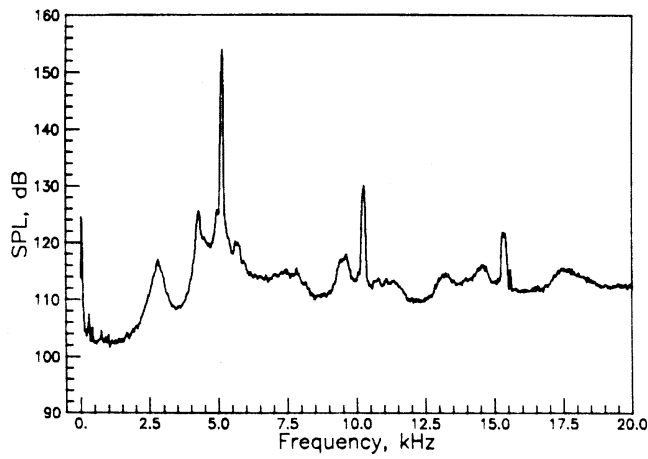


(c) $R/D=2.000$

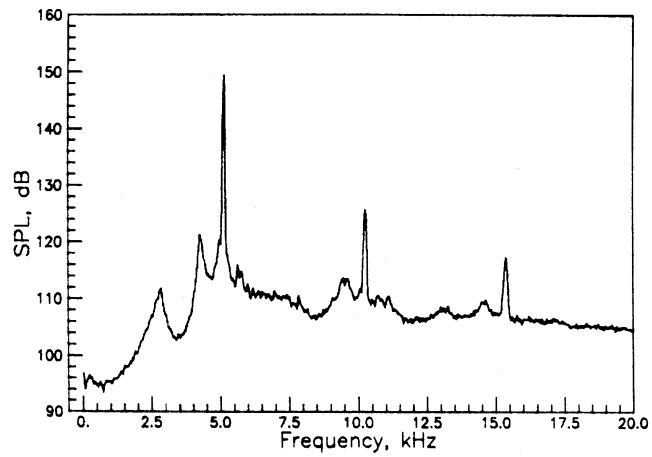
Figure 23. Narrowband spectra for the 0.625 inch lip thickness nozzle at $M_j=1.44$.



(a) $R/D=0.642$

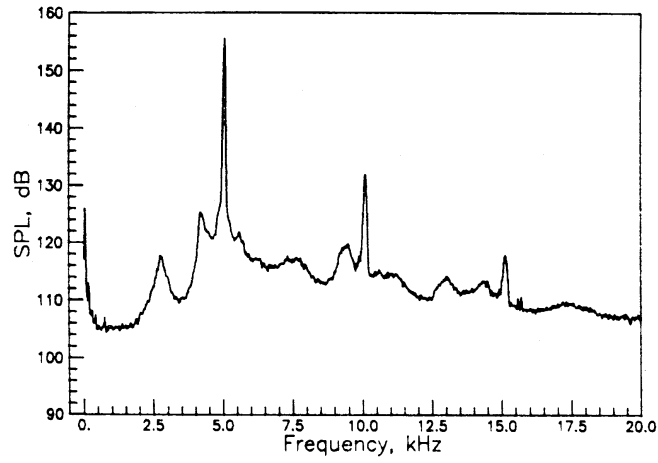


(b) $R/D=0.889$

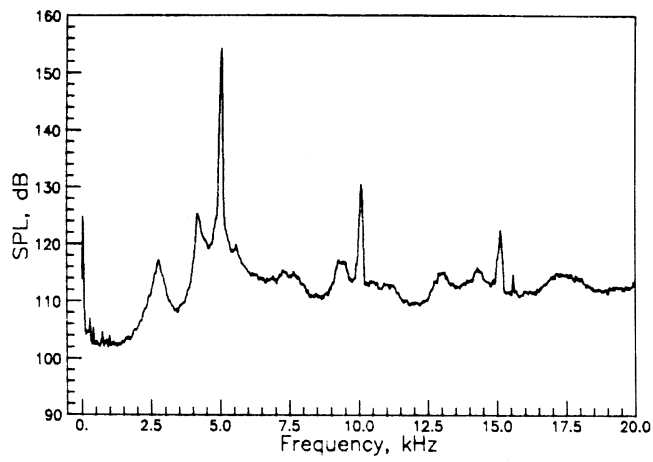


(c) $R/D=2.000$

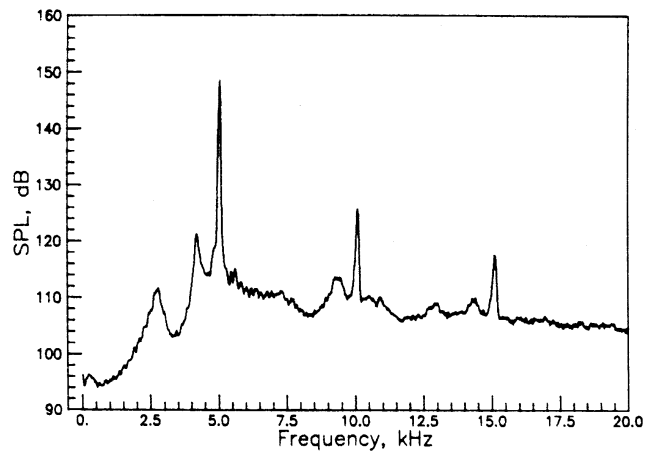
Figure 24. Narrowband spectra for the 0.625 inch lip thickness nozzle at $M_j=1.46$.



(a) $R/D=0.642$

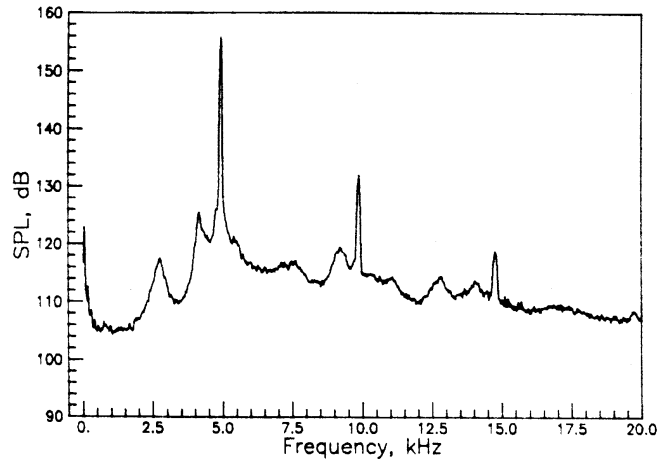


(b) $R/D=0.889$

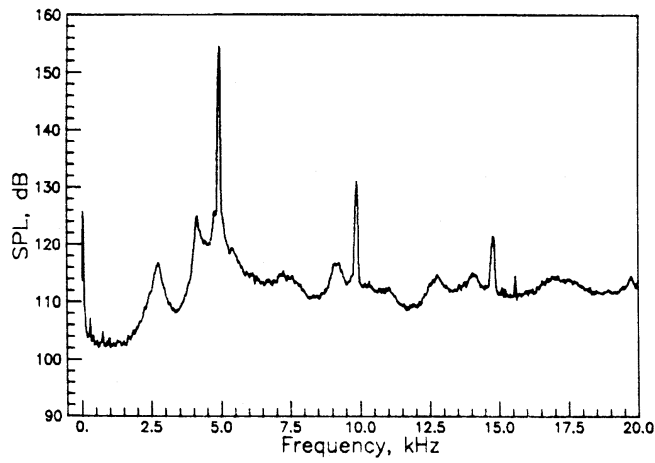


(c) $R/D=2.000$

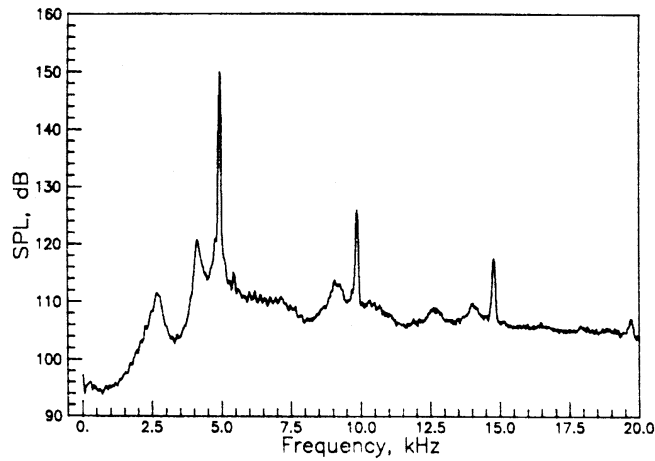
Figure 25. Narrowband spectra for the 0.625 inch lip thickness nozzle at $M_j=1.48$.



(a) $R/D=0.642$

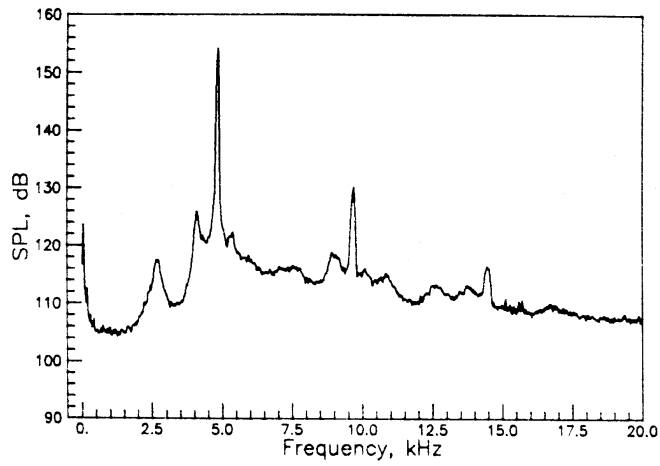


(b) $R/D=0.889$

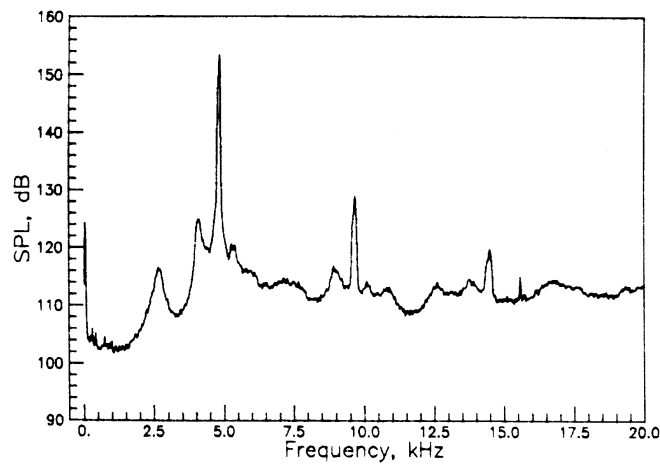


(c) $R/D=2.000$

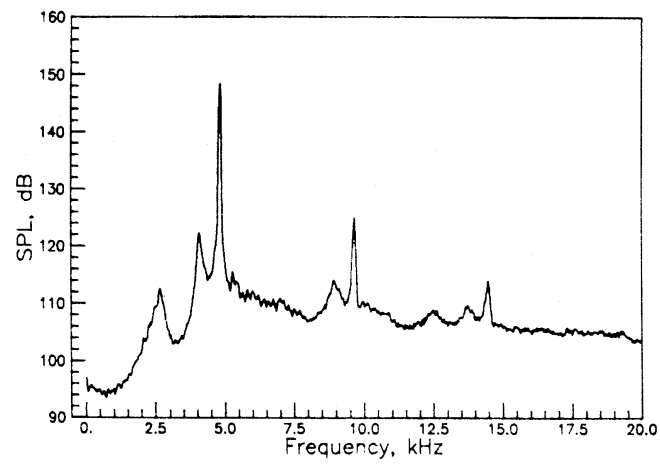
Figure 26. Narrowband spectra for the 0.625 inch lip thickness nozzle at $M_j=1.50$.



(a) $R/D=0.642$

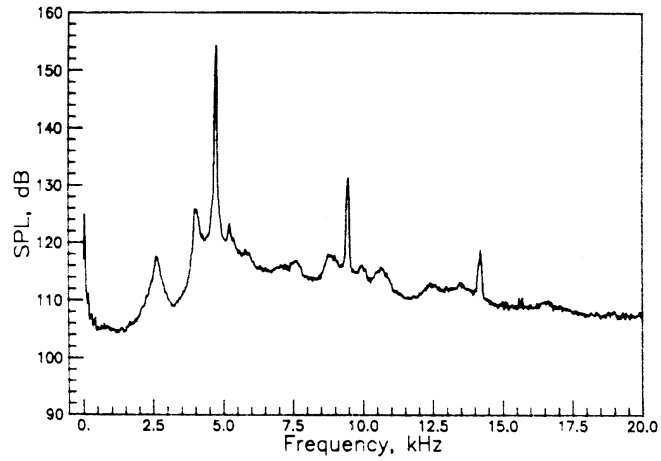


(b) $R/D=0.889$

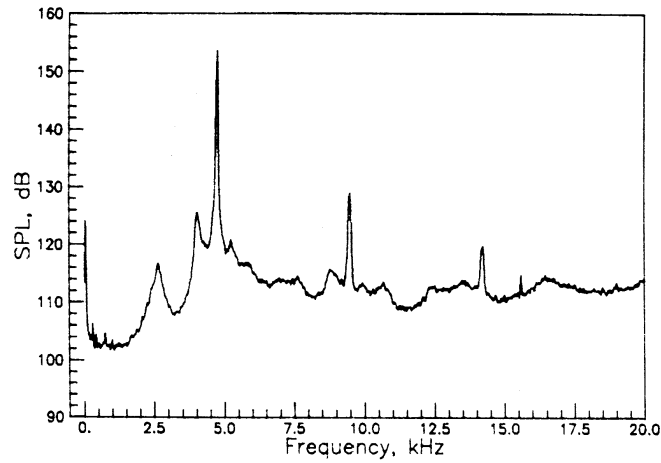


(c) $R/D=2.000$

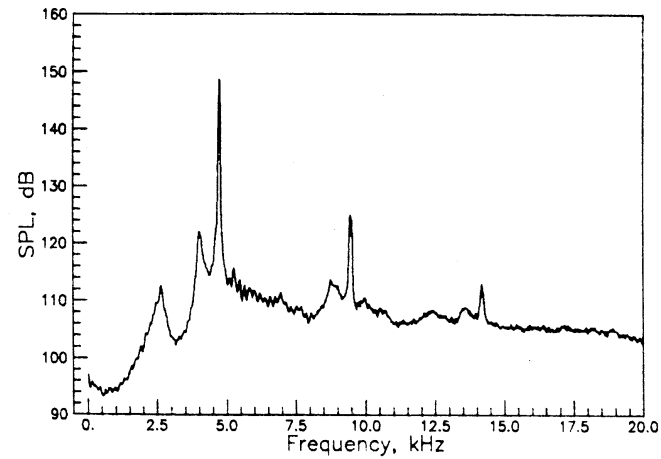
Figure 27. Narrowband spectra for the 0.625 inch lip thickness nozzle at $M_j=1.52$.



(a) $R/D=0.642$

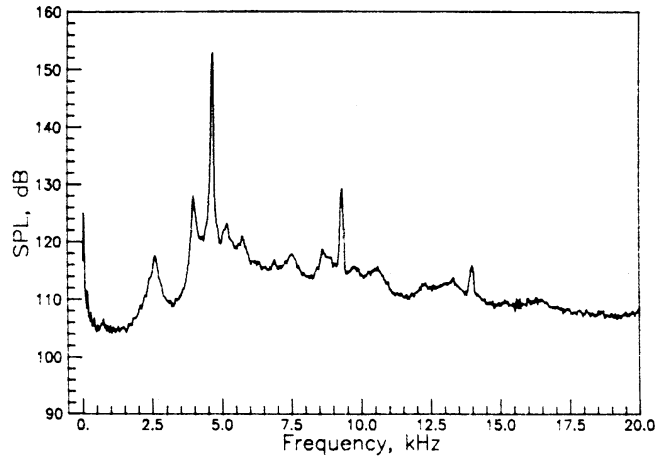


(b) $R/D=0.889$

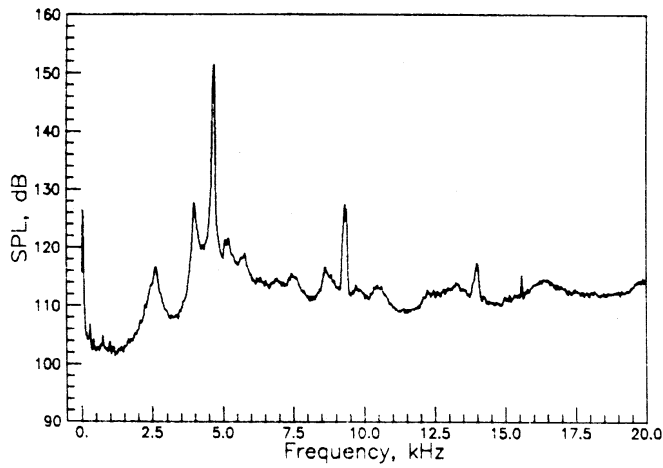


(c) $R/D=2.000$

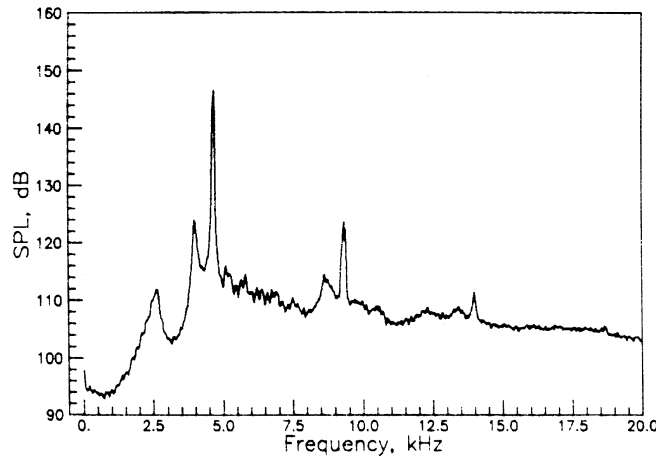
Figure 28. Narrowband spectra for the 0.625 inch lip thickness nozzle at $M_j=1.54$.



(a) $R/D=0.642$

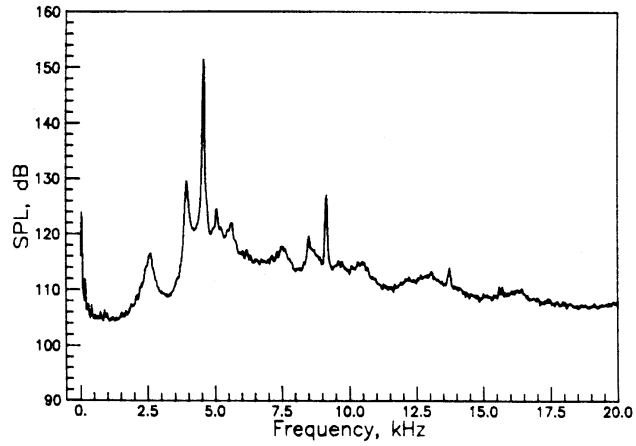


(b) $R/D=0.889$

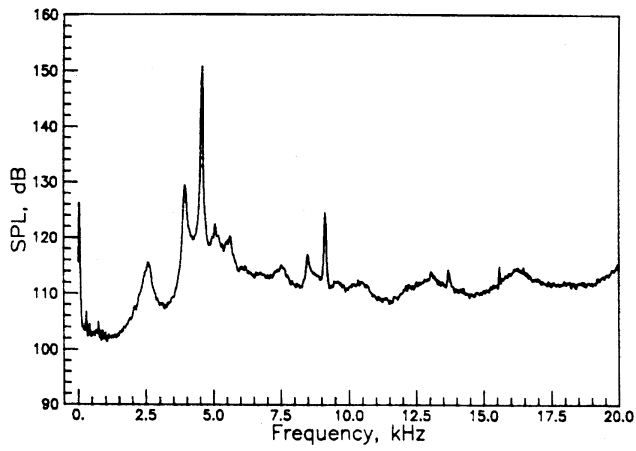


(c) $R/D=2.000$

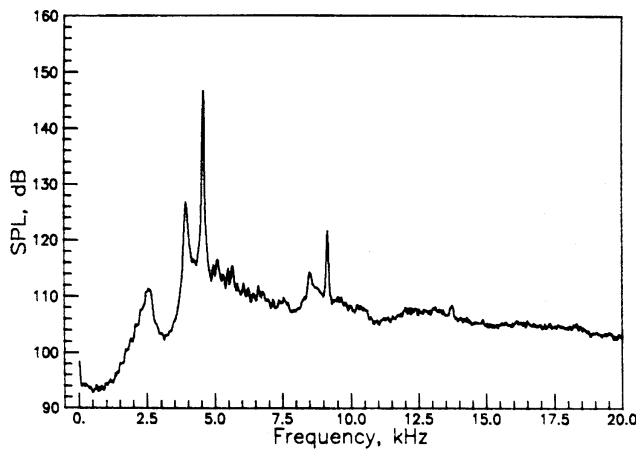
Figure 29. Narrowband spectra for the 0.625 inch lip thickness nozzle at $M_j=1.56$.



(a) $R/D=0.642$

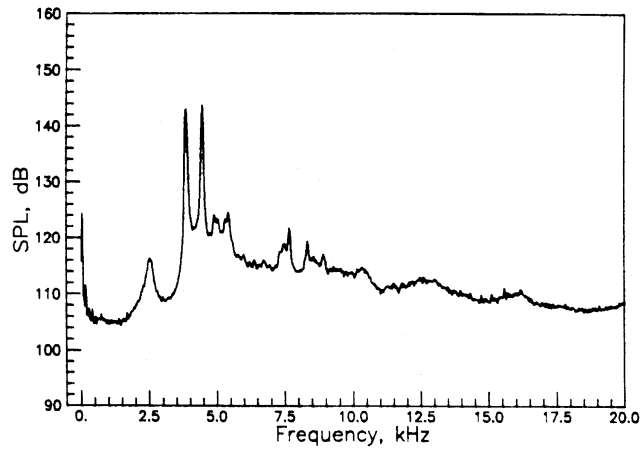


(b) $R/D=0.889$

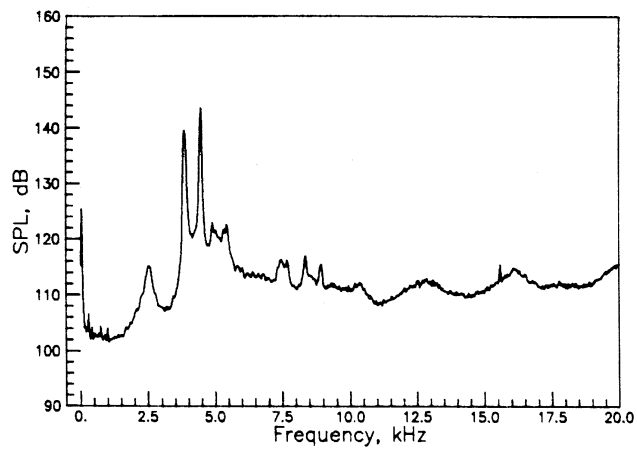


(c) $R/D=2.000$

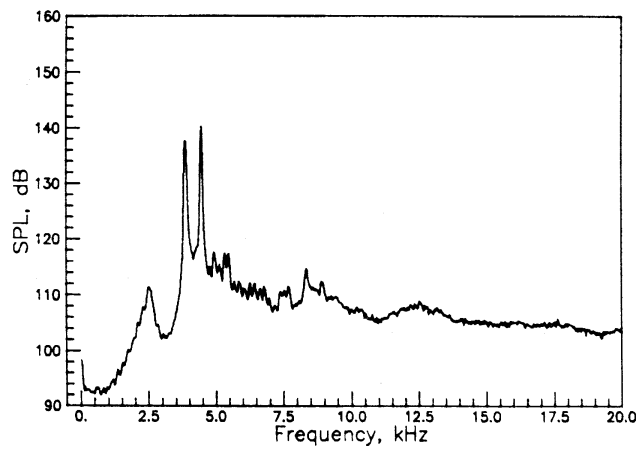
Figure 30. Narrowband spectra for the 0.625 inch lip thickness nozzle at $M_j=1.58$.



(a) $R/D=0.642$

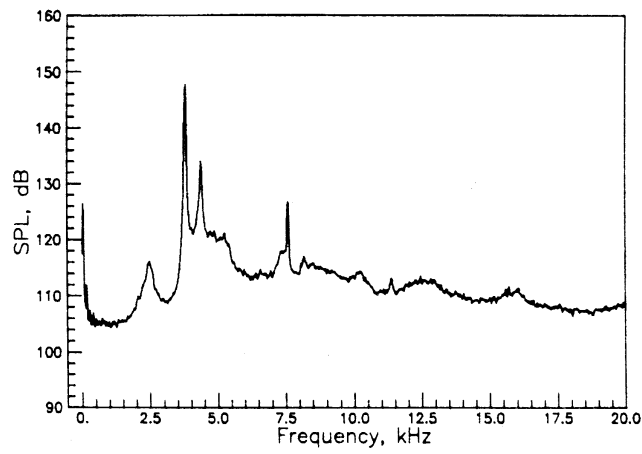


(b) $R/D=0.889$

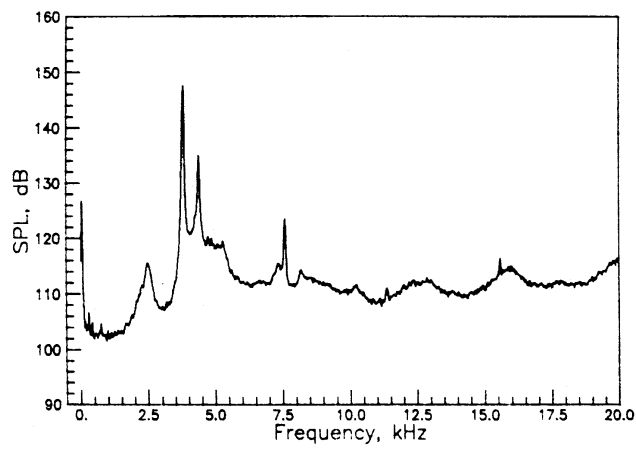


(c) $R/D=2.000$

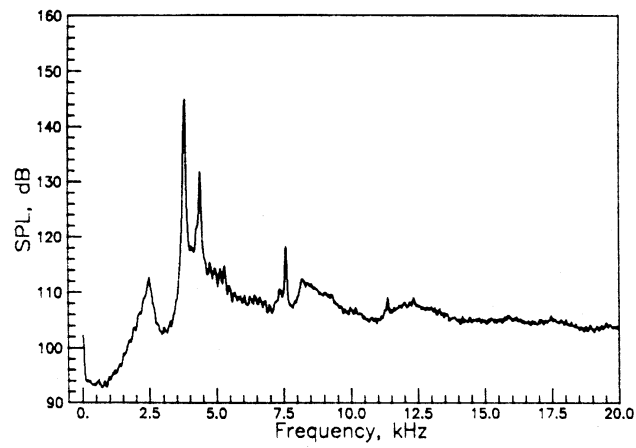
Figure 31. Narrowband spectra for the 0.625 inch lip thickness nozzle at $M_j=1.60$.



(a) $R/D=0.642$

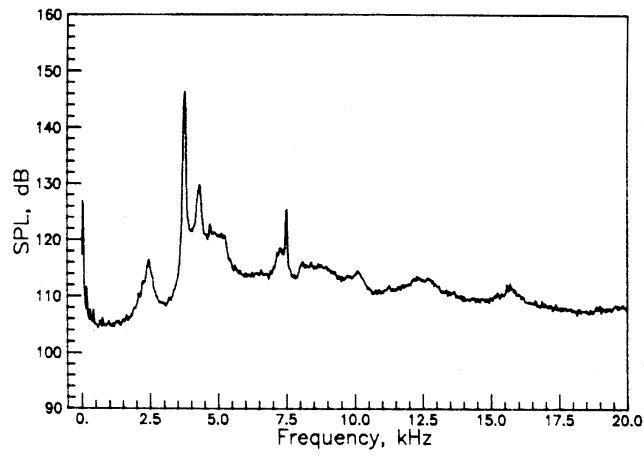


(b) $R/D=0.889$

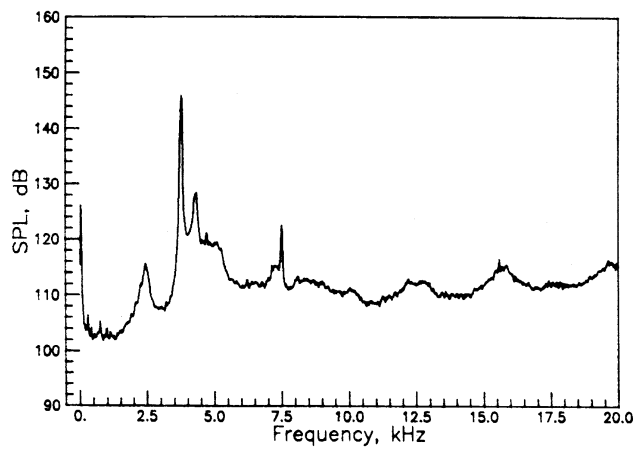


(c) $R/D=2.000$

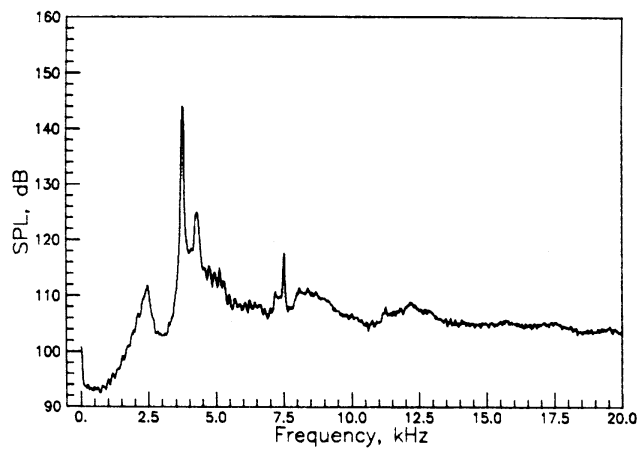
Figure 32. Narrowband spectra for the 0.625 inch lip thickness nozzle at $M_j=1.62$.



(a) $R/D=0.642$

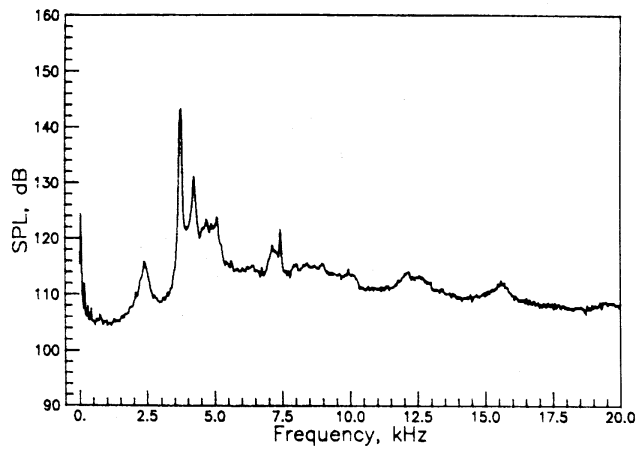


(b) $R/D=0.889$

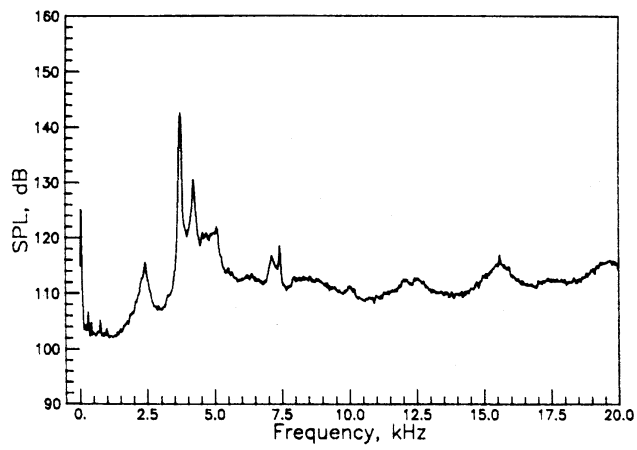


(c) $R/D=2.000$

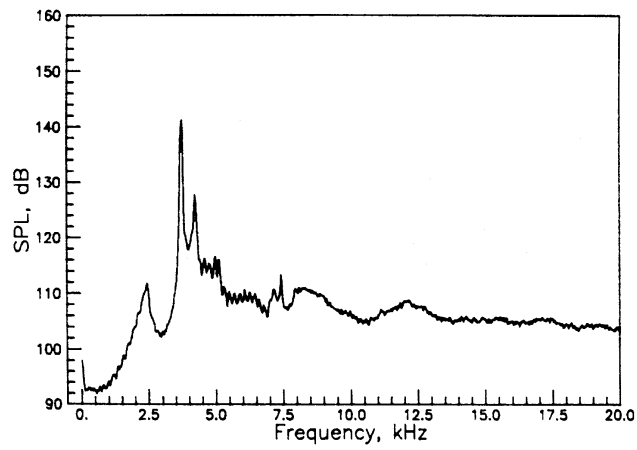
Figure 33. Narrowband spectra for the 0.625 inch lip thickness nozzle at $M_j=1.64$.



(a) $R/D=0.642$

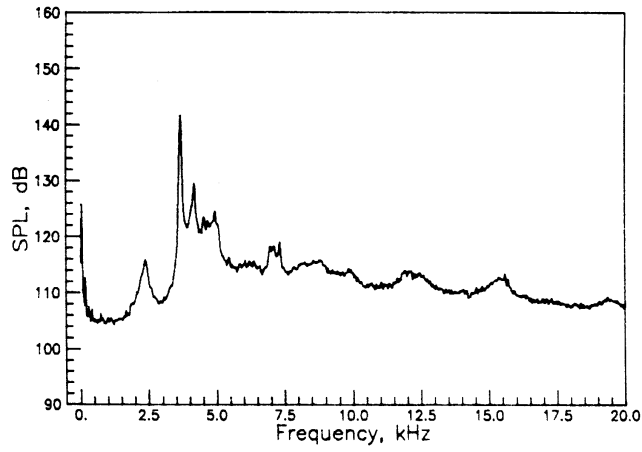


(b) $R/D=0.889$

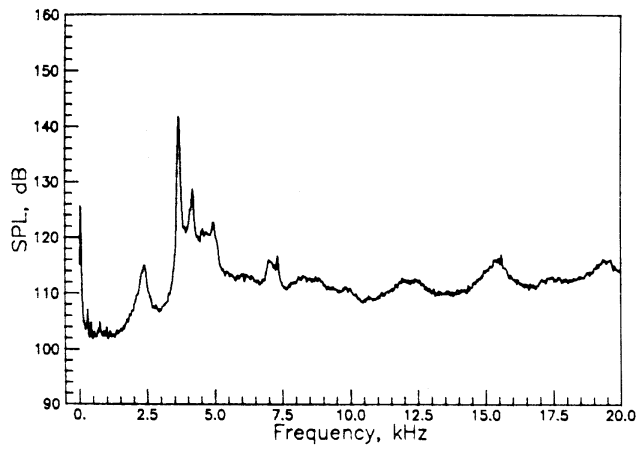


(c) $R/D=2.000$

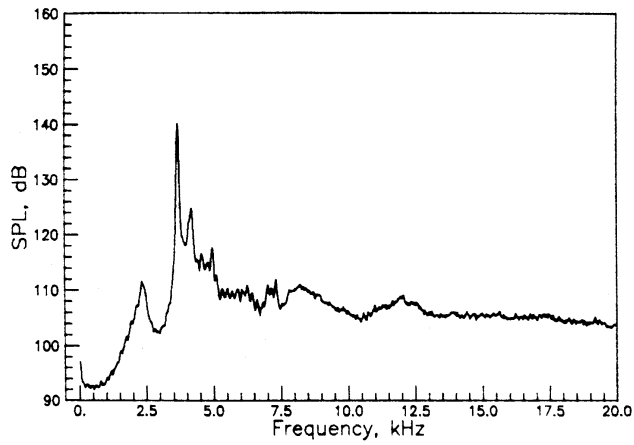
Figure 34. Narrowband spectra for the 0.625 inch lip thickness nozzle at $M_j=1.66$.



(a) $R/D=0.642$

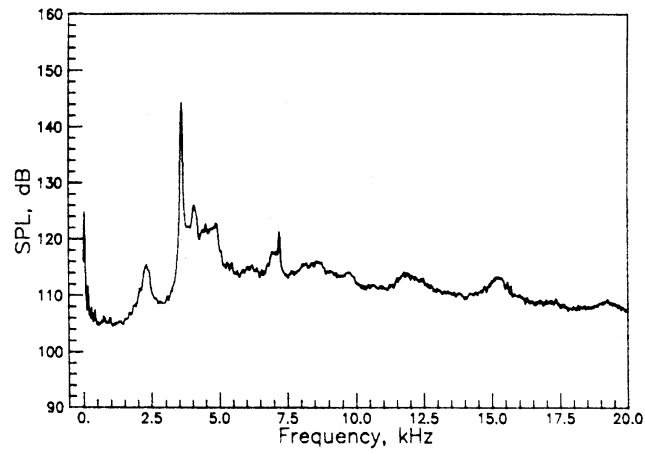


(b) $R/D=0.889$

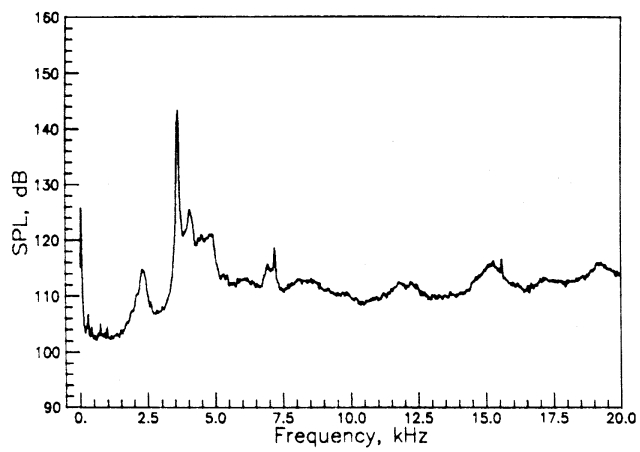


(c) $R/D=2.000$

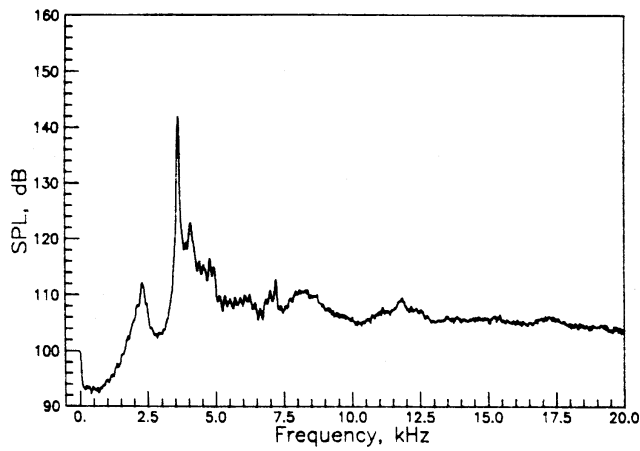
Figure 35. Narrowband spectra for the 0.625 inch lip thickness nozzle at $M_j=1.68$.



(a) $R/D=0.642$

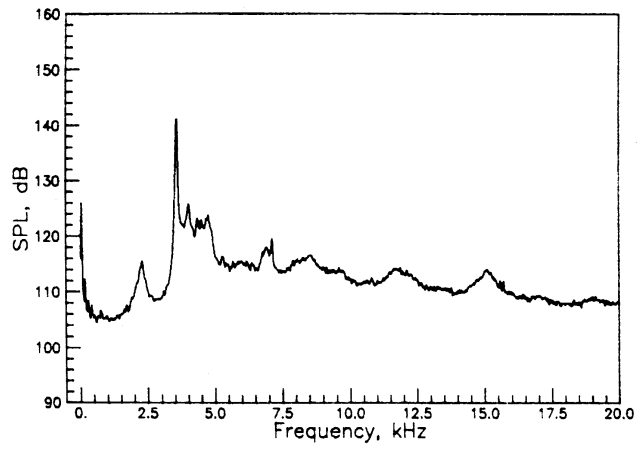


(b) $R/D=0.889$

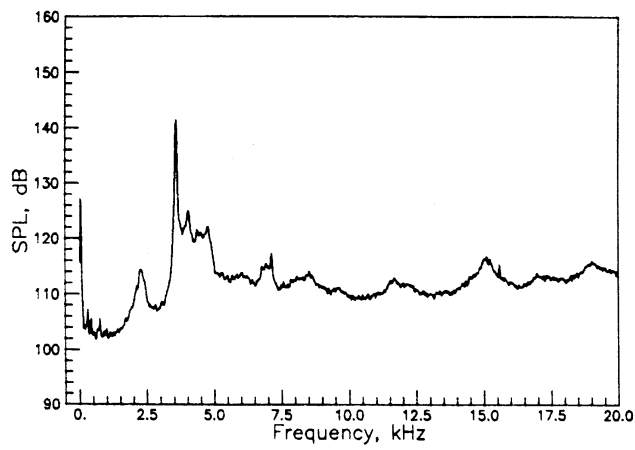


(c) $R/D=2.000$

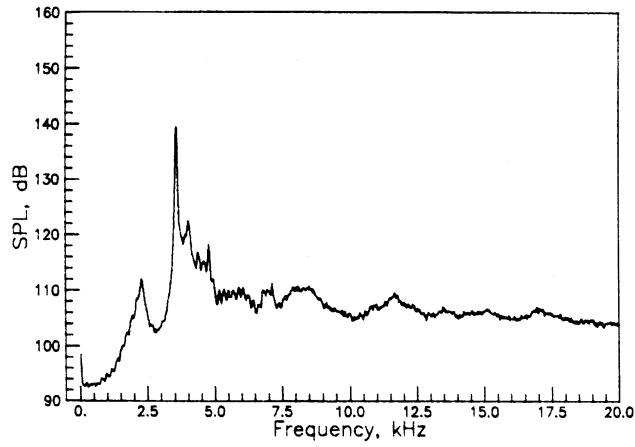
Figure 36. Narrowband spectra for the 0.625 inch lip thickness nozzle at $M_j=1.70$.



(a) $R/D=0.642$

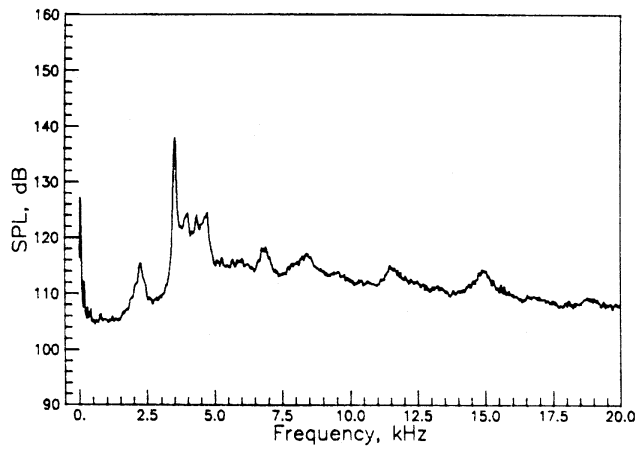


(b) $R/D=0.889$

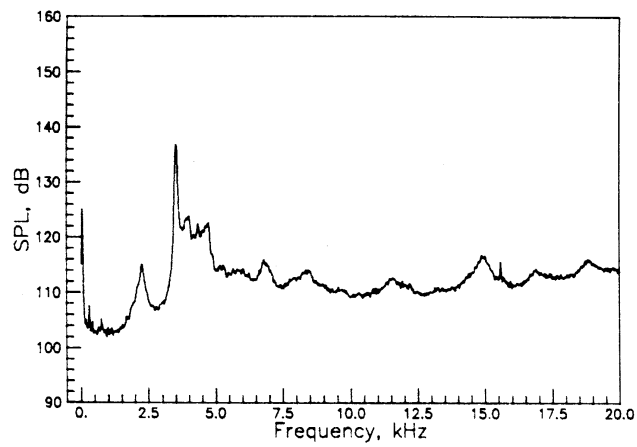


(c) $R/D=2.000$

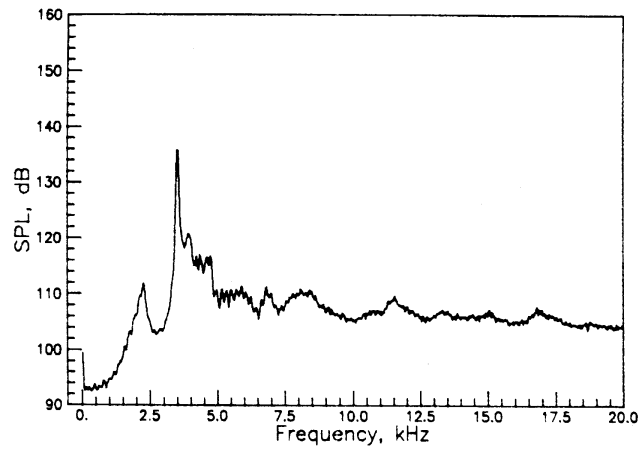
Figure 37. Narrowband spectra for the 0.625 inch lip thickness nozzle at $M_j=1.72$.



(a) $R/D=0.642$

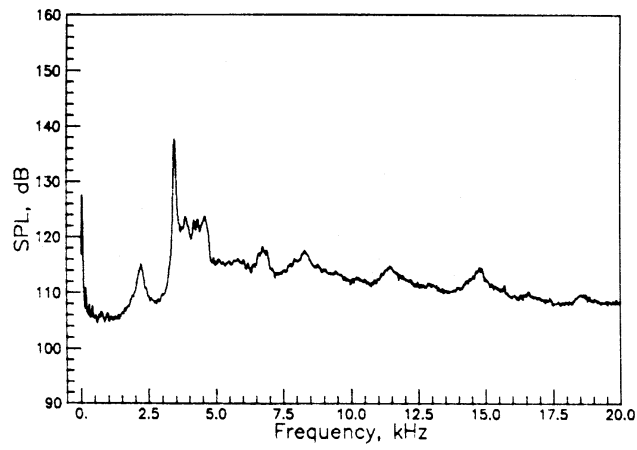


(b) $R/D=0.889$

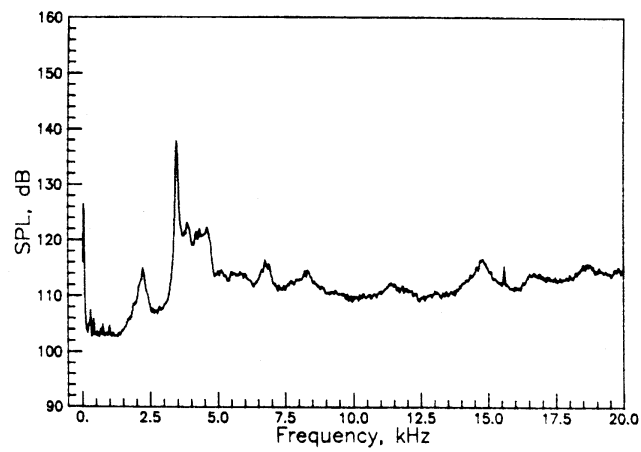


(c) $R/D=2.000$

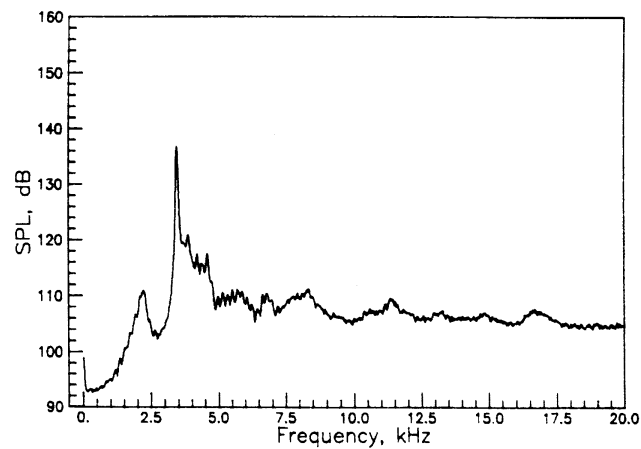
Figure 38. Narrowband spectra for the 0.625 inch lip thickness nozzle at $M_j=1.74$.



(a) $R/D=0.642$

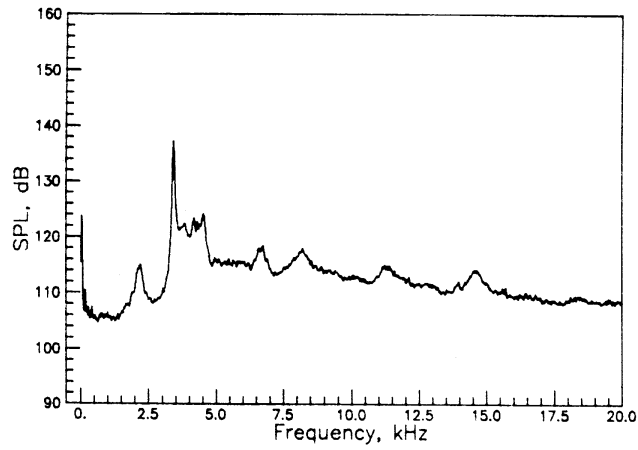


(b) $R/D=0.889$

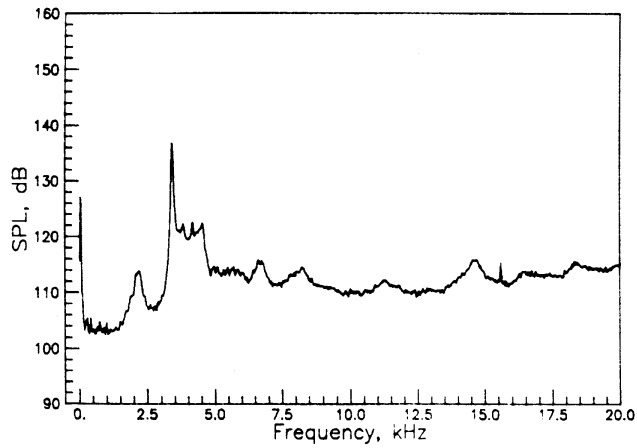


(c) $R/D=2.000$

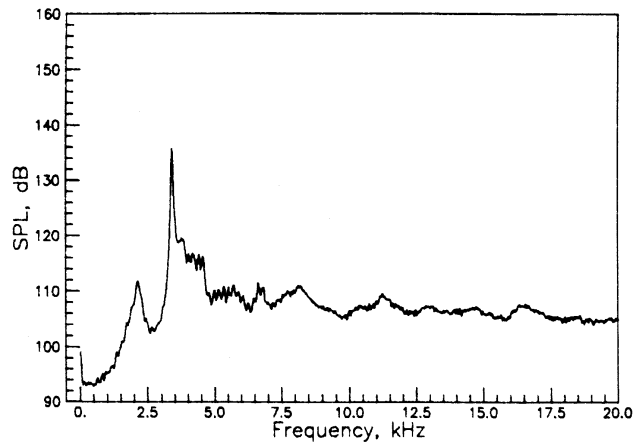
Figure 39. Narrowband spectra for the 0.625 inch lip thickness nozzle at $M_j=1.76$.



(a) $R/D=0.642$

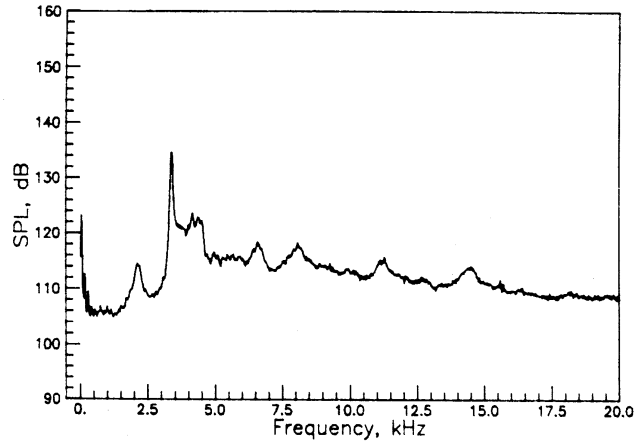


(b) $R/D=0.889$

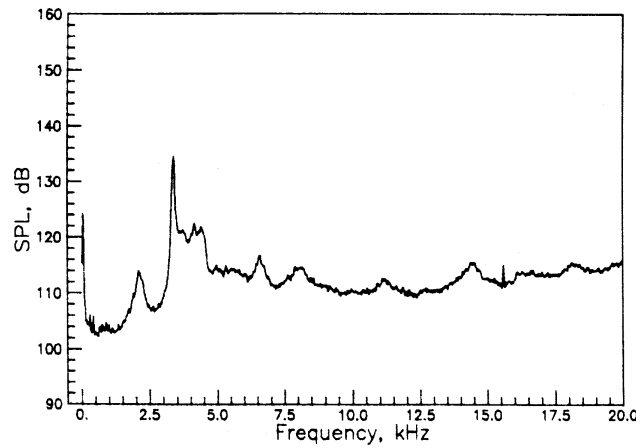


(c) $R/D=2.000$

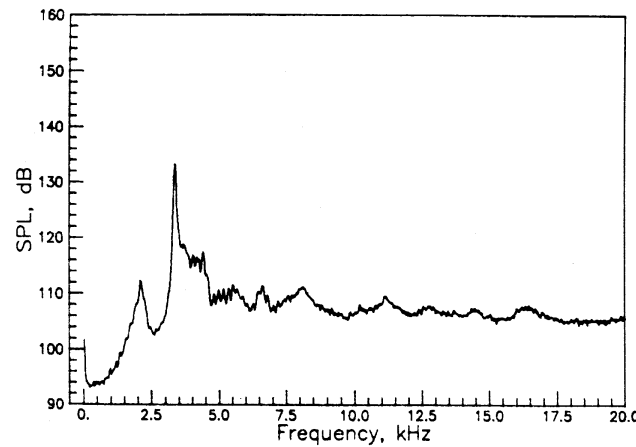
Figure 40. Narrowband spectra for the 0.625 inch lip thickness nozzle at $M_j=1.78$.



(a) $R/D=0.642$

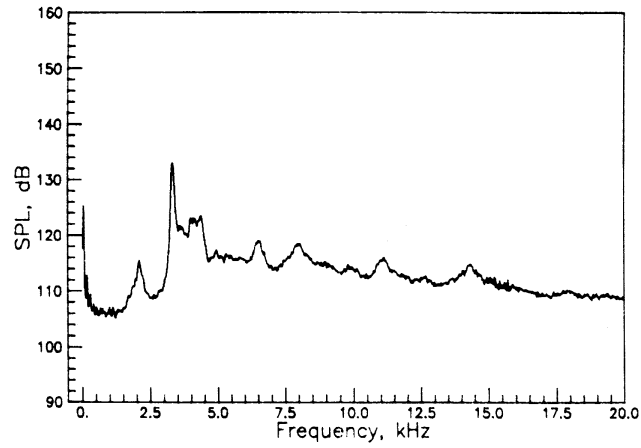


(b) $R/D=0.889$

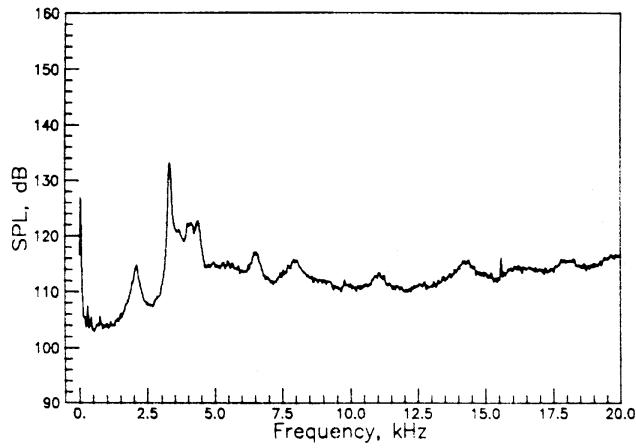


(c) $R/D=2.000$

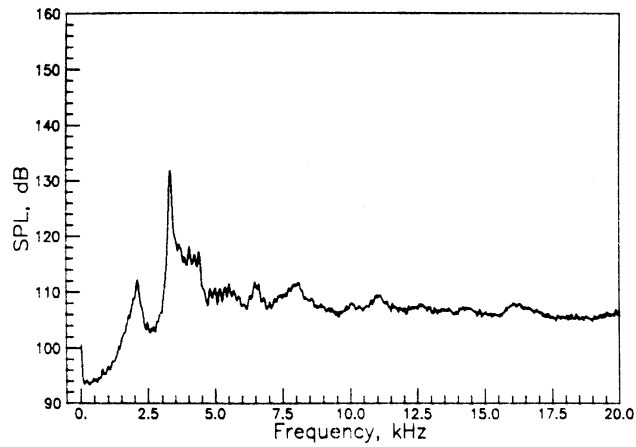
Figure 41. Narrowband spectra for the 0.625 inch lip thickness nozzle at $M_j=1.80$.



(a) $R/D=0.642$

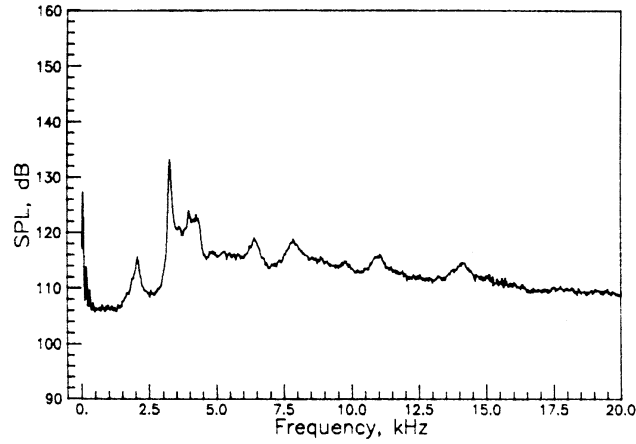


(b) $R/D=0.889$

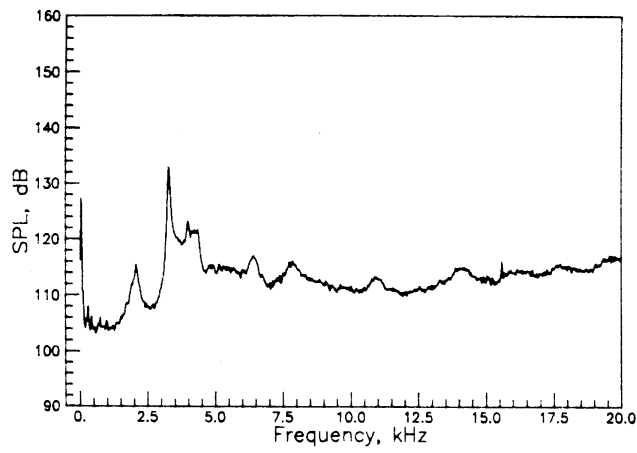


(c) $R/D=2.000$

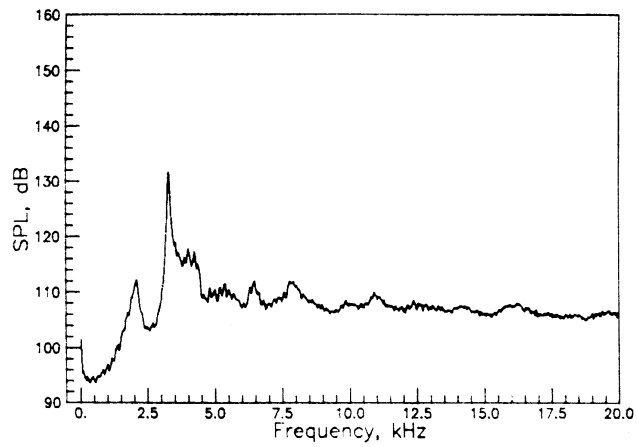
Figure 42. Narrowband spectra for the 0.625 inch lip thickness nozzle at $M_j=1.82$.



(a) $R/D=0.642$

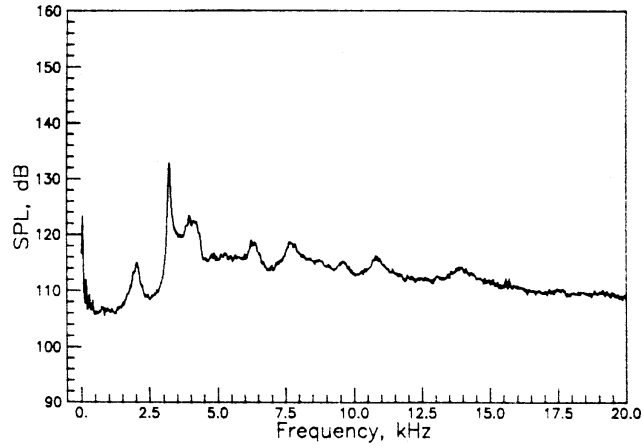


(b) $R/D=0.889$

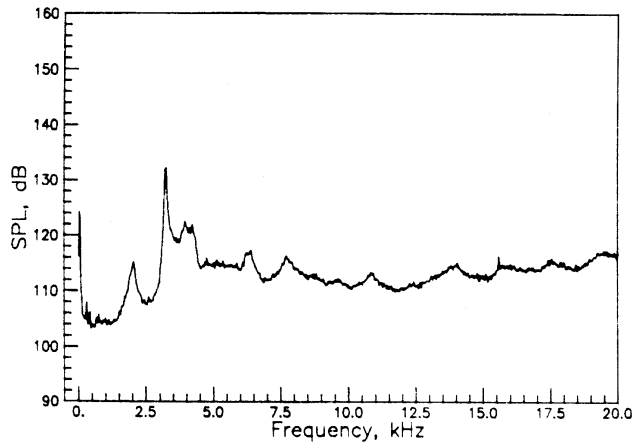


(c) $R/D=2.000$

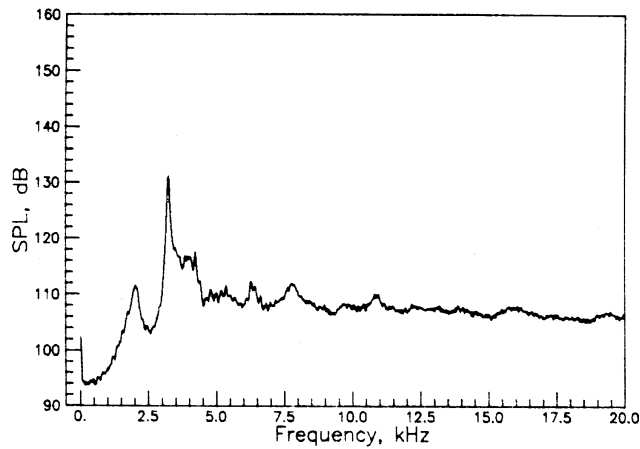
Figure 43. Narrowband spectra for the 0.625 inch lip thickness nozzle at $M_j=1.84$.



(a) $R/D=0.642$

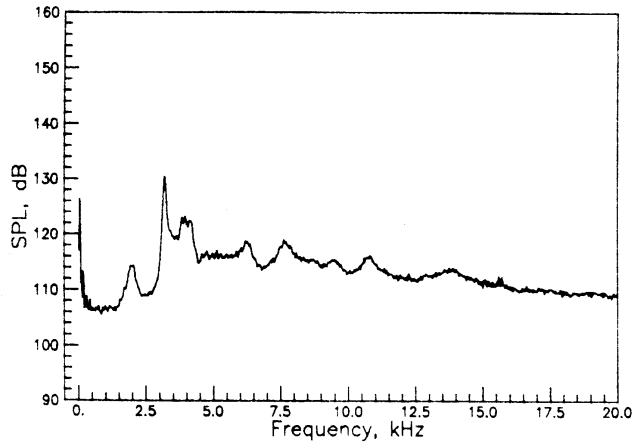


(b) $R/D=0.889$

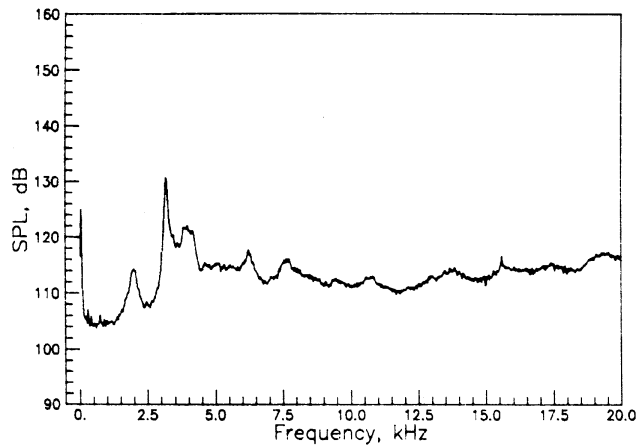


(c) $R/D=2.000$

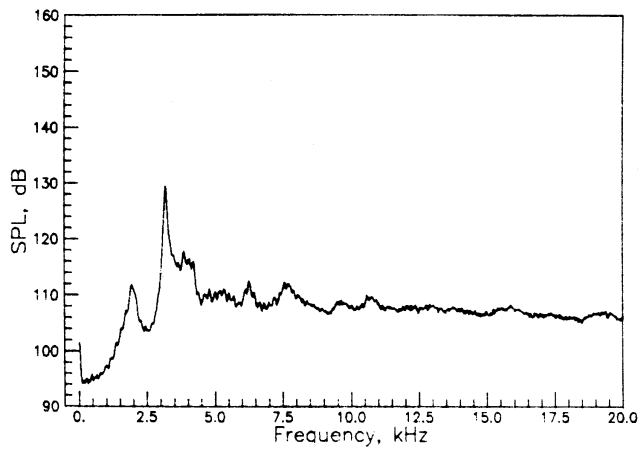
Figure 44. Narrowband spectra for the 0.625 inch lip thickness nozzle at $M_j=1.86$.



(a) $R/D=0.642$

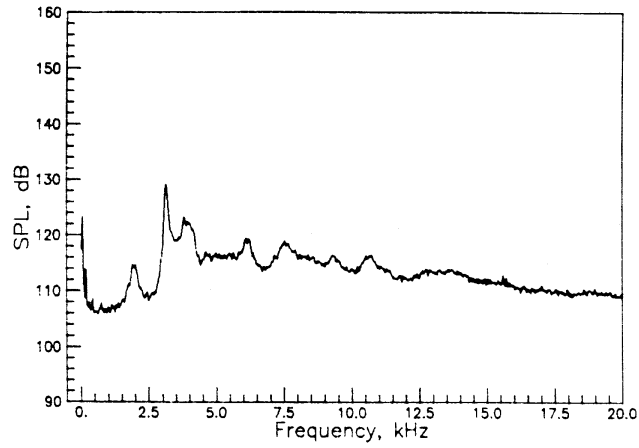


(b) $R/D=0.889$

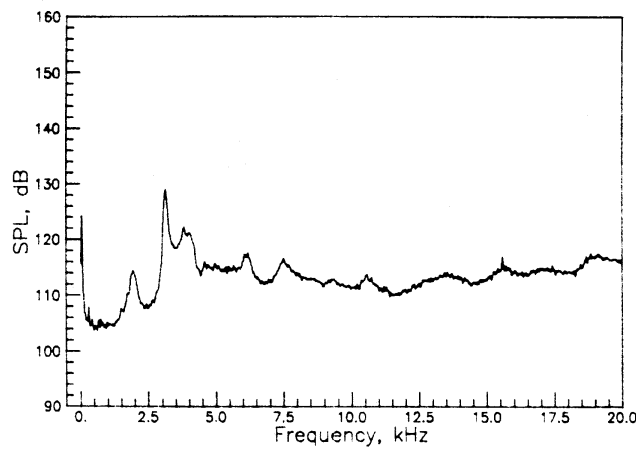


(c) $R/D=2.000$

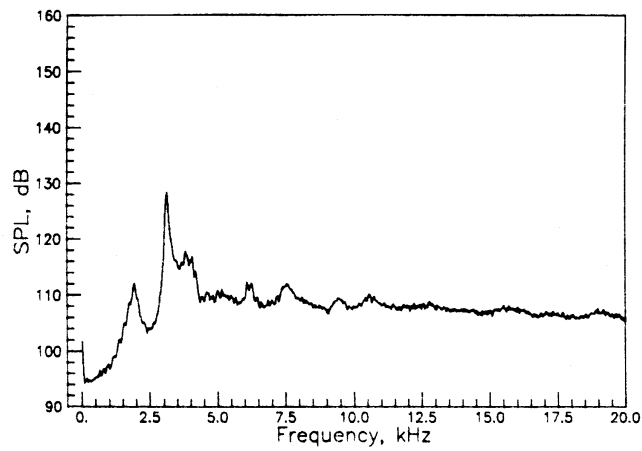
Figure 45. Narrowband spectra for the 0.625 inch lip thickness nozzle at $M_j=1.88$.



(a) $R/D=0.642$

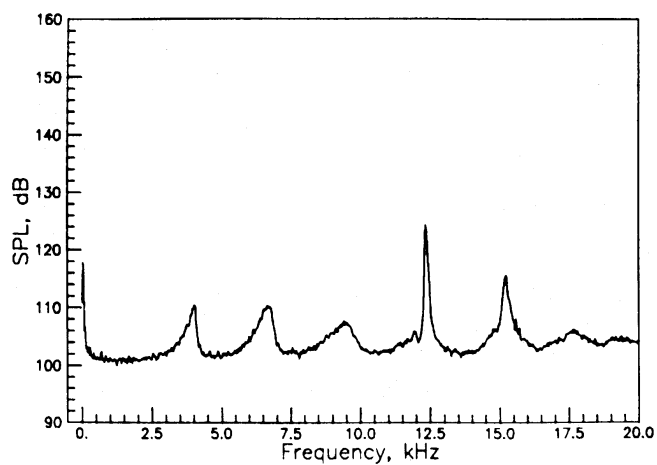


(b) $R/D=0.889$

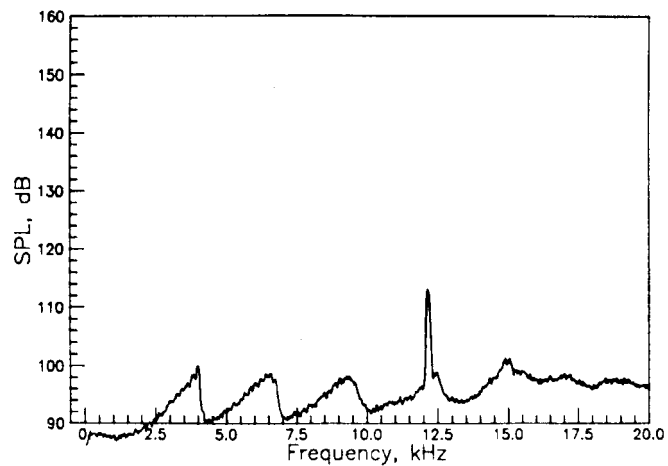


(c) $R/D=2.000$

Figure 46. Narrowband spectra for the 0.625 inch lip thickness nozzle at $M_j=1.90$.

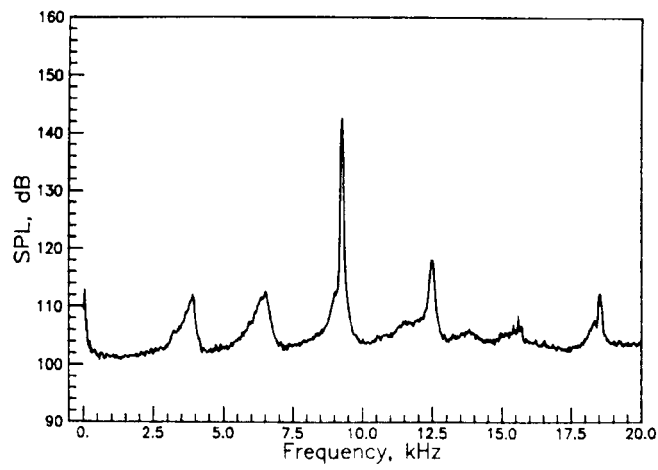


(a) $R/D=0.642$

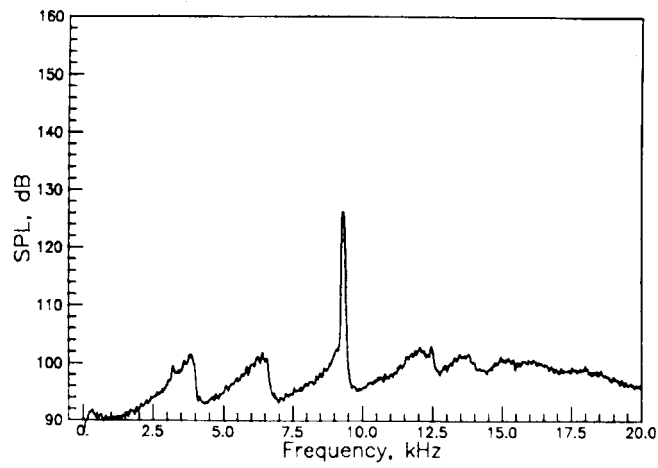


(b) $R/D=2.000$

Figure 47. Narrowband spectra for the 0.200 inch lip thickness nozzle at $M_j=1.04$.

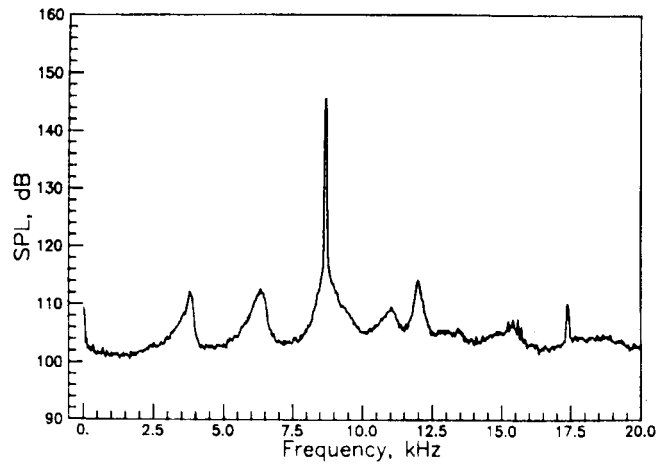


(a) $R/D=0.642$

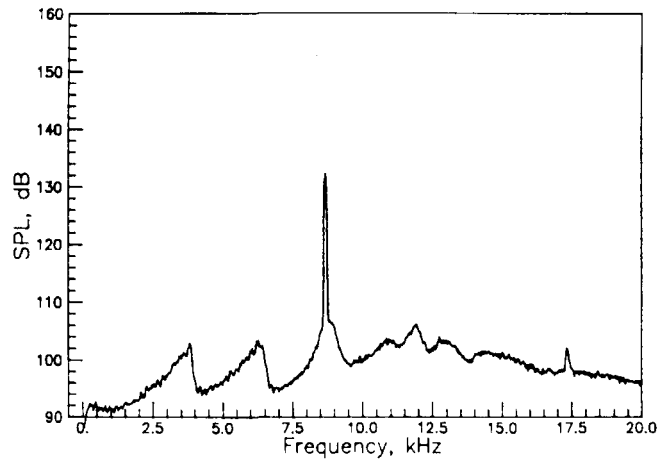


(b) $R/D=2.000$

Figure 48. Narrowband spectra for the 0.200 inch lip thickness nozzle at $M_j=1.07$.

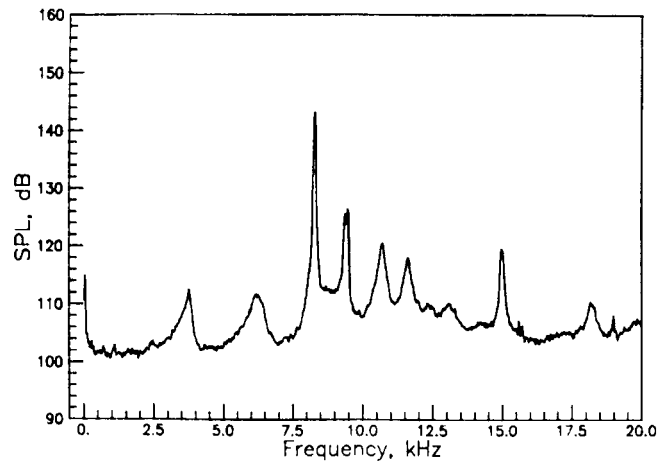


(a) $R/D=0.642$

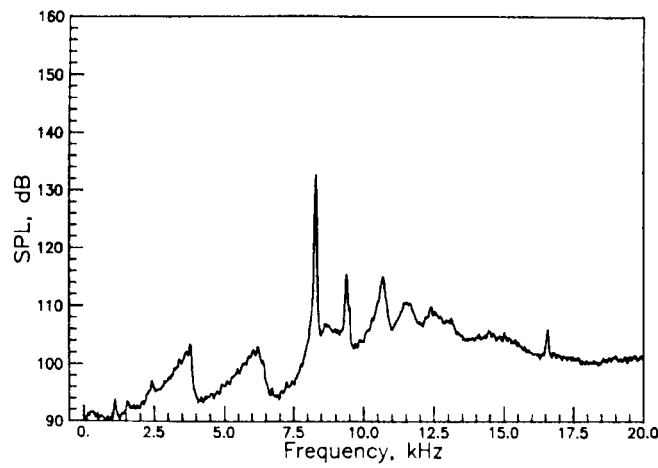


(b) $R/D=2.000$

Figure 49. Narrowband spectra for the 0.200 inch lip thickness nozzle at $M_j=1.09$.

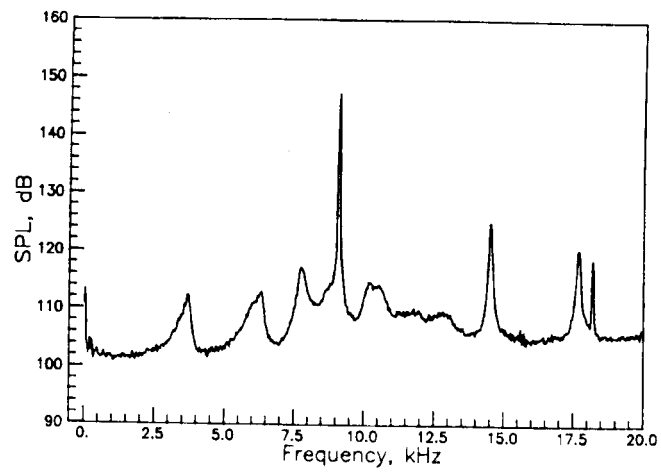


(a) $R/D=0.642$

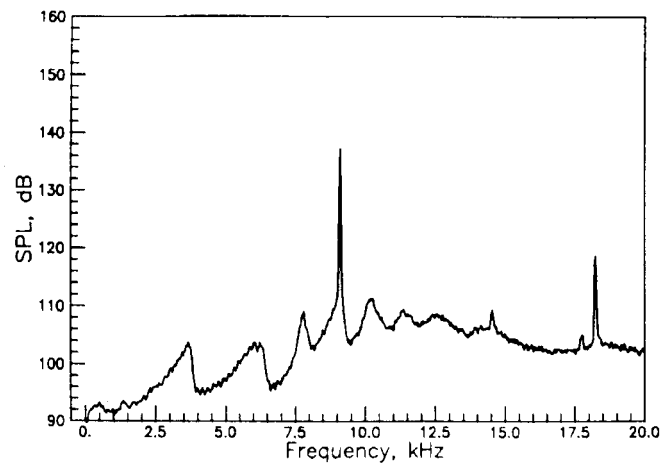


(b) $R/D=2.000$

Figure 50. Narrowband spectra for the 0.200 inch lip thickness nozzle at $M_j=1.11$.

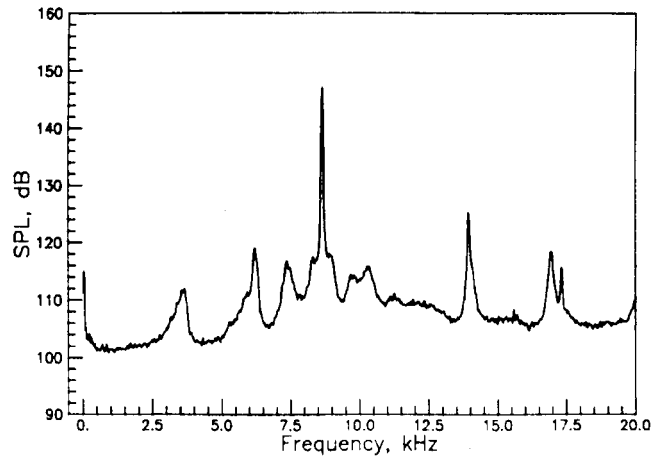


(a) $R/D=0.642$

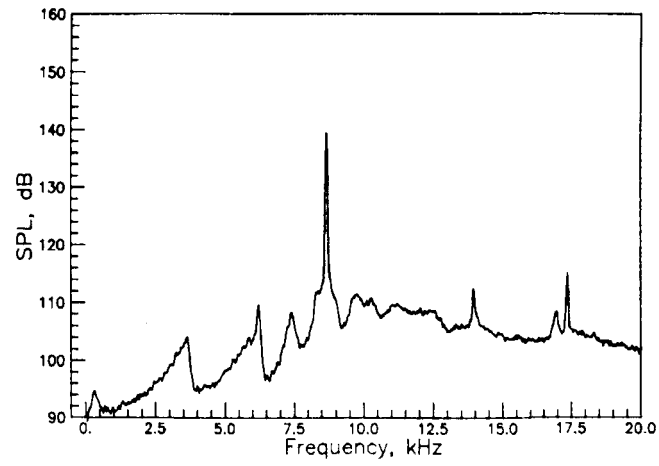


(b) $R/D=2.000$

Figure 51. Narrowband spectra for the 0.200 inch lip thickness nozzle at $M_j=1.13$.

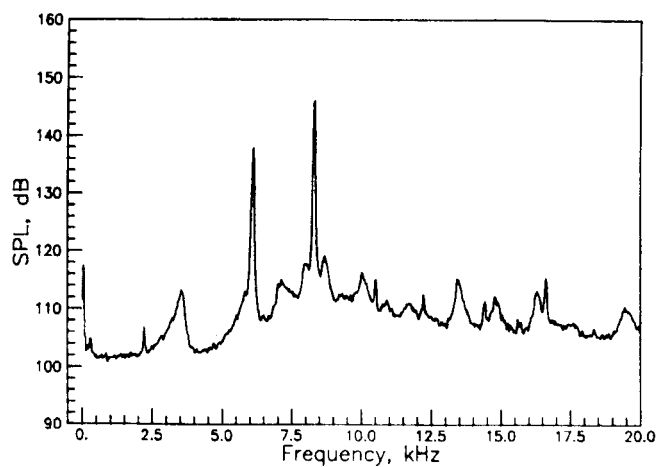


(a) $R/D=0.642$

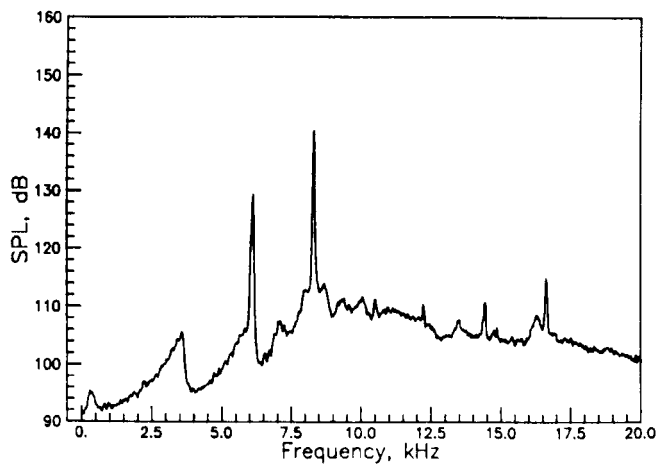


(b) $R/D=2.000$

Figure 52. Narrowband spectra for the 0.200 inch lip thickness nozzle at $M_j=1.15$.

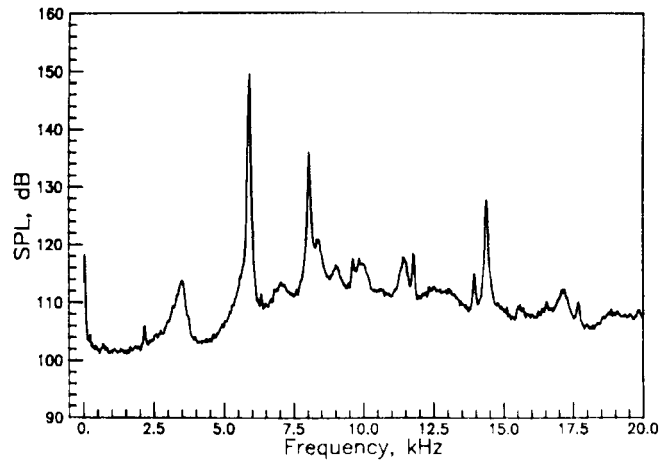


(a) $R/D=0.642$

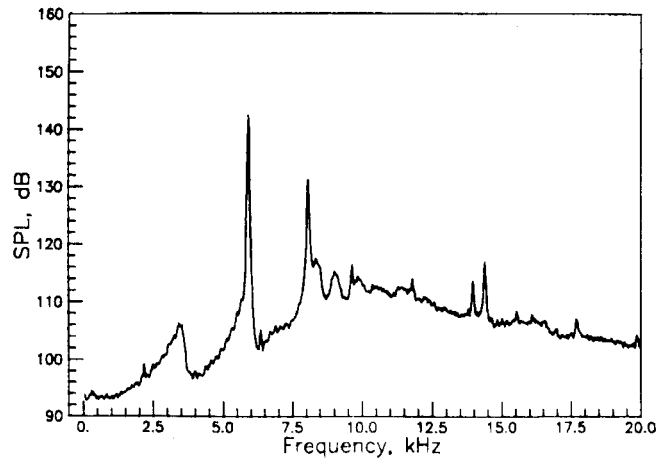


(b) $R/D=2.000$

Figure 53. Narrowband spectra for the 0.200 inch lip thickness nozzle at $M_j=1.17$.

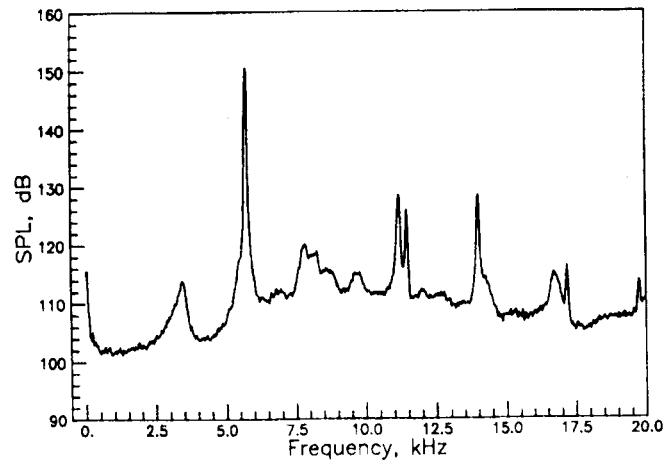


(a) $R/D=0.642$

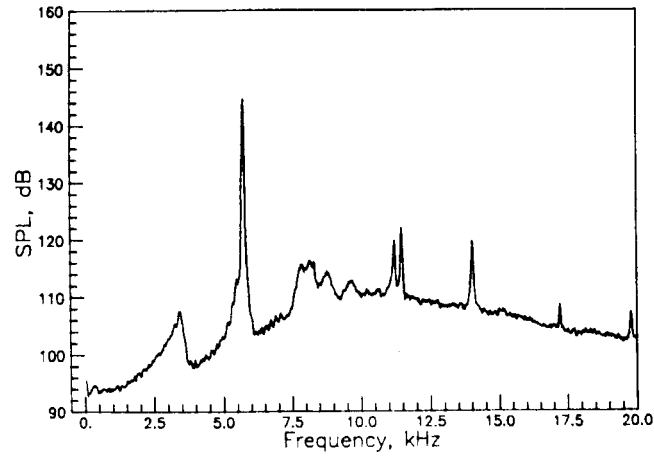


(b) $R/D=2.000$

Figure 54. Narrowband spectra for the 0.200 inch lip thickness nozzle at $M_j=1.19$.

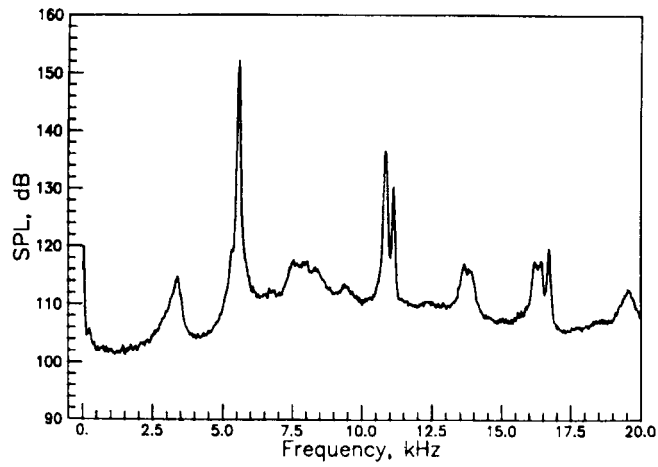


(a) $R/D=0.642$

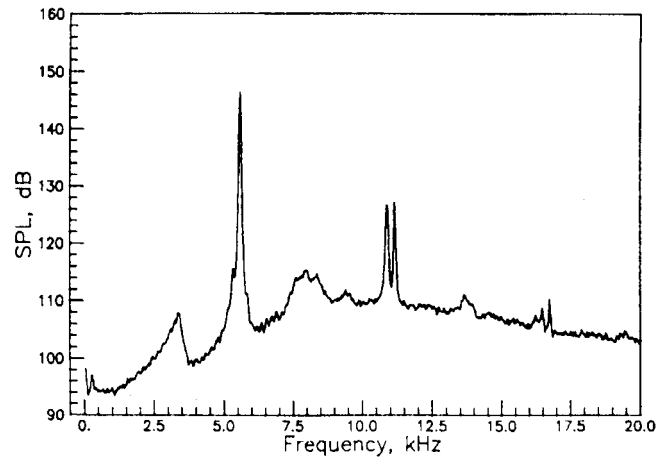


(b) $R/D=2.000$

Figure 55. Narrowband spectra for the 0.200 inch lip thickness nozzle at $M_j=1.21$.

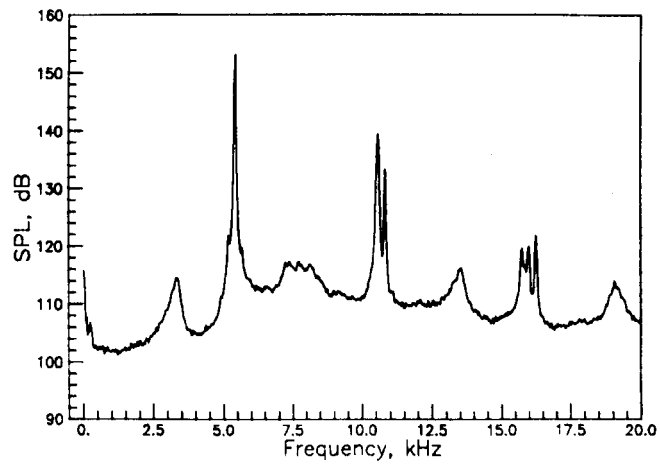


(a) $R/D=0.642$

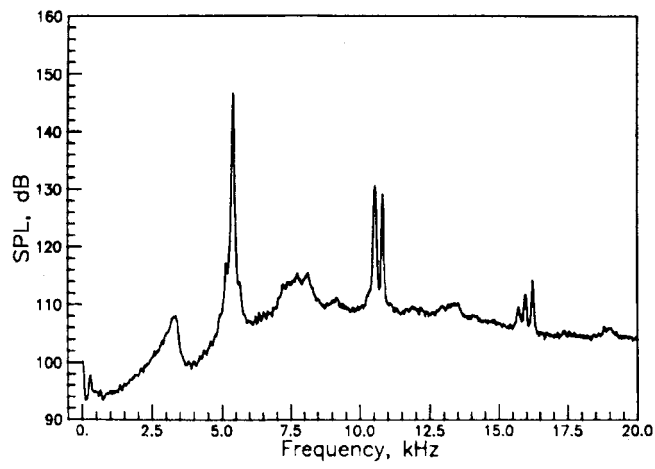


(b) $R/D=2.000$

Figure 56. Narrowband spectra for the 0.200 inch lip thickness nozzle at $M_j=1.23$.

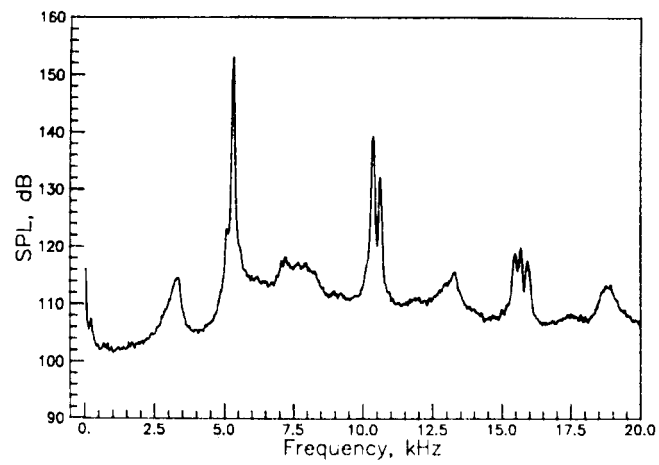


(a) $R/D=0.642$

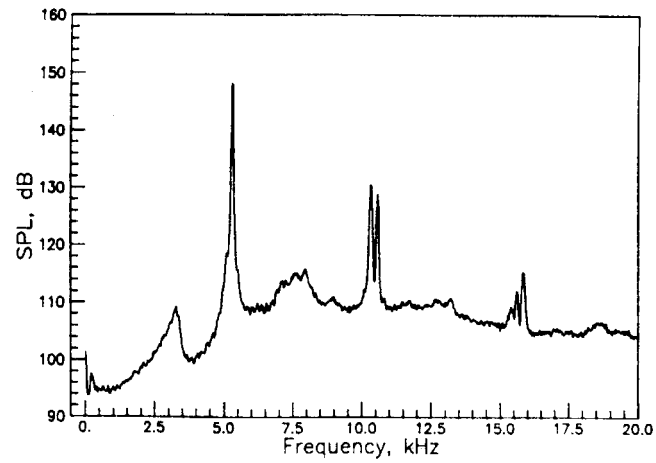


(b) $R/D=2.000$

Figure 57. Narrowband spectra for the 0.200 inch lip thickness nozzle at $M_j=1.25$.

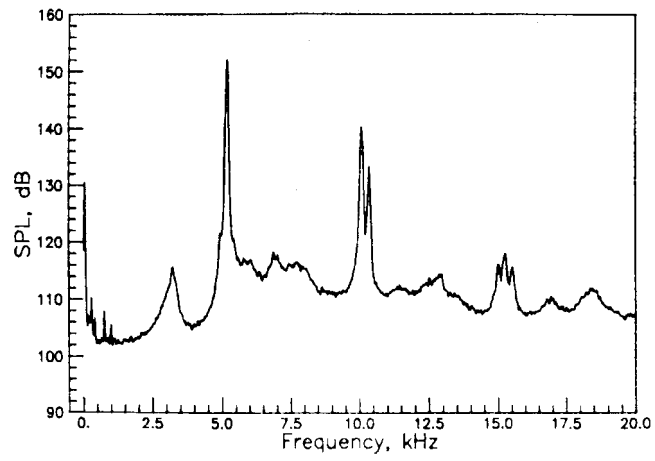


(a) $R/D=0.642$

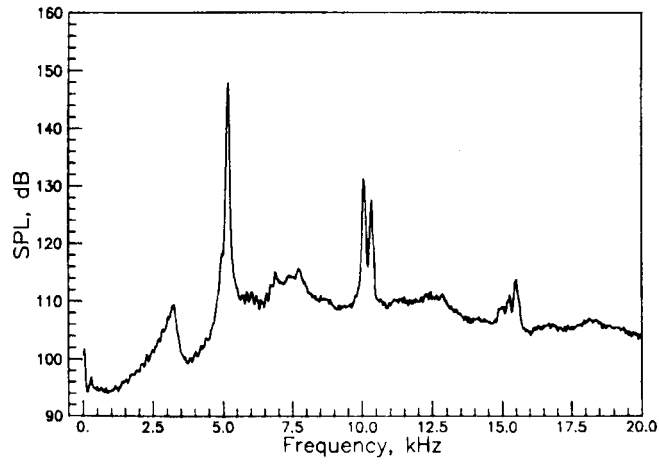


(b) $R/D=2.000$

Figure 58. Narrowband spectra for the 0.200 inch lip thickness nozzle at $M_j=1.27$.

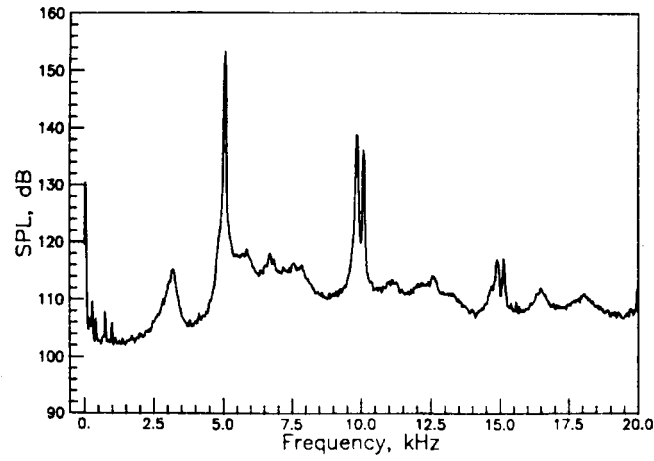


(a) $R/D=0.642$

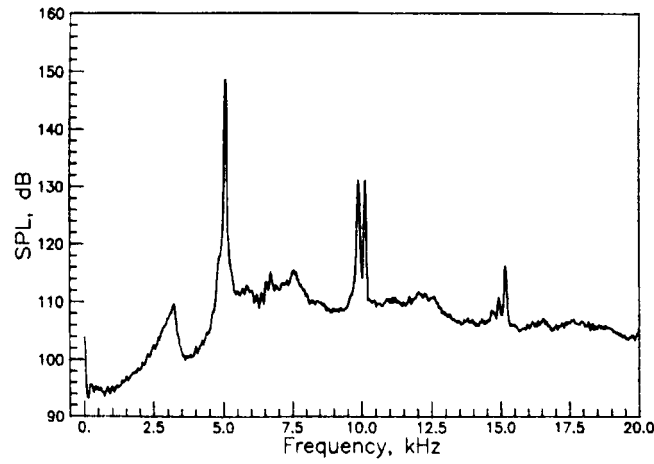


(b) $R/D=2.000$

Figure 59. Narrowband spectra for the 0.200 inch lip thickness nozzle at $M_j=1.29$.

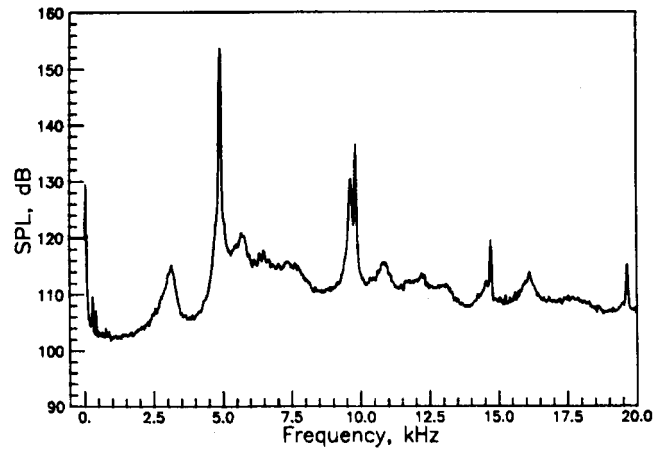


(a) $R/D=0.642$

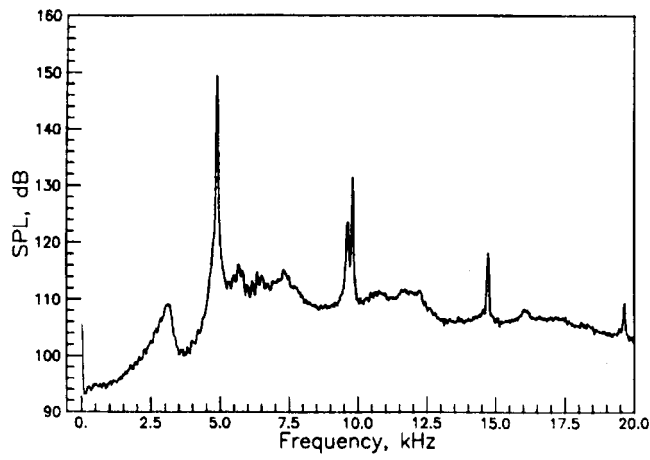


(b) $R/D=2.000$

Figure 60. Narrowband spectra for the 0.200 inch lip thickness nozzle at $M_j=1.31$.

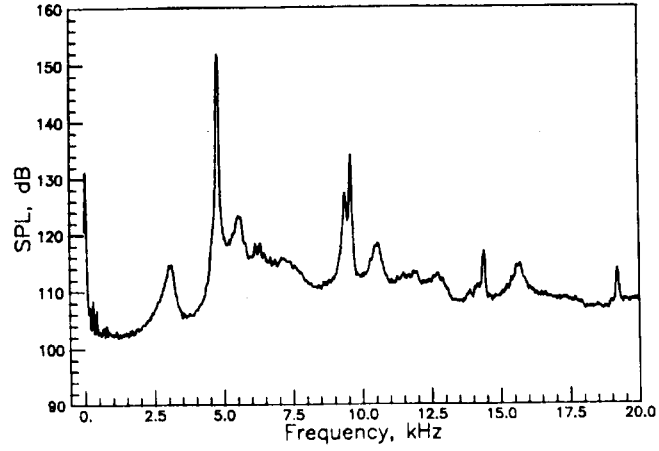


(a) $R/D=0.642$

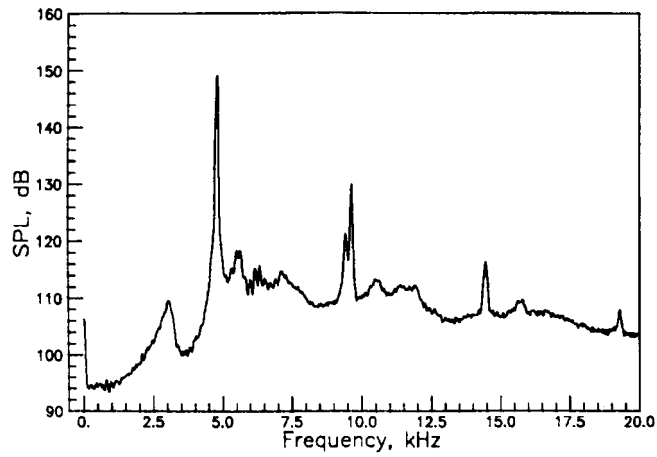


(b) $R/D=2.000$

Figure 61. Narrowband spectra for the 0.200 inch lip thickness nozzle at $M_j=1.33$.

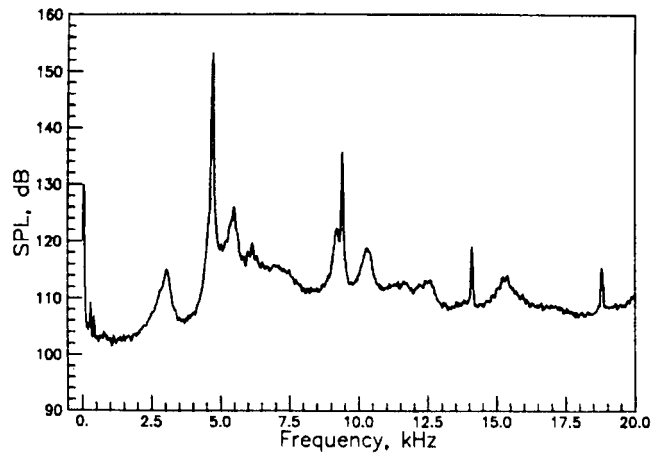


(a) $R/D=0.642$

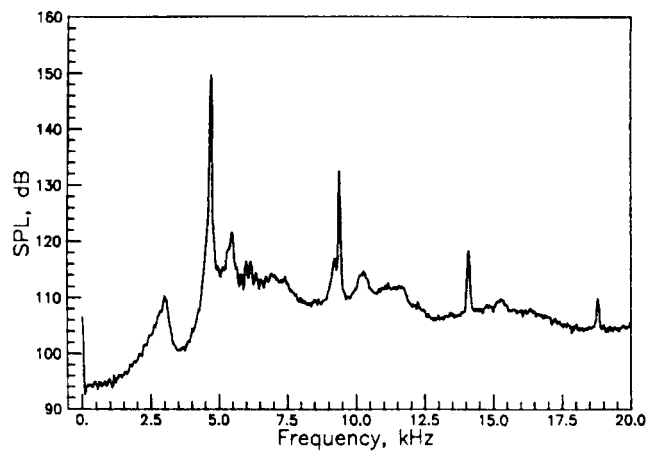


(b) $R/D=2.000$

Figure 62. Narrowband spectra for the 0.200 inch lip thickness nozzle at $M_j=1.35$.

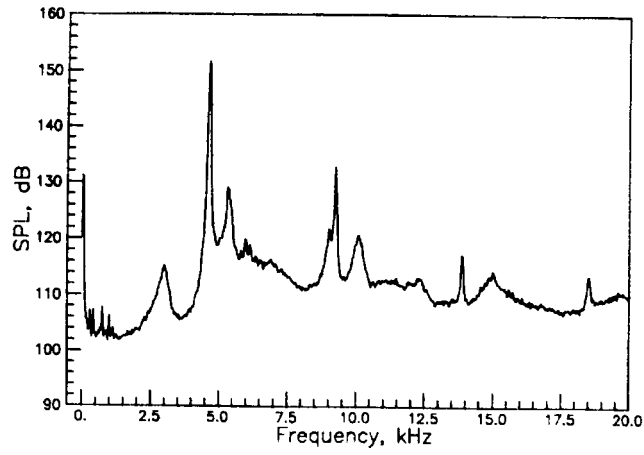


(a) $R/D=0.642$

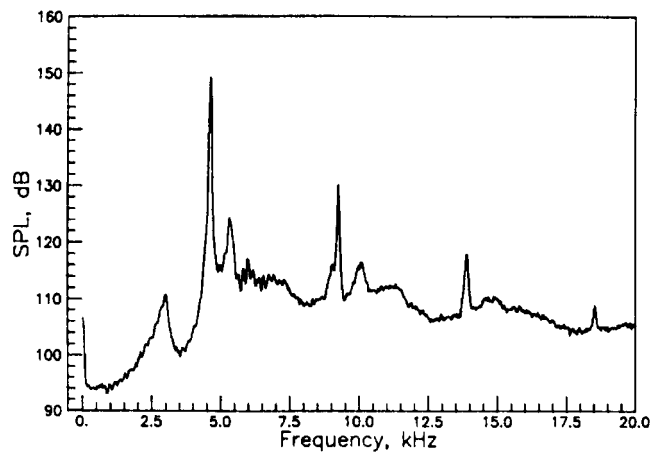


(b) $R/D=2.000$

Figure 63. Narrowband spectra for the 0.200 inch lip thickness nozzle at $M_j=1.37$.

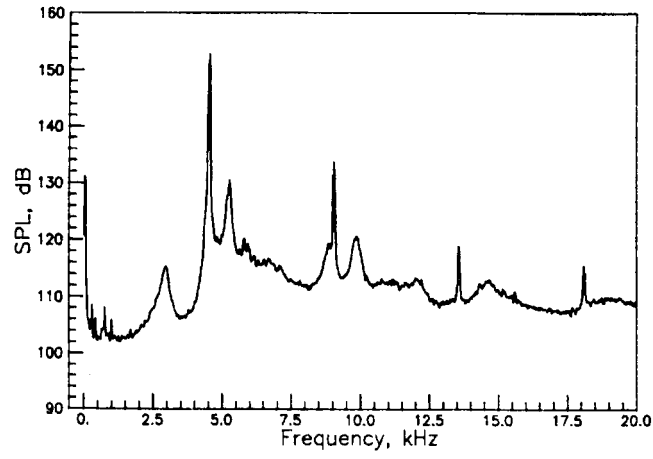


(a) $R/D=0.642$

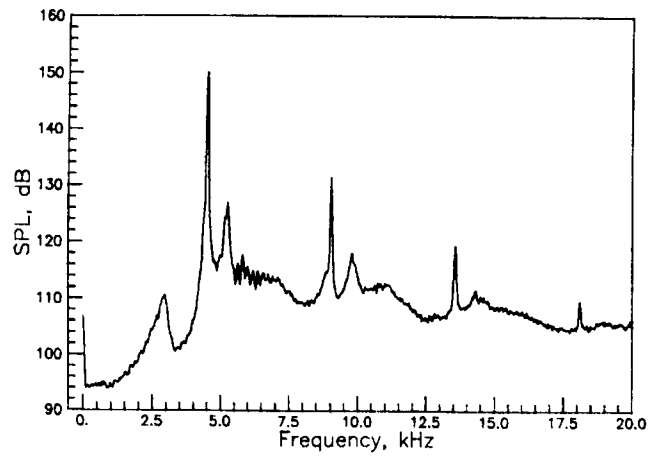


(b) $R/D=2.000$

Figure 64. Narrowband spectra for the 0.200 inch lip thickness nozzle at $M_j=1.39$.

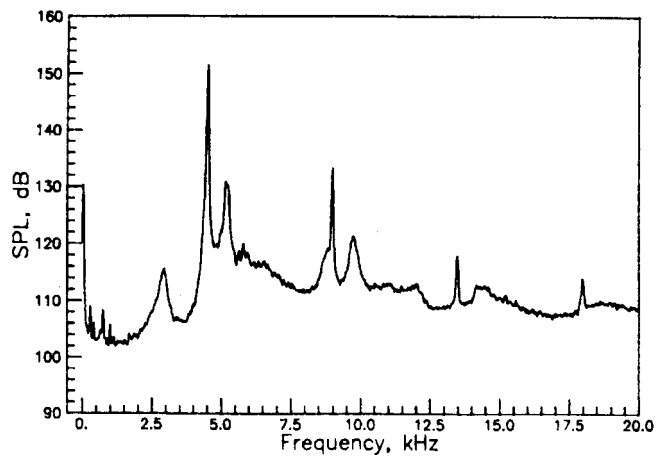


(a) $R/D=0.642$

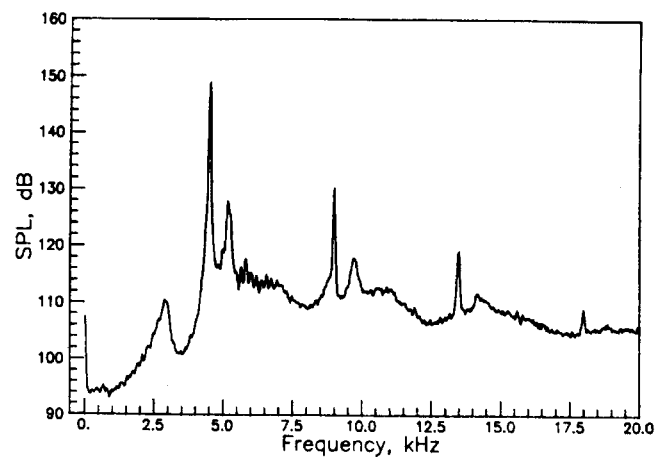


(b) $R/D=2.000$

Figure 65. Narrowband spectra for the 0.200 inch lip thickness nozzle at $M_j=1.41$.

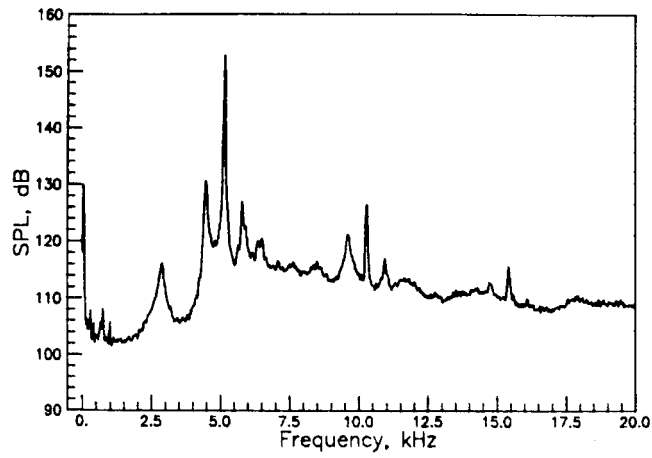


(a) $R/D=0.642$

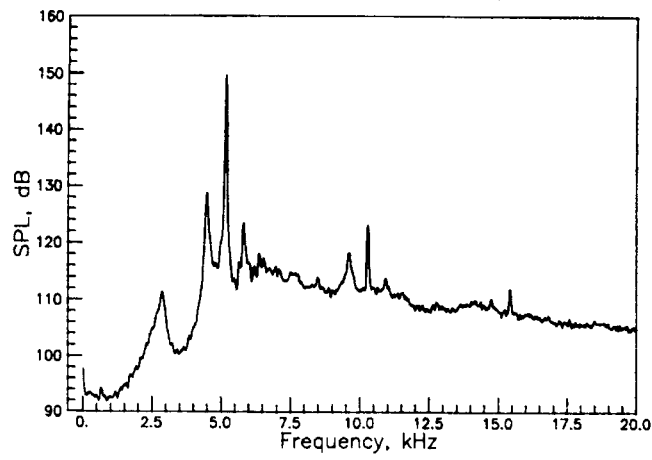


(b) $R/D=2.000$

Figure 66. Narrowband spectra for the 0.200 inch lip thickness nozzle at $M_j=1.42$.

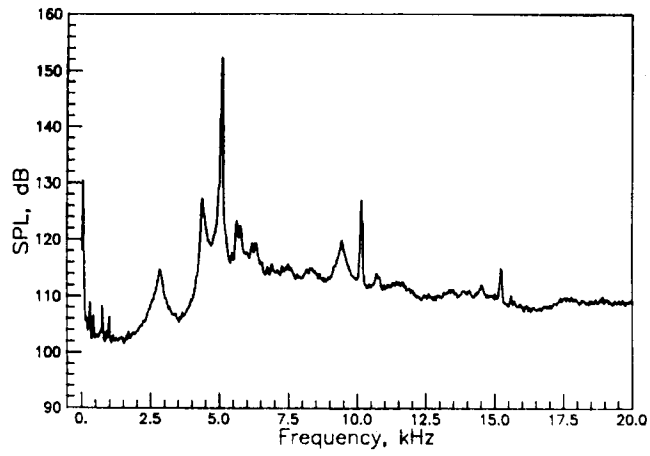


(a) $R/D=0.642$

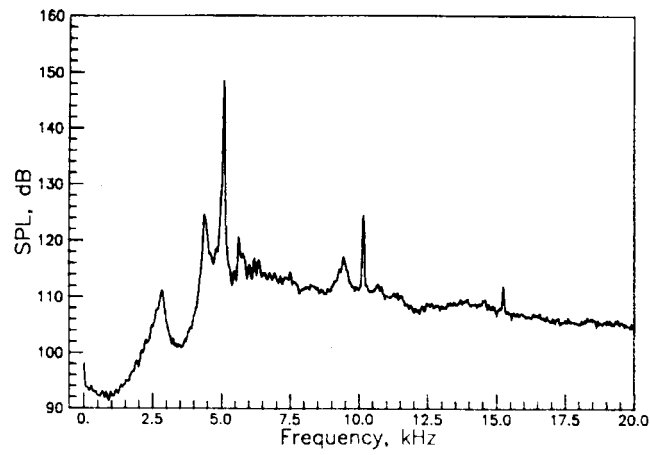


(b) $R/D=2.000$

Figure 67. Narrowband spectra for the 0.200 inch lip thickness nozzle at $M_j=1.44$.

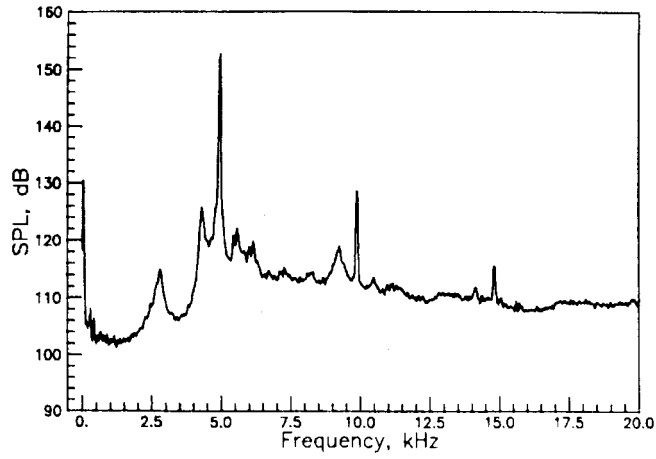


(a) R/D=0.642

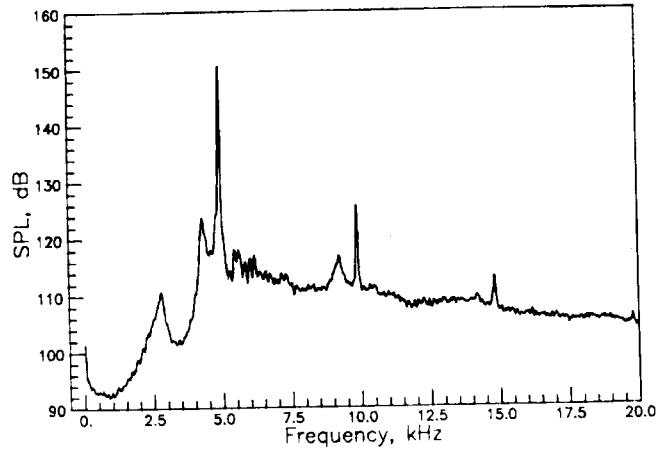


(b) R/D=2.000

Figure 68. Narrowband spectra for the 0.200 inch lip thickness nozzle at $M_j=1.46$.

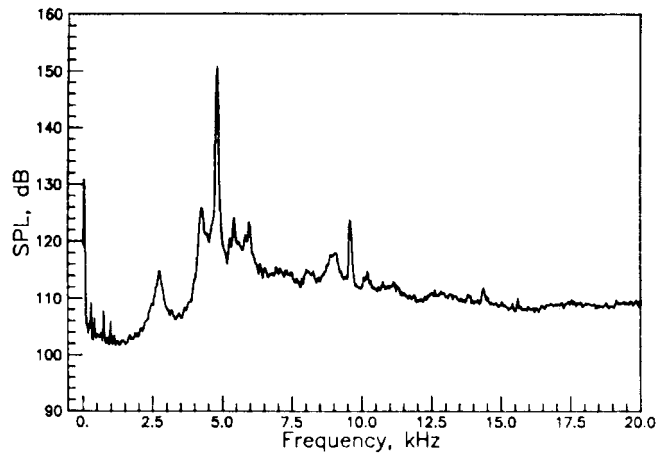


(a) $R/D=0.642$

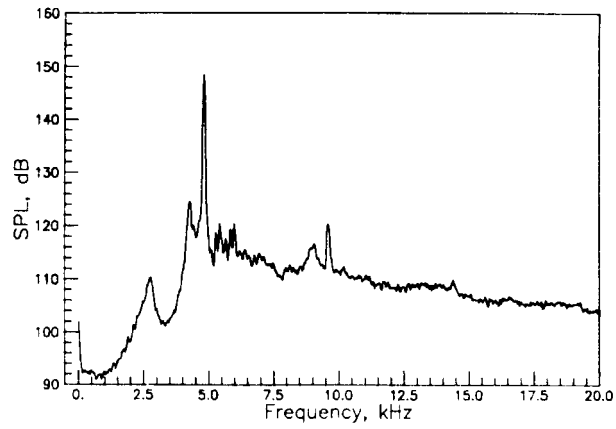


(b) $R/D=2.000$

Figure 69. Narrowband spectra for the 0.200 inch lip thickness nozzle at $M_j=1.48$.

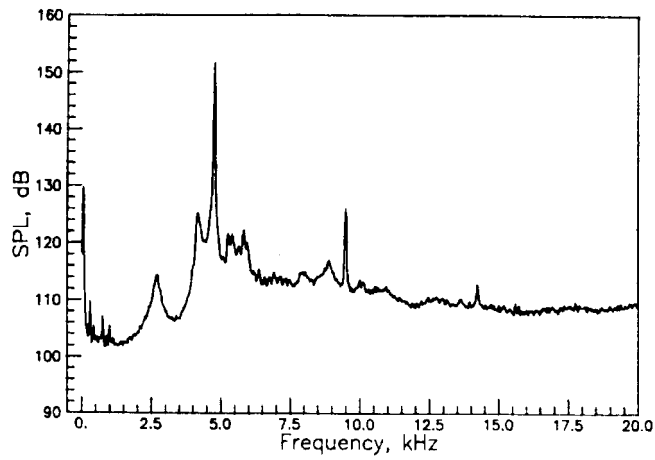


(a) $R/D=0.642$

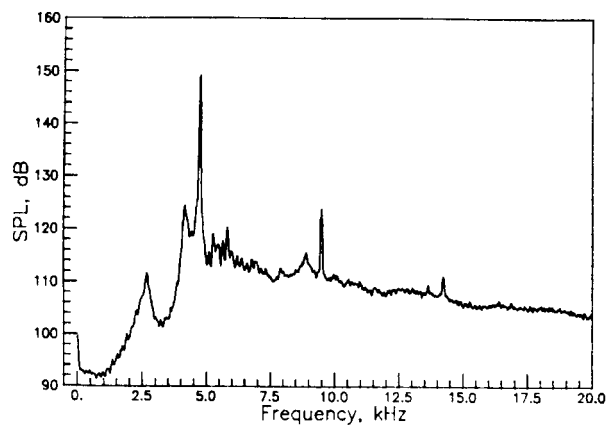


(b) $R/D=2.000$

Figure 70. Narrowband spectra for the 0.200 inch lip thickness nozzle at $M_j=1.50$.

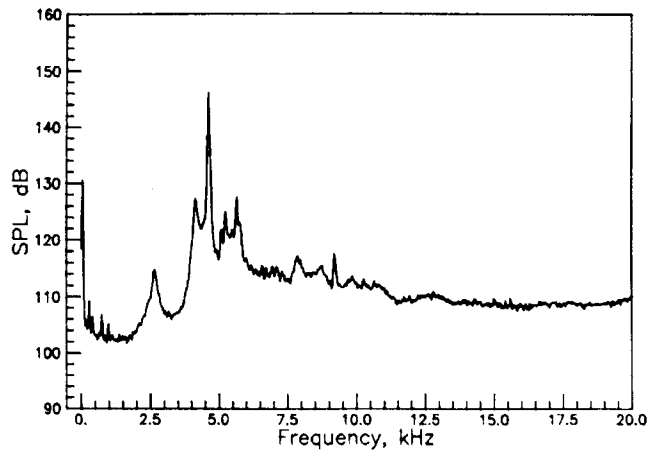


(a) $R/D=0.642$

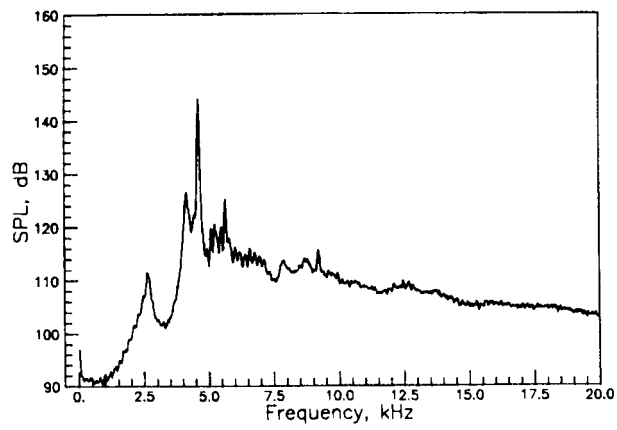


(b) $R/D=2.000$

Figure 71. Narrowband spectra for the 0.200 inch lip thickness nozzle at $M_j=1.52$.

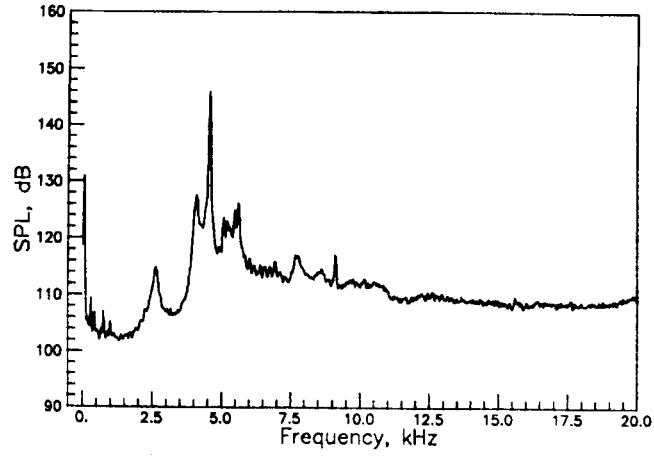


(a) $R/D=0.642$

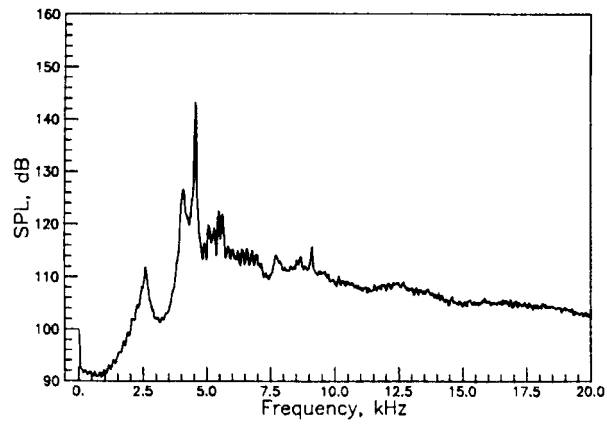


(b) $R/D=2.000$

Figure 72. Narrowband spectra for the 0.200 inch lip thickness nozzle at $M_j=1.54$.

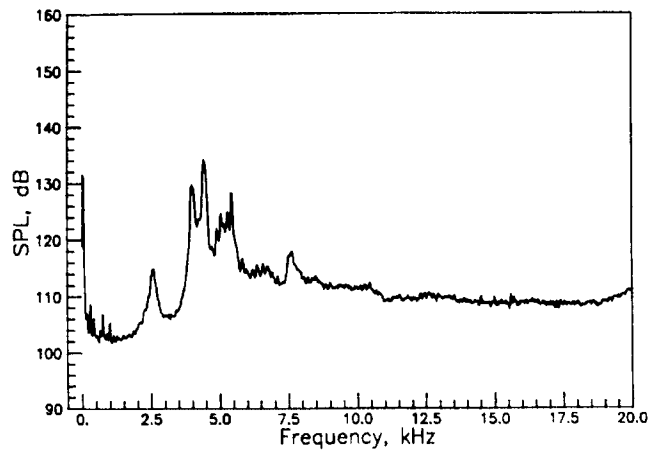


(a) $R/D=0.642$

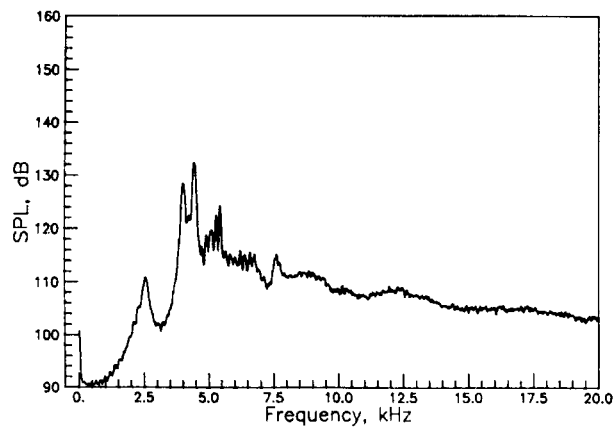


(b) $R/D=2.000$

Figure 73. Narrowband spectra for the 0.200 inch lip thickness nozzle at $M_j=1.56$.

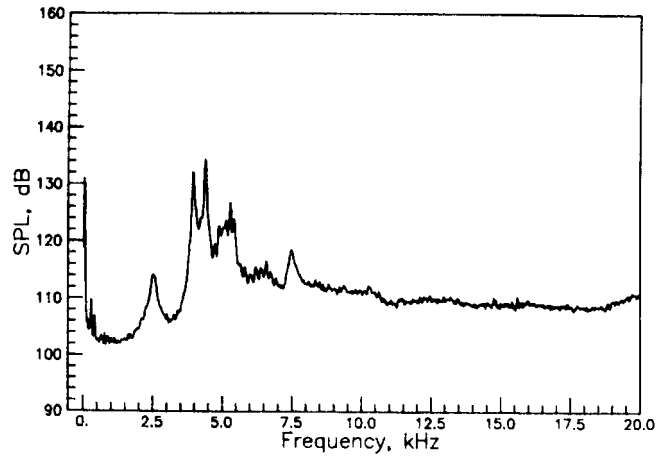


(a) $R/D=0.642$

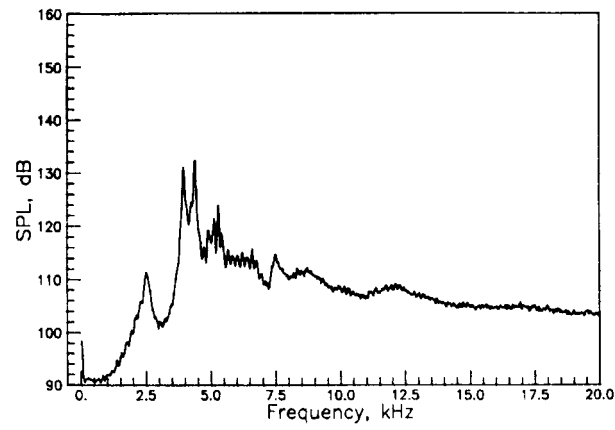


(b) $R/D=2.000$

Figure 74. Narrowband spectra for the 0.200 inch lip thickness nozzle at $M_j=1.58$.

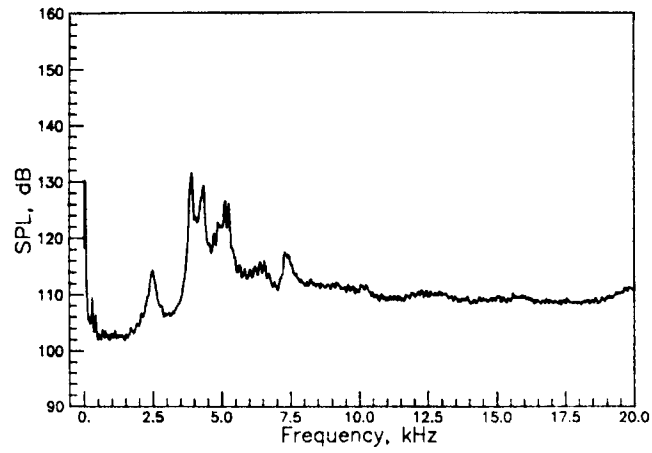


(a) $R/D=0.642$

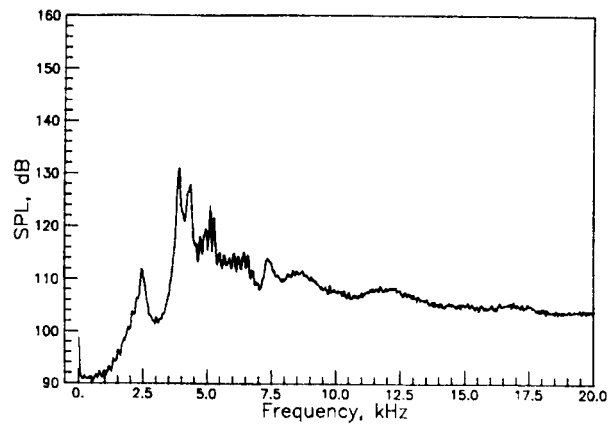


(b) $R/D=2.000$

Figure 75. Narrowband spectra for the 0.200 inch lip thickness nozzle at $M_j=1.60$.

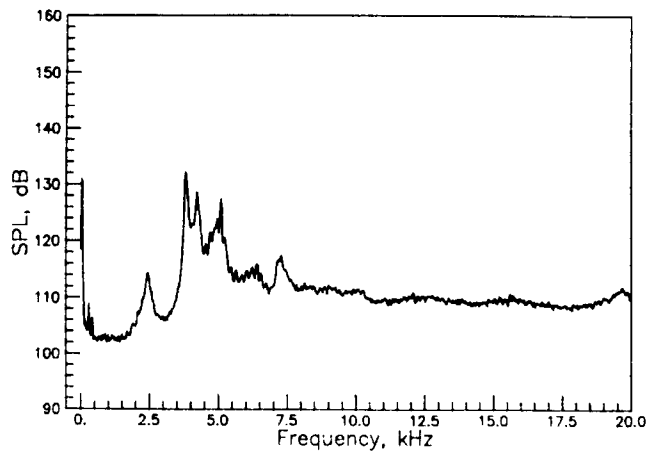


(a) $R/D=0.642$

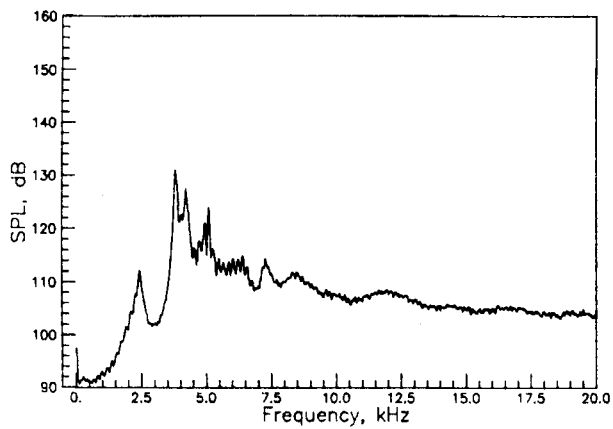


(b) $R/D=2.000$

Figure 76. Narrowband spectra for the 0.200 inch lip thickness nozzle at $M_j=1.62$.

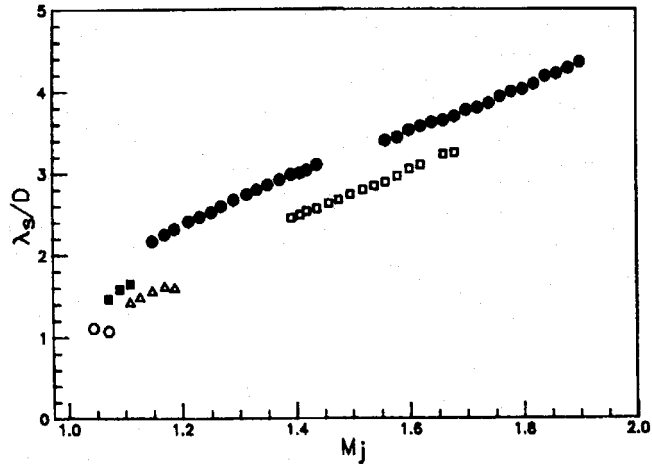


(a) $R/D=0.642$

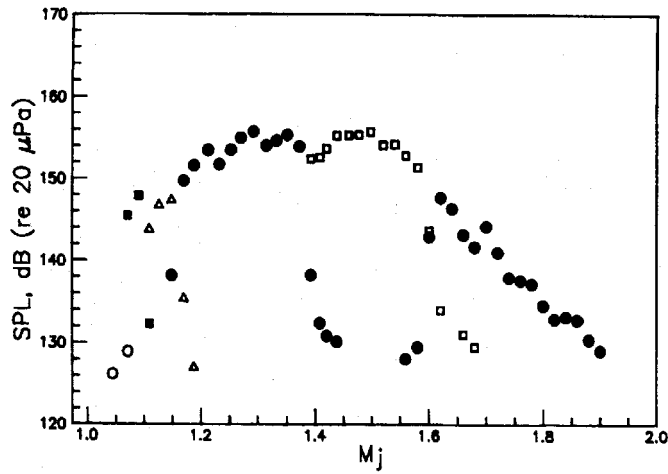


(b) $R/D=2.000$

Figure 77. Narrowband spectra for the 0.200 inch lip thickness nozzle at $M_j=1.64$

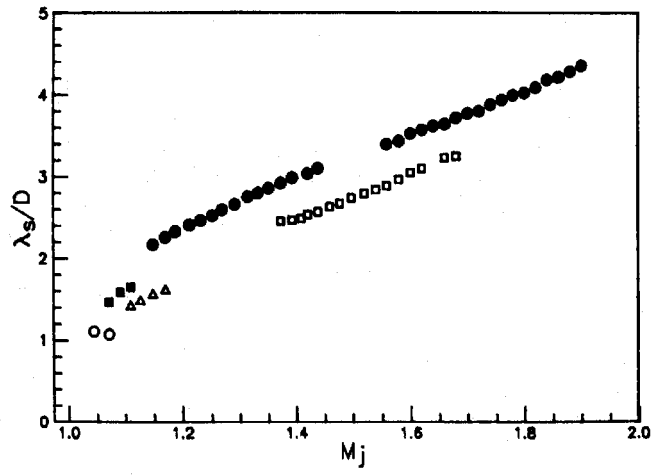


(a) Normalized acoustic wavelength

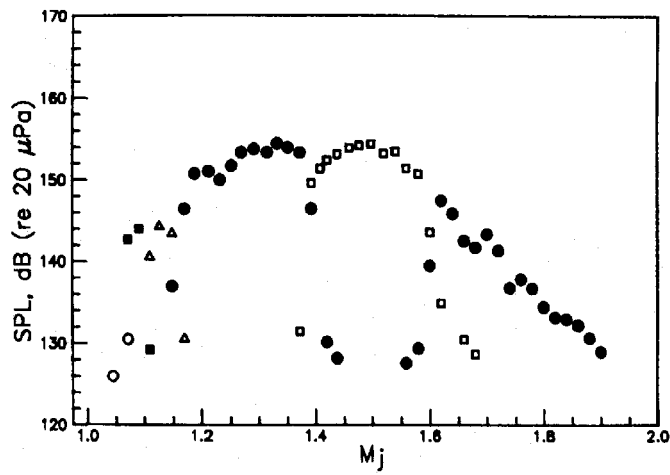


(b) Sound pressure level

Figure 78. Dominant screech components for 0.625 inch lip thickness nozzle at $R/D=0.642$.

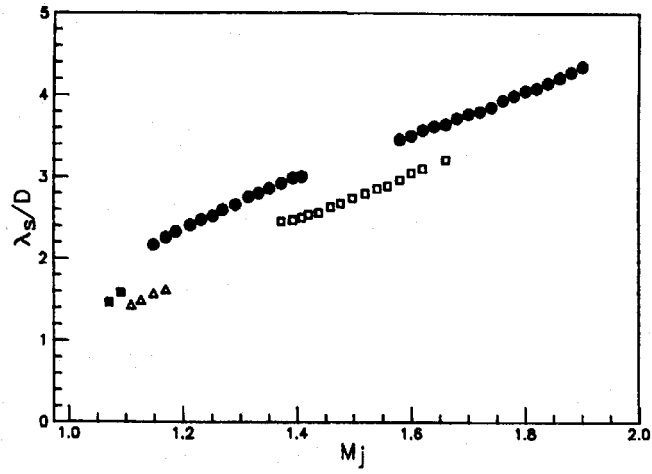


(a) Normalized acoustic wavelength

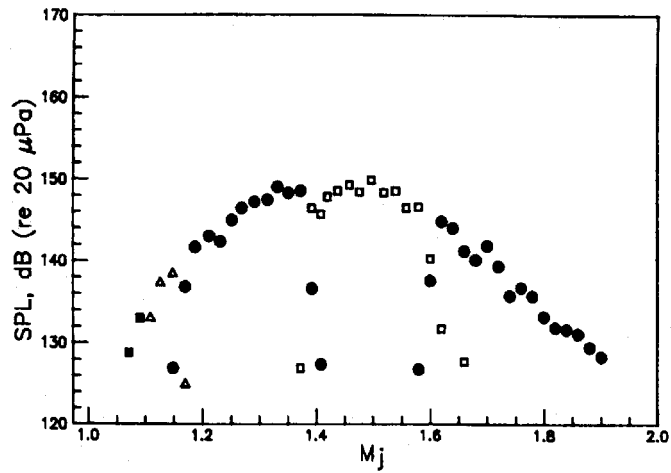


(b) Sound pressure level

Figure 79. Dominant screech components for 0.625 inch lip thickness nozzle at $R/D=0.889$.

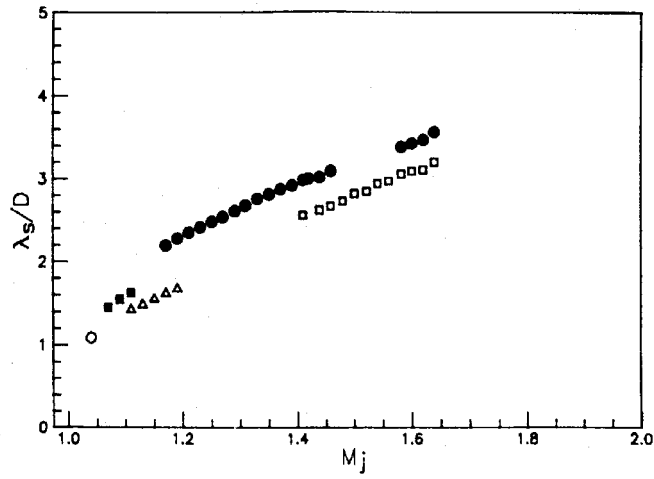


(a) Normalized acoustic wavelength

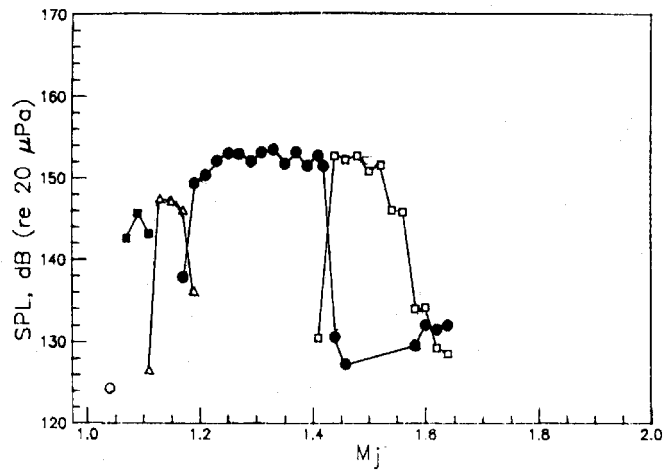


(b) Sound pressure level

Figure 80. Dominant screech components for 0.625 inch lip thickness nozzle at $R/D=2.000$.

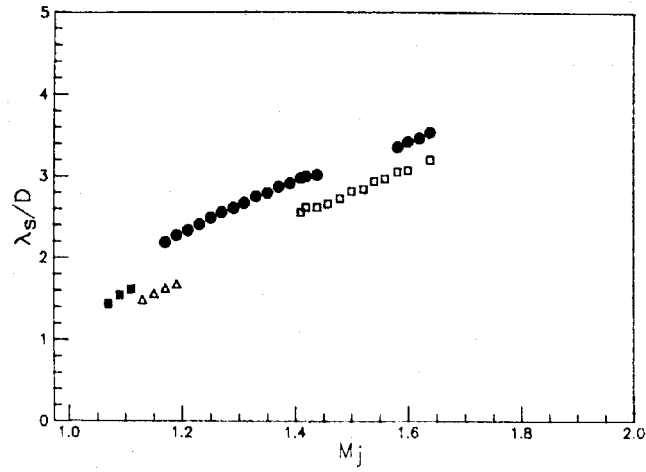


(a) Normalized acoustic wavelength

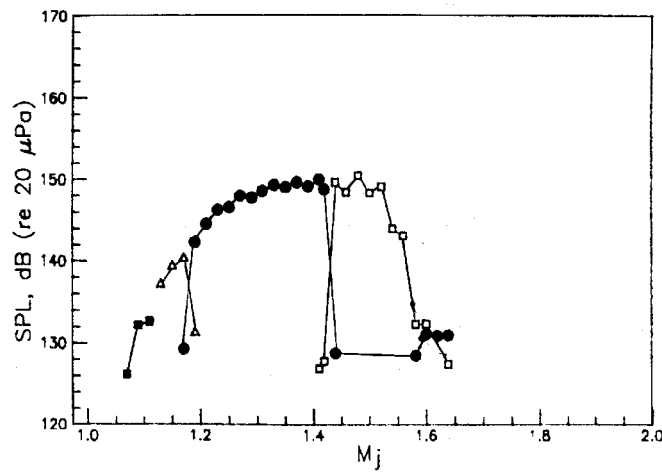


(b) Sound pressure level

Figure 81. Dominant screech components for 0.200 inch lip thickness nozzle at $R/D=0.642$.



(a) Normalized acoustic wavelength



(b) Sound pressure level

Figure 82. Dominant screech components for 0.200 inch lip thickness nozzle at $R/D=2.000$.

REPORT DOCUMENTATION PAGE			Form Approved OMB No. 0704-0188	
Public reporting burden for this collection of information is estimated to average 1 hour per response, including the time for reviewing instructions, searching existing data sources, gathering and maintaining the data needed, and completing and reviewing the collection of information. Send comments regarding this burden estimate or any other aspect of this collection of information, including suggestions for reducing this burden, to Washington Headquarters Services, Directorate for Information Operations and Reports, 1215 Jefferson Davis Highway, Suite 1204, Arlington, VA 22202-4302, and to the Office of Management and Budget, Paperwork Reduction Project (0704-0188), Washington, DC 20503.				
1. AGENCY USE ONLY (Leave blank)		2. REPORT DATE November 1997	3. REPORT TYPE AND DATES COVERED Technical Memorandum	
4. TITLE AND SUBTITLE Near Field Pressure Fluctuations in the Exit Plane of a Choked Axisymmetric Nozzle			5. FUNDING NUMBERS WU 537-05-21-01	
6. AUTHOR(S) Michael K. Ponton, John M. Seiner, and Martha C. Brown				
7. PERFORMING ORGANIZATION NAME(S) AND ADDRESS(ES) NASA Langley Research Center Hampton, VA 23681-2199			8. PERFORMING ORGANIZATION REPORT NUMBER	
9. SPONSORING/MONITORING AGENCY NAME(S) AND ADDRESS(ES) National Aeronautics and Space Administration Washington, DC 20546-0001			10. SPONSORING/MONITORING AGENCY REPORT NUMBER NASA TM-113137	
11. SUPPLEMENTARY NOTES Michael K. Ponton, John M. Seiner; and Martha C. Brown: Langley Research Center, Hampton, VA.				
12a. DISTRIBUTION/AVAILABILITY STATEMENT Unclassified-Unlimited Subject Category 71 Distribution: Nonstandard Availability: NASA CASI (301) 621-0390			12b. DISTRIBUTION CODE	
13. ABSTRACT (Maximum 200 words) Nearfield pressure data are presented for an unheated jet issuing from an underexpanded sonic nozzle for two exit lip thicknesses of 0.200 and 0.625 nozzle diameters. Fluctuating measurements were obtained on the nozzle exit surface as well as in the acoustic nearfield. Narrowband spectra are presented for numerous operating conditions expressed in terms of the fully expanded Mach number based on nozzle pressure ratio.				
14. SUBJECT TERMS Acoustics, Supersonic, Underexpanded			15. NUMBER OF PAGES 91	
			16. PRICE CODE A05	
17. SECURITY CLASSIFICATION OF REPORT Unclassified	18. SECURITY CLASSIFICATION OF THIS PAGE Unclassified	19. SECURITY CLASSIFICATION OF ABSTRACT Unclassified	20. LIMITATION OF ABSTRACT	